EES Batteries

REVIEW

View Article Online
View Journal

Cite this: DOI: 10.1039/d5eb00243e

Thermal energy storage materials for suppressing thermal runaway propagation in lithium-ion batteries: a review

Xinyu Zhang,[a] Lizhi Zhang,[a] Zhengguo Zhang *[a,b,c] and Ziye Ling *[a,b,c]

Thermal runaway propagation in lithium-ion batteries is a major factor leading to fires and explosions in energy storage systems. Thermal energy storage materials, especially phase change materials and thermochemical storage materials, demonstrate significant potential for suppressing thermal runaway propagation due to their high energy storage density and passive heat absorption characteristics. This article systematically reviews the latest research progress in the use of thermal storage materials for suppressing thermal runaway propagation in lithium-ion batteries, focuses on performance enhancement strategies for composite phase change materials in terms of flame retardancy, thermal conductivity regulation, and flexibility. The recent application advances of novel high enthalpy materials such as hydrogels and thermochemical storage materials in inhibiting thermal runaway propagation are introduced. Furthermore, the influencing factors and optimization design of the protective performance of coupled systems integrating thermal storage materials with active cooling are analyzed. Finally, the progress of current research is summarized, and future research directions are outlined, including developing multifunctional thermal storage materials with high enthalpy, improving the long-term stability and compatibility of thermal storage materials in battery systems, constructing intelligent coupled systems, and establishing accurate thermal runaway propagation simulation models. This review aims to provide a reference for thermal protection designs that enhance the safety of lithium-ion battery systems.

Received 24th December 2025,
Accepted 10th May 2026

DOI: 10.1039/d5eb00243e

rsc.li/EESBatteries

Broader context

The widespread adoption of lithium-ion batteries is crucial for the clean energy transition, yet safety concerns due to thermal runaway propagation remain a major obstacle. This review highlights a transformative shift in battery safety strategies by moving beyond traditional passive insulation to active heat absorption using advanced thermal energy storage materials. It provides a systematic and up-to-date analysis of the latest research progress on the use of thermal energy storage materials, including phase change materials, hydrogels, and thermochemical storage materials to suppression thermal runaway propagation. Strategies for enhancing thermal storage material performance in suppressing thermal runaway propagation, such as flame retardancy, thermal conductivity regulation, flexibility, and integration with active cooling systems are also discussed. The insights presented here not only advance the field of battery safety but also contribute to the broader efforts in developing advanced thermal energy storage technologies in the future.

1. Introduction

With the global energy structure transitioning towards cleaner and low-carbon solutions, electrochemical energy storage technologies have garnered increasing attention. Among these, lithium-ion batteries (LIBs) have been widely adopted in electric vehicles, energy storage power stations, and other fields due to their advantages such as high energy density and long cycle life.[1–3] However, as the energy density of LIBs continues to improve and their system scale expands, safety concerns have become increasingly prominent, emerging as a key bottleneck constraining their further development and large-scale application. Under abusive conditions such as overcharging, overheating, or internal short circuits, LIBs are prone to thermal runaway (TR), releasing a substantial amount of heat (up to 800 kJ kg^{-1}).[4–6] Within a battery module, a TR battery can continuously heat adjacent batteries above the TR trigger temperature (150 °C) through heat conduction, convection, and radiation, leading to thermal runaway propagation (TRP). This can result in catastrophic fires or explosions, posing

[a]Key Laboratory of Heat and Mass Transfer and Low-Carbon Conversion, Ministry of Education, School of Chemistry and Chemical Engineering, South China University of Technology, Guangzhou, 510640, China. E-mail: cezhang@scut.edu.cn
[b]Guangdong Engineering Technology Research Center of Efficient Heat Storage and Application, South China University of Technology, Guangzhou, 510640, China. E-mail: zyling@scut.edu.cn
[c]South China Institute of Collaborative Innovation, Dongguan, 523808, China

serious threats to life and property safety.[7–9] As the world's largest electric vehicle market, China reports an average of 31 LIB fire incidents per year. In the U.S., the National Transportation Safety Board recorded 17 fires in Tesla vehicles and 3 in BMW i3 models, with corresponding fleets of approximately 350 000 and 100 000 units, respectively.[10] Some existing studies have attempted to prevent TR by enhancing the thermal stability of internal materials in lithium-ion batteries. Examples include developing high-temperature-resistant electrode materials,[11–13] flame-retardant separators,[14–16] and solid-state electrolytes.[17–19] However, these designs increase the cost and complexity of battery manufacturing, lack universal applicability, and have yet to be widely implemented in practical applications. Therefore, there remains a critical need to develop technologies that prevent the TRP within battery packs, thereby minimizing damage and enhancing the overall safety of battery systems.

The key to preventing TRP lies in maintaining the temperature of batteries adjacent to a TR cell below the TR trigger temperature. Various strategies have been proposed to suppress TRP. Active cooling systems, such as forced air cooling and liquid cooling, manage battery temperatures within a safe range by removing heat through airflow or coolant circulation.[20,21] However, these systems are structurally complex, energy-intensive, and often inadequate in handling the instantaneous high-temperature impact generated during a TR event. Low-thermal-conductivity materials, such as aerogels, delay heat transfer to adjacent batteries through their extremely low thermal conductivity.[22,23] Yet, this approach does not fundamentally eliminate the heat generated during TR and may still fail under sustained high-temperature conditions.[24] In this context, thermal energy storage materials exhibit significant potential for suppressing TRP. On one hand, these materials effectively absorb the enormous heat released during TR through phase change or thermochemical reactions; on the other hand, their near-constant temperature during the heat storage process helps maintain adjacent cells below the thermal runaway trigger threshold, thereby forming an effective thermal buffer barrier. Among them, solid–liquid phase change materials (PCMs), characterized by relatively high energy storage density and moderate volume change, represent the most extensively studied thermal storage material system to date.[25,26] However, their energy storage density typically falls below 300 kJ kg^{-1}, which remains insufficient when confronting extreme thermal runaway in high-energy-density batteries.[27] In recent years, novel thermal storage materials, such as hydrogels utilizing water's liquid–gas phase change and thermochemical storage materials (TCMs) with endothermic decomposition capabilities, have attracted considerable attention for suppressing TRP. These materials offer high evaporation or decomposition enthalpies (exceeding 1000 kJ kg^{-1}), surpassing the thermal storage capacity of traditional solid–liquid PCMs.[28,29] Additionally, coupling thermal storage materials with active cooling systems to achieve synergistic rapid heat absorption and continuous heat dissipation has become an important research direction for enhancing suppressing TRP performance.[30,31]

Although numerous reviews have explored the application of thermal storage materials in LIBs thermal management, these studies have largely concentrated on conventional solid–liquid PCMs, with the optimization objective often being the enhancement of thermal conductivity to maintain battery temperature within the optimal range—typically below 50 °C for maximum temperature and within 5 °C for maximum temperature difference.[32–36] This fundamentally differs from the objective of suppressing TRP under extreme abuse conditions, which requires controlling the temperature of adjacent cells below the TR trigger threshold (approximately 150 °C), withstanding instantaneous high-temperature shock, and emphasizing the fire resistance and high-temperature insulation capabilities of the materials. Currently, reviews specifically addressing the application of thermal storage materials for TRP suppression under extreme conditions remain scarce, particularly regarding systematic summaries of performance enhancement strategies for PCMs and the utilization of novel high-enthalpy thermal storage materials such as hydrogels and thermochemical storage materials in TRP mitigation.

This review summarizes the latest research progress in utilizing thermal storage materials to suppress TRP. The overall structure is as follows: chapter 2 introduces TR and TRP mechanisms of LIBs, as well as TRP suppression methods. Chapter 3 presents the types and working principles of thermal storage materials. Chapter 4 discusses the application of CPCMs in TRP protection and optimization strategies for their key properties, including flame retardancy, thermal conductivity, and flexibility. Chapter 5 introduces the application of novel thermal storage materials (hydrogels and TCMs) in TRP suppression. Chapter 6 analyzes the design of coupled systems integrating thermal storage materials with active cooling methods (*e.g.*, liquid cooling) and methods for enhancing their TRP suppression performance. Finally, chapter 7 summarizes current research findings and explores future research directions.

2. Thermal runaway and its propagation in LIBs

2.1 Structure and working principle of LIBs

LIBs primarily consist of a cathode, an anode, an electrolyte, and a separator.[37] The cathode is mainly responsible for storing and releasing lithium ions, with common cathode materials including lithium cobalt oxide ($LiCoO_2$), lithium manganese oxide ($LiMn_2O_4$), and lithium iron phosphate ($LiFePO_4$).[38,39] The anode is primarily responsible for absorbing or releasing lithium ions, typically utilizing graphite or other carbon-based materials.[40] The electrolyte acts as the conduction medium for lithium ions and is an organic solution containing lithium salts, such as lithium hexafluorophosphate and lithium tetrafluoroborate.[41,42] The separator is used to isolate the cathode and anode to prevent short circuits while allowing the free passage of lithium ions. It is mainly made of polyolefin films, such as polypropylene (PP) and polyethylene

(PE).[43] The principle of LIBs charging and discharging is the intercalation and deintercalation of lithium ions between the cathode and anode. During charging, lithium ions detach from the crystal lattice structure of the cathode material, travel through the electrolyte and separator, and intercalate into the anode. Concurrently, electrons flow from the cathode to the anode *via* the external circuit to maintain charge balance. The discharging process is the reverse of charging, forming a reversible cycle.[44] The structure and working principle of LIBs are illustrated in Fig. 1.[45]

Based on the casing material and packaging method, commercial lithium-ion batteries are mainly classified into three categories: cylindrical, prismatic, and pouch cells.[46] Among them, cylindrical batteries feature a wound structure encased in steel or aluminum shells. They offer mature manufacturing processes, low cost, and good consistency, but suffer from low space utilization and relatively small capacity, often requiring a large number of cells to form a module in practical applications. Prismatic batteries are typically encapsulated in aluminum shells and fabricated *via* lamination or winding processes. They exhibit advantages such as efficient heat dissipation, high space utilization, and robust reliability, yet are limited by higher cost and lack of standardized specifications.[47] Pouch batteries, usually packaged with aluminum–plastic composite films, possess high energy density, flexible shape adaptation, and light weight, but are challenged by low mechanical strength, susceptible to external mechanical damage and internal gas expansion.[48]

2.2 Mechanism of thermal runaway

TR in LIBs is typically triggered by the following scenarios: (1) mechanical abuse: when a battery is subjected to penetration, crush, or impact, the separator may rupture, leading to an internal short circuit and the release of a substantial amount of Joule heat; (2) electrical abuse: conditions such as overcharge, over-discharge, or excessive current can induce internal short circuits and vigorous side reactions, generating significant heat; (3) thermal abuse: elevated temperatures can initiate exothermic decomposition reactions of the cathode and anode materials as well as the electrolyte, causing a rapid temperature rise.[7] Furthermore, factors such as battery aging, manufacturing defects, and inconsistencies among individual cells within a battery pack can significantly increase the risk of TR.[49] The root cause of TR lies in a series of self-accelerating exothermic chain reactions occurring inside the battery. These reactions cause the rate of heat generation to far exceed the rate of heat dissipation, ultimately leading to the loss control of temperature. The chain reactions involved in the thermal runaway process can be divided into five primary stages:

(1) Decomposition of the solid-electrolyte interphase (SEI): the SEI is a surface passivation layer formed during the initial charging of LIBs due to the reaction between the graphite anode material and the electrolyte at the solid–liquid interface. It effectively prevents direct reaction between the anode and the electrolyte.[50] The SEI layer is primarily composed of metastable components (*e.g.*, $ROCO_2Li$, $(CH_2OCO_2Li)_2$, ROLi, *etc.*) and stable components (*e.g.*, LiF, Li_2CO_3, *etc.*). Its decomposition temperature is influenced by the lithium salt and typically occurs in the range of 80–120 °C.[37] The thermal decomposition of the SEI is essentially a process in which metastable components transform into stable components, accompanied by the release of heat and gases, as represented by eqn (1)–(3). Owing to its lowest decomposition temperature, SEI decomposition is recognized as the initial exothermic reaction during TR.[51]

$$(CH_2OCO_2Li)_2 \rightarrow Li_2CO_3 + C_2H_4 + CO_2 + 0.5O_2 \quad (1)$$

$$2Li + (CH_2OCO_2Li)_2 \rightarrow 2Li_2CO_3 + C_2H_4 \quad (2)$$

$$Li_2CO_3 + 2HF \rightarrow 2LiF + CO_2 + H_2O \quad (3)$$

(2) Reaction between the anode and the electrolyte: the exothermic decomposition of the SEI layer further elevates the internal temperature of the battery. Meanwhile, after the decomposition of the SEI layer, the lithiated anode becomes directly exposed to the electrolyte. When the temperature rises to 100–250 °C, the intercalated lithium in the anode reacts exothermically with carbonate-based organic solvents (*e.g.*, EC, PC, DMC, EMC, *etc.*), further increasing the battery temperature. For the $Li_{0.86}C_6$ + 1.0 M $LiPF_6$/EC + DEC system, the total heat release can reach 2600.9 J g^{-1}. As the amount of intercalated lithium increases, the activation energy decreases, while the reaction heat increases.[52] Simultaneously, these reactions generate substantial amounts of flammable gases, such as C_2H_4 and CO.[53] Taking DMC as an example, the reactions are represented by eqn (4)–(6).

$$2Li^+ + C_3H_6O_3(DMC) + 2e^- \rightarrow CO + 2CH_3OLi \quad (4)$$

$$Li^+ + C_3H_6O_3(DMC) + e^- + 0.5H_2 \rightarrow CH_4 + CH_3OCO_2Li \quad (5)$$

$$2Li + C_3H_6O_3(DMC) \rightarrow C_2H_6 + Li_2CO_3 \quad (6)$$

(3) Separator melting and internal short circuit: the melting of the separator plays a critical role in the TR process of LIBs. Under normal operating conditions, the separator physically

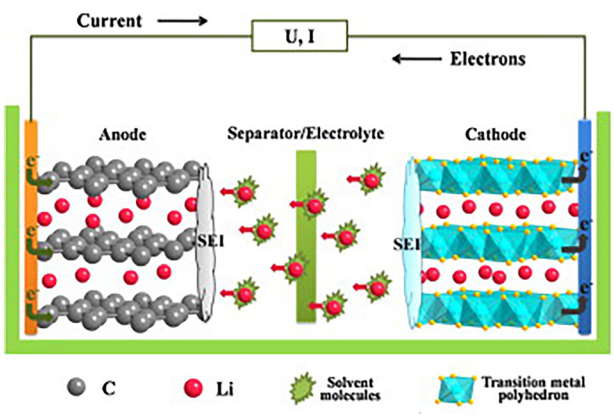

Fig. 1 Structure and working principles of LIB (charging). Reproduced with permission from ref. 45. Copyright 2012, Elsevier.

isolates the cathode and anode while allowing lithium-ion transport. When the battery temperature exceeds approximately 135–166 °C, polyolefin-based separators (*e.g.*, PE and PP) undergo melting and shrinkage, leading to direct contact between the electrodes and triggering a large-scale internal short circuit.[54] This short circuit releases substantial Joule heat, causing a rapid temperature surge that accelerates subsequent exothermic reactions, including cathode decomposition and electrolyte combustion.[55] Therefore, the separator melting event marks a critical transition from gradual self-heating to catastrophic TR.

(4) Cathode decomposition and its reaction with the electrolyte: under high-temperature conditions, the decomposition of cathode materials releases oxygen, which undergoes a vigorous oxidation reaction with the electrolyte, generating substantial heat and gas. This process serves as the critical turning point where the thermal runaway chain reaction escalates into its severe stage. The thermal stability of cathode materials is governed by their crystal structure. Layered structures (LCO, NCM, NCA) exhibit the poorest thermal stability due to their relatively weak interlayer bonding, with decomposition onset temperatures ranging from 180–200 °C.[55] During structural collapse, a large amount of lattice oxygen is released, forming reactive oxygen species, resulting in intense TR behavior. The spinel structure (LMO) possesses a three-dimensional tunnel framework that is more stable than layered structures, with a decomposition onset temperature of approximately 220 °C.[56] Its oxygen release is lower than that of layered structures, leading to a comparatively milder TR reaction. The olivine structure (LFP) features a stable PO_4 tetrahedral framework, and owing to the exceptionally strong P–O bonds, it releases almost no reactive oxygen, achieving the highest thermal stability. Its decomposition temperature range is 190–285 °C, and typically exhibits no open flames or only weak flames during TR.[57,58] The decomposition reactions of the common cathode materials LCO, NCM, and LFP are presented in eqn (7)–(9), respectively.[37]

$$4LiCoO_2(LCO) \rightarrow 2Li_2O + 2Co_3O_4 + 3O_2 \quad (7)$$

$$Li_x(NiCoMn)_{1/3}O_2(NCM) \rightarrow Li_x(NiCoMn)_{1/3}O_{2-y} + y/2O_2 \quad (8)$$

$$(1-x)LiFePO_4(LFP) + xFePO_4 \rightarrow (1-x)LiFePO_4 + x/2Fe_2P_2O_7 + 1/4O_2 \quad (9)$$

(5) Electrolyte decomposition: during thermal runaway of lithium-ion batteries, the electrolyte serves as both a heat source and a fuel source. When the temperature rises to 100–120 °C, $LiPF_6$ undergoes thermal decomposition to produce PF_5 and toxic HF.[59] PF_5 acts as a strong Lewis acid that catalyzes the decomposition of carbonate solvents, generating flammable gases such as C_2H_4, CO, and H_2, along with substantial heat release. In the temperature range of 200–300 °C, the decomposition reactions intensify, producing large quantities of combustible gases and increasing the internal pressure of the battery.[60] When the temperature exceeds the flash point of the solvent, the generated gases ignite upon exposure to high temperatures or sparks, triggering violent combustion. Taking diethyl carbonate (DEC) as an example, its decomposition reaction is represented by eqn (10)–(14).

$$LiPF_6 \rightarrow LiF + PF_5 \quad (10)$$

$$C_2H_5OCOOPF_4 + PF_5 \rightarrow C_2H_5OCOOPF_4 + HF + C_2H_4 \quad (11)$$

$$C_2H_5OCOOPF_4 \rightarrow PF_3O + CO_2 + C_2H_4 + HF \quad (12)$$

$$C_2H_5OCOOPF_4 \rightarrow PF_3O + CO_2 + C_2H_5F \quad (13)$$

$$C_2H_5OCOOPF_4 + HF \rightarrow PF_4OH + CO_2 + C_2H_5F \quad (14)$$

Beyond the aforementioned reactions, some researchers have proposed more detailed subdivisions of the TR process, accounting for factors such as binder decomposition and reactions between the binder and electrode materials.[61] The processes occurring at different stages of TR are illustrated in Fig. 2.[62]

Through Accelerating Rate Calorimetry (ARC) testing, researchers have identified three characteristic temperatures during the TR process of LIBs: self-heating starting temperature (T_1), trigger temperature (T_2), and maximum temperature (T_3), as shown in Fig. 3.[63] Specifically, self-heating onset temperature typically occurs between 90–120 °C, corresponding to the initiation of SEI decomposition and the onset of self-exothermic reactions. It is defined by a battery self-heating rate exceeding 0.02 °C min^{-1}. TR trigger temperature marks the transition from gradual to rapid temperature rise, usually occurring between 130–180 °C, which corresponds to separator meltdown leading to large-scale internal short circuits. The criterion for TR trigger temperature is a heating rate exceeding 60 °C min^{-1}. Maximum temperature represents the peak temperature reached during TR, reflecting the intensity of the runaway reaction, and often exceeds 300 °C.[64] In summary, during TR in LIBs, internal chemical reactions mutually reinforce each other, releasing substantial heat. The generated flammable gases and high pressure may further lead to fire or explosion. Within a battery pack, if the heat released by a TR cell raises the temperature of adjacent cells above TR trigger temperature, it may induce TR in those neighboring cells, thereby triggering TRP.

2.3 Thermal runaway propagation and its influencing factors

The pathways through which energy is released during battery TR can be primarily categorized into internal and external paths. The internal path mainly refers to the rapid release of energy stored within the battery in the form of heat. The external path primarily involves the combustion and explosion of the substantial amounts of flammable gas mixtures generated during TR, triggered by factors such as high-temperature particles or electrostatic sparks.[63] Within a battery pack, the substantial heat released by a TR cell continuously heats adjacent cells through heat conduction *via* solid components such as the cell casing, tabs, and busbars, as well as thermal convection and radiation induced by high-temperature ejecta and

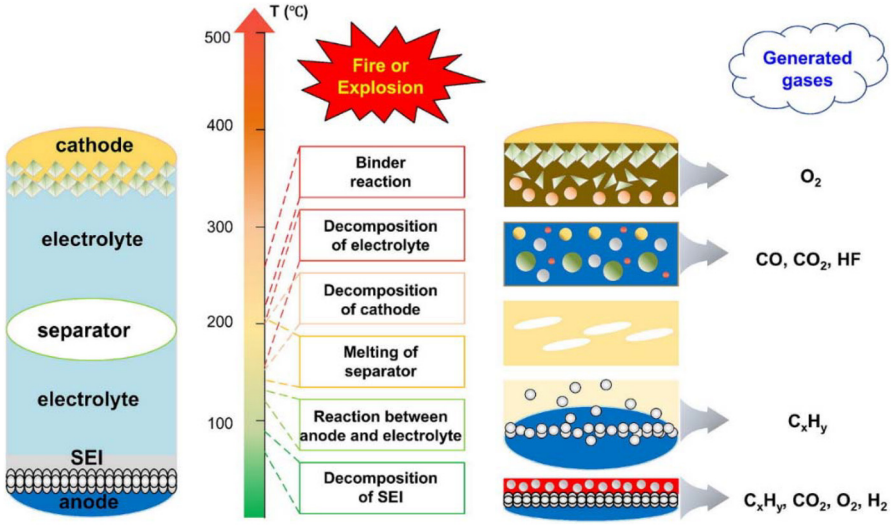

Fig. 2 An overview of the TR process of LIBs in stages. Reproduced with permission from ref. 62. Copyright 2025, Elsevier.

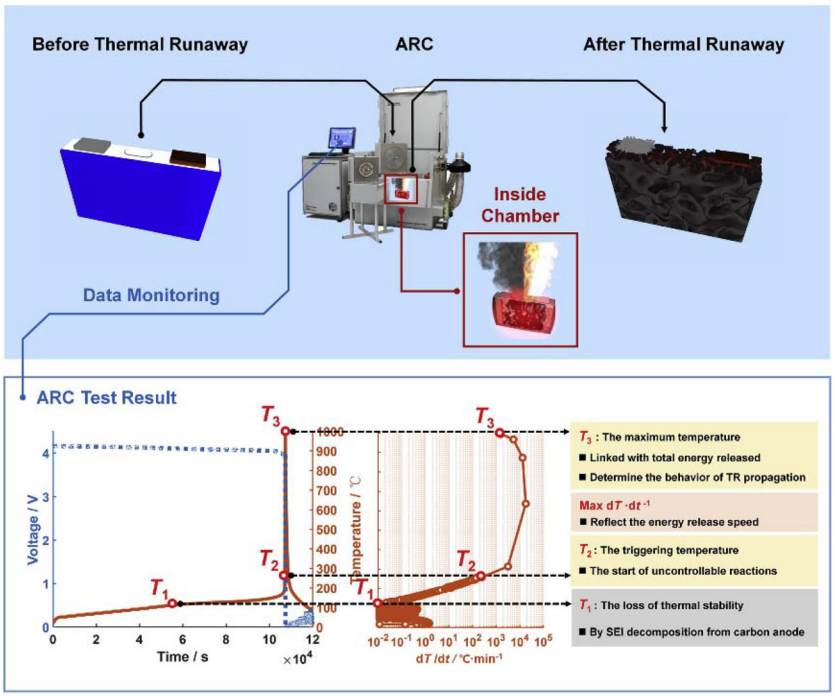

Fig. 3 ARC test for thermal stability of lithium-ion batteries (T_1: self-heating starting temperature, T_2: trigger temperature, and T_3: maximum temperature of sample during TR). Reproduced with permission from ref. 63. Copyright 2020, Elsevier.

flames.[65] If the temperature of other cells in the pack exceeds the TR trigger temperature, TRP may be initiated. Current research indicates that as little as 12% of the heat generated by a TR cell is sufficient to induce TR in an adjacent cell, with the majority of this heat transferred through thermal conduction *via* the cell casing.[66]

Multiple factors influence TRP behavior, including the battery's state of charge (SOC), inter-cell spacing, and the method of TR initiation. Huang *et al.*[67] compared TRP behavior in LIBs triggered by overcharge *versus* overheating. Their study found that while overcharge-triggered cells produced more heat and flammable gas during TR, overheating-triggered TRP propagated faster in an open environment. This is attributed to the higher casing temperature during overheating, leading to more rapid heat transfer between adjacent cells. Li *et al.*[68] investigated the influence of battery SOC on TRP. Their results showed that higher SOC corresponds to a lower TR trigger temperature and greater heat release, thereby accelerating TRP.

As the SOC increased from 50% to 100%, the TRP time decreased significantly from 307 s to 87 s. Huang *et al.*[69] compared TRP behavior in LIBs with NCM and LFP cathodes. Their research indicated that NCM batteries exhibit more intense reactions during TR, with higher peak TR temperatures and longer durations compared to LFP batteries, making them more prone to triggering TRP. Huang *et al.*[70] explored the influence of battery pack connection methods on TRP. They found that due to the heat transfer *via* electrical connectors, TRP propagation speed is faster in series and parallel connected packs compared to unconnected cells. In parallel connections, the connectors not only provide a heat transfer path but can also conduct electricity to other LIBs, presenting a higher TRP risk. Lopez *et al.*[71] found that the probability of TRP occurrence decreases significantly as the distance between batteries increases. It is worth pointing out that the shape and packaging format of the battery are also key factors influencing the path and rate of thermal runaway propagation. Zhang *et al.*[72] compared the thermal runaway behavior of prismatic and pouch cells and found that although pouch batteries release less energy during thermal runaway, the lateral flame generated during TR is more likely to trigger TRP. In summary, heat transfer between cells plays a crucial role in TRP. The key to preventing TRP lies in reducing heat transfer to adjacent cells and maintaining their temperature below the TR trigger threshold.

2.4 Suppression strategies for thermal runaway propagation

Current suppression strategies for TRP can be broadly classified into three categories: heat dissipation based on active cooling systems, heat blocking based on thermal insulation materials and heat absorption based on thermal storage materials.[24] These suppression strategies will be discussed separately in the following sections.

2.4.1 Heat dissipation based on active cooling systems. Active cooling systems involves dissipating heat from a TR cell through means such as air or liquid flow, or by spraying water mist or fire suppressants, thereby maintaining the temperature of adjacent cells below the TR trigger temperature. For instance, Xu *et al.*[73] investigated the effectiveness of a microchannel liquid cooling plate in suppressing TRP *via* numerical simulation. They found that at a flow rate of 10 L min^{-1}, the system could maintain the maximum temperature of adjacent cells below 60 °C, effectively preventing TRP. Han *et al.*[74] developed an optimized air cooling system utilizing sleeves and non-uniform fins, which successfully prevented TRP. Qin *et al.*[75] designed an integrated system based on a closed-loop $C_6F_{12}O$ spray cooling (Fig. 4). Their study demonstrated that $C_6F_{12}O$ spray cooling could significantly remove TR heat, successfully blocking TRP. While active cooling systems offer robust and sustained heat dissipation capacity, they have disadvantages such as structural complexity, high cost, and a potential risk of failure under the extreme temperatures of a TR event.

2.4.2 Heat blocking based on thermal insulation materials. Placing materials with extremely low thermal conductivity, such as aerogels, between cells can effectively delay the transfer of TR heat to adjacent cells (Fig. 5).[76] Wei *et al.*[77] fabricated polyimide aerogel for TRP suppression and found that increasing the aerogel thickness from 0.5 mm to 1.5 mm extended the TRP delay time from 182 s to 259 s. Zhao *et al.*[78] prepared a flexible Al_2SiO_5 fiber membrane. Their research showed that under heating, this membrane could extend the time for the cell to reach the TR trigger temperature by 1608 s. Although low-conductivity materials like aerogels effectively slow heat transfer, they cannot eliminate the substantial heat generated during TR, the accumulated heat may still raise adjacent cell temperatures above the TR trigger point, leading to TRP. Sun *et al.*[79] studied the effectiveness of different thermal insulation materials in suppressing TRP. They found that while nanofibers and aerogels delayed the TRP time, they could not completely prevent its occurrence. Furthermore, using aerogel for insulation might lead to heat accumulation within the battery pack, potentially exacerbating the severity of TR. Zhou *et al.*[80] found that wrapping cells with aerogel resulted in a higher peak TR temperature.

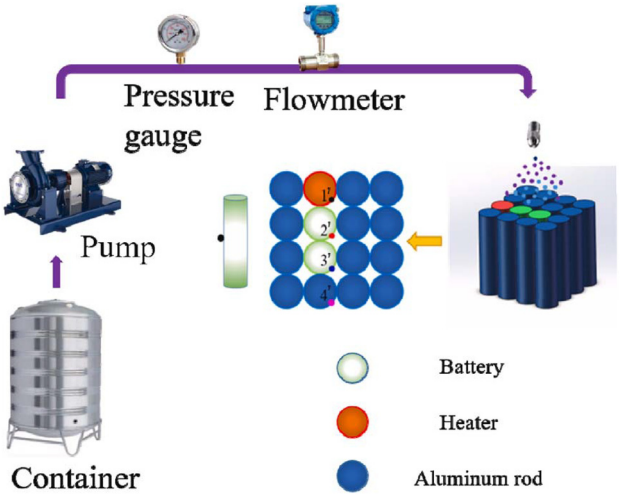

Fig. 4 The schematic figure of the integrated system. Reproduced with permission from ref. 75. Copyright 2021, Elsevier.

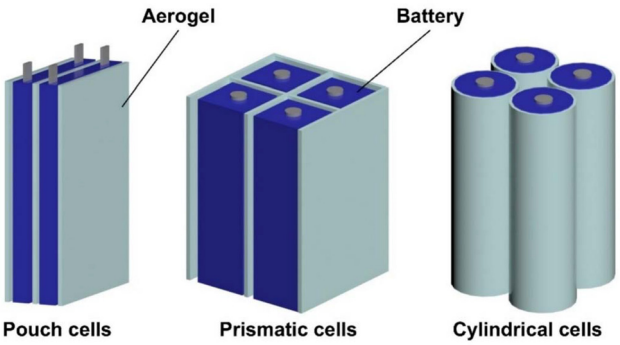

Fig. 5 Aerogel products application in pouch, prismatic and cylindrical cells. Reproduced with permission from ref. 76. Copyright 2025, Elsevier.

2.4.3 Heat absorption based on thermal storage materials. Compared to thermal insulation materials, which can only delay heat transfer but cannot eliminate heat, thermal storage materials can directly absorb the heat released by a TR cell, thereby suppressing the temperature of adjacent cells below the TR trigger threshold. Galazutdinova *et al.*[81] applied PCMs to suppress TRP in battery packs (Fig. 6), the results indicated that the heat generated during TR was effectively absorbed, adjacent cell temperatures were contained below 63.5 °C, and TRP was completely prevented. In summary, thermal storage materials offer advantages such as rapid passive heat absorption, simple structure, and no requirement for external energy, presenting a highly promising technical pathway for completely preventing TRP. However, the effectiveness of TRP suppression depends on the intrinsic properties of thermal storage materials, including energy storage density and the temperature range of heat storage. The following sections will elaborate on the main categories and working principles of thermal storage materials, as well as their applicability as TRP suppression materials.

3. Types of thermal storage materials

3.1 Classification of thermal storage materials

To effectively suppress TRP, thermal storage materials must operate below the TR trigger temperature of LIBs, and possess sufficiently high energy storage density to handle the substantial heat release during a TR event. Based on their working principles, thermal storage materials can be primarily classified into three categories: sensible heat storage materials, latent heat storage materials, and TCMs. Sensible heat storage materials absorb or release heat through temperature change. Their storage capacity depends on the material's specific heat capacity, mass, and the temperature change range. Sensible heat storage offers relatively low energy storage density, typically in the range of 10–50 kW h m^{-3}.[82] Latent heat storage materials, also known as PCMs, store or release thermal energy through phase transitions of a substance. They provide a higher energy storage density, typically ranging from 84–140 kW h m^{-3}.[83] TCMs involve reversible chemical reactions to achieve conversion between thermal energy and chemical energy. Compared to sensible and latent heat storage, they offer significantly higher energy storage density, which can reach 200–840 kW h m^{-3}.[84] Due to their relatively low energy density, sensible heat storage materials are generally inadequate for absorbing the large amount of heat generated during battery TR. In contrast, PCMs and thermochemical storage materials offer higher energy densities and maintain an almost constant temperature during the energy storage process. Consequently, PCMs and thermochemical storage materials are the primary focus for TRP suppression and will be discussed in detail in the following sections.

3.2 Phase change materials

PCMs can be primarily classified according to the phase transition involved: solid–solid, solid–liquid, liquid–gas PCMs and solid–gas PCMs.[85] Solid–solid phase change materials, although free from liquid leakage risks and endowed with good shape stability, generally exhibit low phase change enthalpy (typically below 100 kJ kg^{-1}), which limits their capacity to absorb the substantial heat generated during TR. Liquid–gas and solid–gas PCMs, despite possessing exceptionally high enthalpy (exceeding 1000 kJ kg^{-1}), but during the phase transition, the volume expands dramatically and is accompanied by gas generation.[86] In contrast, solid–liquid PCMs achieve a favorable balance among energy storage density (typically 150–300 kJ kg^{-1}), minimal volume change, and the absence of gas generation, are therefore the most widely adopted for the application of TRP suppression.[87]

Based on their chemical composition, solid–liquid PCMs can be further divided into organic and inorganic PCMs.

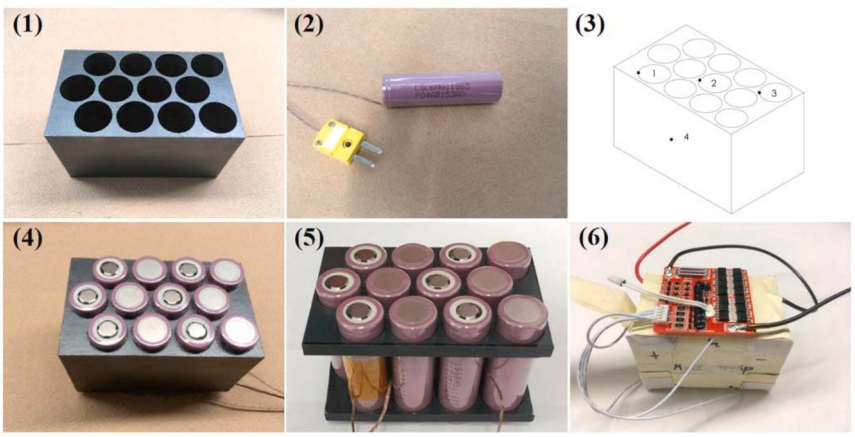

Fig. 6 Assembly of the battery packs: (1) graphite matrix impregnated with PCM (CPCM), (2) thermocouple attached to a cell, (3) position of thermocouples in the pack, (4) cells inserted into CPCM, (5) cells inserted into PVC holders, (6) soldering of the voltage sense wires and BMS. Reproduced with permission from ref. 81. Copyright 2021, Elsevier.

Organic PCMs, such as paraffin waxes, fatty acids, and polyethylene glycol (PEG), offer advantages including high stability, negligible supercooling, and the absence of phase separation, along with high energy storage density per unit mass. However, they are also associated with drawbacks such as high cost and flammability.[88] Inorganic PCMs encompass materials like hydrated salts, molten salts, metals, and alloys. They typically provide high energy storage density per unit volume and possess higher thermal conductivity. Their disadvantages include a tendency for supercooling, phase separation and strong corrosiveness. Among various PCMs, organic types like paraffin and inorganic hydrated salts, whose phase change temperatures are typically below the TR trigger temperature of LIBs, are most frequently employed for TRP suppression.[89]

Pure PCMs face the issue of liquid leakage during the solid–liquid phase transition. To address this and maintain shape stability, they are often composited with support materials to form CPCMs. Current preparation methods for CPCMs primarily include porous carrier adsorption, microencapsulation, and chemical grafting. Porous carrier adsorption involves immobilizing the PCM within the pores of a carrier material through capillary forces, hydrogen bonding, *etc*. Commonly used porous carriers include expanded graphite, porous carbon, and metal foams.[86] This method features a simple process, but carries a risk of leakage during long-term cycling. It's suitable for the preparation of high-thermal-conductivity CPCMs, for instance, Huang *et al.*[90] prepared a CPCM by loading a $LiNO_3$/KCl eutectic salt onto expanded graphite. Their study showed that as the mass fraction of expanded graphite increased from 10% to 30%, the enthalpy of the CPCM decreased from 178.10 kJ kg^{-1} to 142.41 kJ kg^{-1}, but its thermal conductivity increased significantly, but the thermal conductivity increased from 1.85 times that of the pure eutectic salt to 7.56 times. Microencapsulation entails encapsulating the PCM within a dense shell. Methods for preparing phase change microcapsules include sol–gel, emulsion polymerization, *in situ* polymerization, and spray drying.[91] This method can completely encapsulate the PCM to prevent leakage, but the process is relatively complex. It's suitable for the preparation of high-stability CPCMs and for reducing the corrosiveness of PCMs such as hydrated salts. For example, Fang *et al.*[92] prepared phase change microcapsules by encapsulating paraffin with SiO_2. Their results indicated an encapsulation efficiency of 87.5% for the paraffin within the SiO_2 shell, and the microcapsules achieved an enthalpy of 165.68 kJ kg^{-1}. Chemical grafting involves fixing the PCM onto a polymer support skeleton *via* chemical bonds to maintain shape stability. This method achieves molecular-level immobilization, fundamentally preventing PCM leakage. However, due to the limited grafting ratio, the resulting heat storage density is relatively low. It's suitable for the preparation of CPCMs requiring exceptional shape stability and long-term reliability. Chen *et al.*[93] chemically crosslinked PEG onto a glucose-based skeleton, producing a CPCM that exhibited no liquid leakage and possessed an enthalpy of 108.70 kJ kg^{-1}.

The enthalpy of solid–liquid PCMs is typically below 300 kJ kg^{-1}. In contrast, liquid–gas PCMs can offer significantly higher enthalpy values. Water is an environmentally friendly and cost-effective liquid–gas PCM. Its boiling point (100 °C) is below the typical TR trigger temperature of LIBs (150 °C), and it possesses a very high enthalpy of vaporization (up to 2500 kJ kg^{-1}),[94] making it suitable for battery TRP suppression.[95] Researchers have similarly attempted to composite water with carrier materials to achieve shape stability. Hydrogels, a class of highly hydrophilic three-dimensional network structures formed by crosslinking one or more polymers, exhibit exceptional water absorption capacity (water content can exceed 95%) and good flexibility, making them excellent carriers for water.[96] For instance, Cui *et al.*[97] fabricated an hydrogel *via* the polymerization and crosslinking of polyvinyl alcohol (PVA), which achieved a high evaporation enthalpy of 1642 kJ kg^{-1}.

3.3 Thermochemical storage materials

TCMs absorb or release heat through the breaking and formation of chemical bonds, offering an energy storage density per unit volume that can exceed twice that of latent heat storage materials.[98] A key advantage of this storage mode is the high energy density associated with the chemical reaction process, coupled with negligible energy loss. For thermochemical storage below 250 °C, widely studied reaction media currently include crystalline hydrates, hydroxides, and their composites.[99–101] Among these, hydrated salts, which utilize hydration/dehydration reactions for thermal energy storage and release, represent the simplest reaction principle in terms of mechanism, the reaction is represented by eqn (15).[102] The endothermic decomposition of hydrated salts typically occurs within the temperature range of 100–150 °C, with decomposition enthalpies potentially exceeding 1000 kJ kg^{-1}, meeting the requirements for TRP suppression.[103] For example, Ma *et al.*[104] prepared composite microcapsules with SiO_2 shells encapsulating a mixture of $CH_3COONa{\cdot}3H_2O$ and $Na_2HPO_4{\cdot}12H_2O$. Their study showed that the thermal decomposition of these microcapsules occurred between 100–120 °C, with a total enthalpy as high as 509.18 kJ kg^{-1}. Heating stage tests demonstrated that even after heating at 120 °C for 30 minutes, the backside temperature of the microcapsule material could be maintained below 65 °C, indicating its potential application in suppressing TRP.

$$\text{Salt}\cdot a\text{H}_2\text{O} + \Delta H \rightleftharpoons \text{Salt}\cdot b\text{H}_2\text{O} + (a-b)\text{H}_2\text{O} \qquad (15)$$

In summary, PCMs exhibit promising potential for suppressing battery TRP due to their high energy storage density. Preparing CPCMs effectively overcomes the inherent limitations of pure PCMs and provides diverse technical options for enhancing TRP suppression performance. Novel thermal storage materials, such as hydrogels and TCMs, have achieved significant improvements over the thermal storage performance of traditional solid–liquid PCMs, holding promise for breakthroughs in TRP suppression. Some commonly used

Table 1 The thermal properties of some thermal energy storage materials used for suppressing TRP

Thermal storage materials	Type	Phase change temperature (°C)	Phase change enthalpy (kJ kg^{-1})	Decomposition temperature (°C)	Decomposition enthalpy (kJ kg^{-1})	Ref.
Paraffin	Organic PCM	50–52	196	—	—	105
Lauric acid	Organic PCM	43.5–48.2	187.21	—	—	106
PEG 6000	Organic PCM	62.8	171.2	—	—	107
PEG 8000	Organic PCM	62.7	170.3	—	—	108
KCl/$LiNO_3$	Inorganic PCM	142	308	—	—	109
Water	Liquid–gas PCM	100	2500	—	—	94
$Na_2HPO_4{\cdot}12H_2O$	Inorganic PCM & TCM	~36	270	93–110	1281	27
$CH_3COONa{\cdot}3H_2O$	Inorganic PCM & TCM	58	225	106–140	568	110

thermal energy storage materials for suppressing TRP and their thermal properties are shown in Table 1. The following chapters will focus on detailing the specific applications of thermal storage materials and their composites in inhibiting battery TRP, along with strategies for performance optimization.

4. CPCMs for suppressing TRP

4.1 Flame-retardant CPCMs

The TR process in LIBs is often accompanied by high temperatures and flames, imposing stringent requirements on the flame retardancy of CPCMs. Organic PCMs inherently suffer from flammability and therefore require compounding with flame retardants to enhance their fire resistance. Commonly used flame retardants types include: phosphorus-based flame retardants (*e.g.*, phosphorus oxides, phosphates), nitrogen-based flame retardants (*e.g.*, dicyandiamide, melamine), silicon-based flame retardants (*e.g.*, silicon dioxide, silica gel), metal hydroxides (*e.g.*, $Mg(OH)_2$, $Al(OH)_3$), intumescent flame retardants (*e.g.*, nitrogen-phosphorus compounds, expandable graphite). Their mechanisms of action differ: phosphorus-based retardants primarily form a dense char layer on the material surface to isolate oxygen and scavenge radicals to interrupt combustion reactions. Nitrogen-based and metal hydroxide retardants act mainly by decomposing endothermically and releasing non-combustible gases to dilute flammable gases and oxygen concentrations. Silicon-based retardants can form a dense silicon–carbon barrier on the surface, isolating heat and oxygen. Intumescent flame retardants decompose to generate gases, leading to the formation of a porous, expanded char layer that acts as a physical barrier.[111] Based on their preparation methods, flame-retardant CPCMs can be primarily categorized into two approaches: incorporating flame retardants into the CPCM matrix, and encapsulating the CPCM with a flame-retardant coating or shell. Beyond the use of flame retardants additives, inorganic PCMs offer the inherent advantage of non-flammability, presenting benefits in the preparation of flame-retardant CPCMs. The following sections will detail the preparation strategies for flame-retardant CPCMs and their applications in TRP suppression.

4.1.1 Internal incorporation of flame retardants. Incorporating flame retardants directly into the CPCM matrix during preparation is a straightforward method for fabricating flame-retardant CPCMs. Weng *et al.*[112] prepared a CPCM by crosslinking octadecyl acrylate with 1,6-hexanediol diacrylate and incorporated $Al(OH)_3$ as a flame retardant during synthesis. Their study revealed that $Al(OH)_3$ undergoes endothermic decomposition at approximately 200–300 °C, effectively reduces the temperature, and generating water vapor that dilutes the concentration of combustible gases. Additionally, the resulting Al_2O_3 nanoparticles aggregate on the surface of the CPCM to form a dense protective layer, while simultaneously embedding into the pyrolytic carbon layer of the polymer to inhibit cracking, thereby blocking oxygen and heat transfer. Flame retardancy test results showed that the addition of 15 wt% $Al(OH)_3$ extended the ignition time of the CPCM by 92 s. In battery pack TR tests, the flame-retardant CPCM delayed TRP time by 85 s. $Al(OH)_3$ exhibits a relatively high decomposition temperature. In contrast, the decomposition temperature of $CH_3COONa{\cdot}3H_2O$ (100–140 °C) is lower than the TR trigger temperature, making it more suitable for suppressing TRP. Mei *et al.*[113] combined $CH_3COONa{\cdot}3H_2O$ with paraffin and demonstrated that $CH_3COONa{\cdot}3H_2O$ absorbs a substantial amount of heat through phase change and thermal decomposition, while also diluting the concentration of combustible gases by generating water vapor, thereby reducing the combustion time of paraffin by 40.5%. In TR test triggered by a heating rod, this flame-retardant CPCM extended the time for the battery to reach the TR trigger temperature by 47.1% compared to pure paraffin.

The type of flame retardants significantly influences the effectiveness of CPCMs in suppressing TRP. Dai *et al.*[105] prepared flame-retardant CPCMs by separately adding ammonium polyphosphate (APP) and a mixture of $Al(OH)_3$ and $Mg(OH)_2$ (AMTH) to a paraffin/expanded graphite composite. Their study revealed that the CPCM containing AMTH delayed the time for the battery to reach the TR trigger temperature by 385 s compared to the one containing APP, and also reduced the peak TR temperature by 400 °C. The reason lies in the fact that the char layer formed by APP decomposition inadequately encapsulates the molten liquid paraffin to isolate oxygen, whereas AMTH effectively lowers the battery temperature through endothermic decomposition. Mei *et al.*[114] compared the TR suppression effects of three flame retardants (phenoxy cyclophosphazene (TRRH), $Mg(OH)_2$, and $CH_3COONa{\cdot}3H_2O$) after being added to paraffin. Their results

showed that the addition of TRRH enhances the flame retardancy of the CPCM through free radical scavenging and the generation of non-flammable gases, extending the TR trigger time by 61.94%, but the lack of endothermic capacity results in a rapid temperature rise of the battery. In contrast, $Mg(OH)_2$ and $CH_3COONa{\cdot}3H_2O$, which undergo endothermic decomposition, were more effective in delaying temperature rise. Among them, $CH_3COONa{\cdot}3H_2O$, possessing higher latent heat, offered the best protection. The peak temperature of TR was reduced by 44.10%, and the TR trigger time was delayed by 74.77%.

Utilizing multiple flame retardants to achieve a synergistic effect can yield superior flame retardancy and TRP protection compared to using a single flame retardant. Chen *et al.*[115] prepared a CPCM of melamine-PEG borate phosphate (P-BPM)/expanded graphite/APP (Fig. 7). In vertical burning tests, the CPCM containing only MA failed to achieve a UL-94 V-0 rating, whereas the CPCM containing the composite flame retardant successfully met this standard. This improvement is attributed to the nitrogen–phosphorus synergy between MA and APP, which promoted the formation of a thick char layer on the CPCM surface, thereby enhancing flame retardancy. In a heating plate simulation of TR, compared to the CPCM containing only MA, the one with the composite flame retardant delayed the time for a simulated battery to reach a high-temperature threshold by 418 s. Shen *et al.*[116] fabricated a CPCM by compositing polyamide and epoxy resin with MOF/expanded graphite and adding a composite flame retardant of APP and expandable graphite (EGA). Their research found that the CPCM with the composite flame retardant achieved a UL-94 V-0 rating, while CPCMs with APP or EGA alone failed to reach this level. This is because at high temperatures, APP promotes

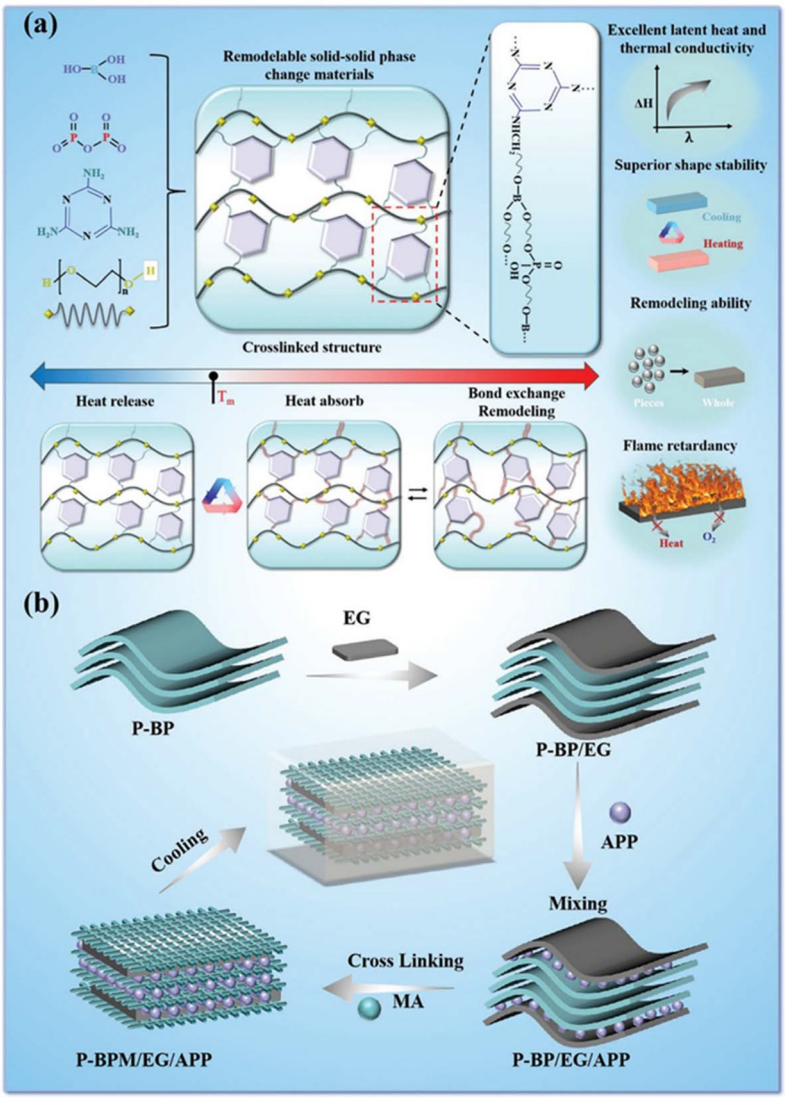

Fig. 7 (a) Synthesis and chemical structure design of P-BPM. (b) CPCM structure design. Reproduced with permission from ref. 115. Copyright 2025, John Wiley and Sons.

the dehydration and carbonization of the polyamide matrix to form a dense insulating char layer, while EGA rapidly expands to thicken the char layer, with the two acting synergistically to enhance flame retardancy. TRP test results indicated that a 10 mm thick layer of this CPCM could reduce the peak TR temperature by 60 °C and completely prevent TRP.

To achieve optimal flame retardancy, the component ratio within composite flame retardants requires optimization. Yang *et al.*[117] fabricated a flame-retardant CPCM by adding methyl phenyl silicone resin (MPS) and triphenyl phosphate (TPP) to a composite of paraffin/expanded graphite/styrene–butadiene–styrene block copolymer. Their study demonstrated that the most complete and dense char layer was formed when the mass ratio of MPS to TPP was 1 : 2, resulting in the optimal improvement in the flame retardancy of the CPCM. Heating rod simulation of TRP showed that using this composite flame retardant CPCM could prevent TRP completely. Beyond enhancing flame retardancy, combining inorganic and organic flame retardants can improve the dispersion of inorganic flame retardants within organic PCM matrices. Zhao *et al.*[118] innovatively proposed encapsulating the inorganic flame retardant AHP with the organic flame-retardant melamine cyanurate to form microcapsules. These microcapsules (AHP@MCA) were then added, along with APP, to a PEG2000/epoxy resin/expanded graphite composite to prepare a flame-retardant CPCM. The results showed that the AHP@MCA microcapsules were uniformly distributed within the CPCM without agglomeration (Fig. 8). This CPCM achieved a UL-94 V-0 rating. Heating plate simulation of TRP indicated that, compared to the CPCM without flame retardant, this flame-retardant CPCM delayed the TRP initiation time by 510 s.

Incorporating flame retardants into CPCMs effectively enhances their flame retardancy and TRP suppression performance. However, as the solid–liquid phase change cycles repeatedly, flame retardants may undergo phase separation and agglomeration, leading to a degradation in flame-retardant properties. Fixing flame retardants onto the CPCM carrier is beneficial for improving their dispersion and stability. Han *et al.*[107] chemically grafted the phosphorus-based flame retardant phenylphosphonic acid (PPA) onto triphenylmethane-4,4′,4″-triisocyanate (TTI) backbone and prepared a CPCM *via* crosslinking polymerization with PEG 6000. At high temperatures, PPA decomposes to capture free radicals in the combustion chain reaction and catalyzes the dehydration and carbonization of the polymer. Additionally, the benzene rings in PPA and TTI act synergistically to enhance the densification and stability of the char layer. CPCM with a grafted flame-retardant group content of only 5 wt% achieved a UL-94 V-2 rating and reduced the total heat transfer in the battery pack by 38.5% during TRP experiments. Huang *et al.*[108] *in situ* grew flame-retardant aluminum–magnesium layered double hydroxide (Mg/Al-LDH) on a carbon foam (CF) skeleton and subsequently adsorbed PEG 8000 to fabricate a flame-retardant CPCM (Fig. 9). Mg/Al-LDH decomposes at high temperatures to form a MgO/Al_2O_3 oxide protective layer and inert gases, effectively isolating oxygen and diluting combustible gases. Meanwhile, the carbon skeleton, which possesses good thermal stability and mechanical strength, cooperates with LDH to form a char layer, thereby delaying the combustion process. Microcalorimetry revealed that compared to pure PEG, this flame-retardant CPCM exhibited a 12.34% reduction in peak heat release rate. ARC tests demonstrated that this CPCM could extend the time for a battery to reach the TR trigger temperature by 8003 s.

4.1.2 Flame-retardant coatings or shells. When flame retardants are located within the CPCM matrix, only those exposed at the surface can fully exert their flame-retardant function, which increases the overall amount of retardant required.[119] In contrast, encapsulating the CPCM with a flame-retardant coating or shell can improve the utilization efficiency of the flame retardant and minimize its impact on properties such as latent heat. Shen *et al.*[120] prepared a flame-retardant coating by mixing epoxy resin, boron nitride, and a composite flame retardant (CFR). They applied this coating to the surface of a CPCM fabricated by melt-blending paraffin, expanded graphite, and ethylene-vinyl acetate copolymer, resulting in a sandwich-structured flame-retardant CPCM, as shown in Fig. 10. Upon exposure to flame, the coating preferentially forms a dense char layer as a protective barrier on the CPCM surface, significantly enhancing flame retardant efficiency. Compared to directly mixing the flame retardant into the CPCM, the sandwich-structured CPCM improved its flame retardancy rating from UL-94 V-1 to V-0 and increased its phase change enthalpy by 8%. In a heating rod simulation of TR, the sandwich-type CPCM delayed the time to reach the TR trigger temperature by 263 s compared to the mixed-type CPCM. Increasing the thickness of the flame-retardant coating is beneficial for enhancing flame retardancy, but it reduces the PCM content, thereby weakening the phase change heat absorption capacity. Qiu *et al.*[26] prepared a CPCM by incorporating ethylene propylene diene monomer into a paraffin/expanded graphite composite. They then coated the CPCM surface with a composite flame retardant of expanded graphite and APP using polydimethylsiloxane as a binder and investigated the effect of coating thickness. Their results indicated that when the coating thickness is 167 μm, the inability to form a continuous and dense char layer on the CPCM surface leads to flame retardancy failure. When the thickness was increased to 265 μm, the CPCM reached a UL-94 V-0 rating. Further increasing the coating thickness provided limited improvement in flame retardancy while causing a significant reduction in enthalpy. TRP tests demonstrated that this flame-retardant CPCM could maintain the temperature of cells adjacent to the TR cell below 70 °C, effectively preventing TRP.

Besides using flame-retardant coatings, methods such as *in situ* polymerization or sol–gel processes can be employed to form flame-retardant shells on the CPCM surface. Jiang *et al.*[121] used *in situ* polymerization to encapsulate a paraffin/expanded graphite CPCM with a shell of Aluminum–Phenylphosphinate (PADP), fabricating a core–shell structured flame-retardant CPCM. Their study showed that the paraffin/expanded graphite CPCM was easily ignited 6 s after exposure

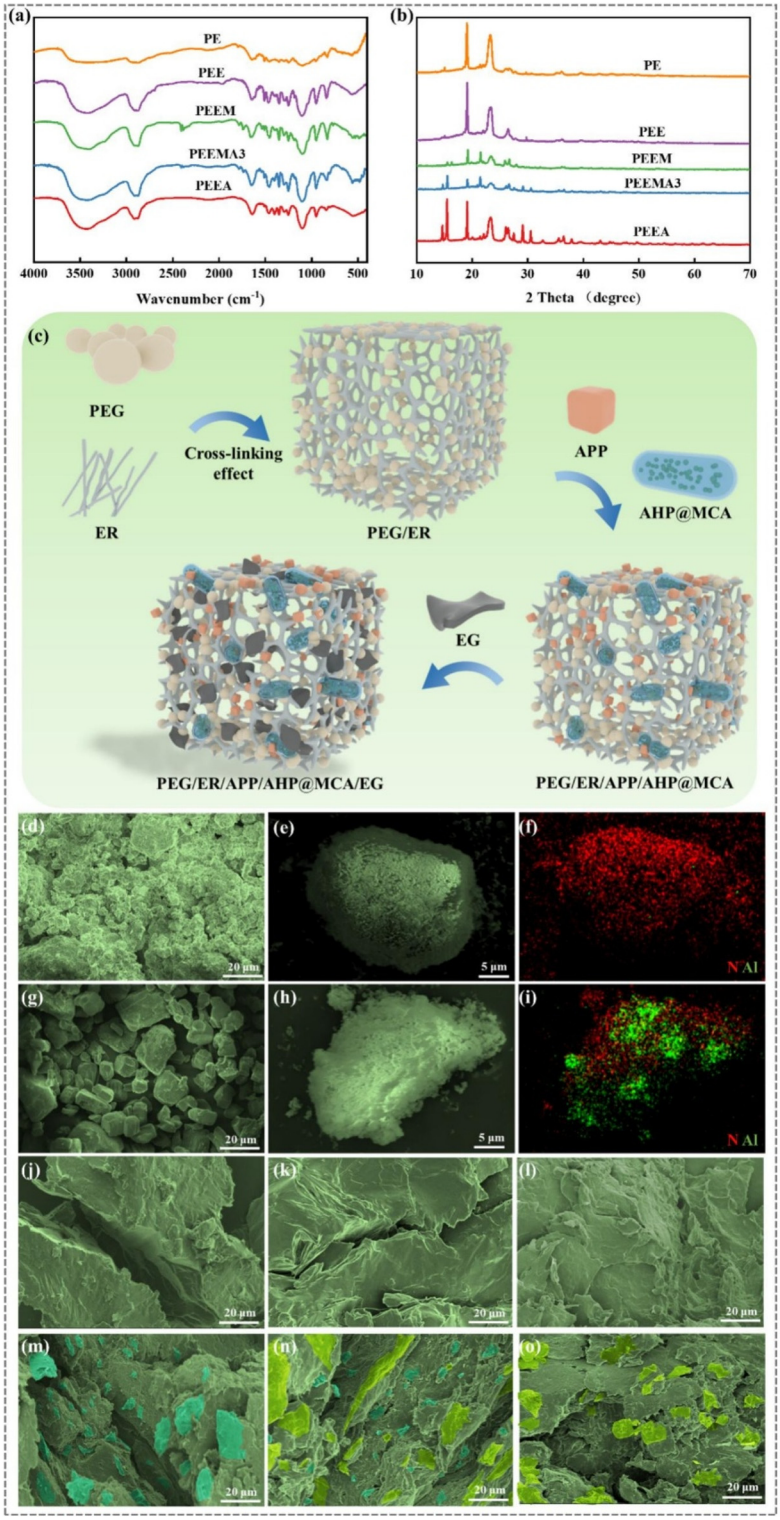

Fig. 8 (a) FT-IR spectra of CPCM, (b) XRD spectra of CPCM, (c) preparation process design of the flame retardant CPCM, and SEM images of (d) AHP, (e) AHP@MCA microcapsules, (f) EDS of AHP@MCA microcapsules, (g) APP, (h) worn-out AHP@MCA microcapsules, (i) EDS of worn-out AHP@MCA microcapsules, (j) PEG2000, (k) PE, (l) PEE, (m) PEEM, (n) PEEMA3 and (o) PEEA. Reproduced with permission from ref. 118. Copyright 2025, Elsevier.

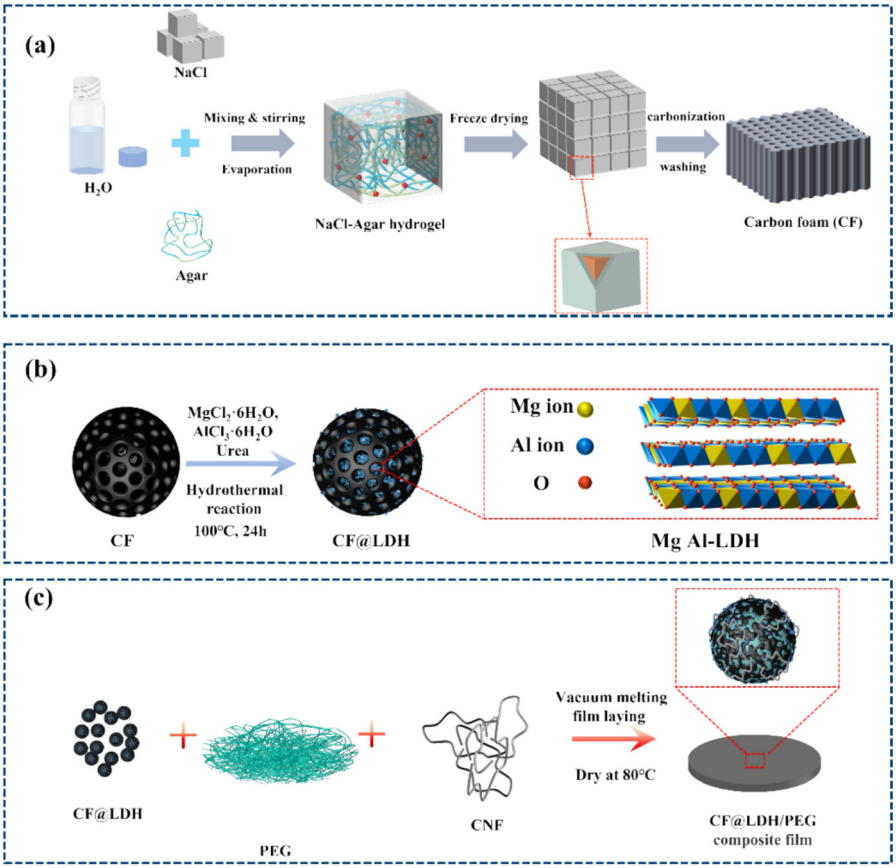

Fig. 9 Preparation processes of (a) CF, (b) CF@LDH and (c) CF@LDH/PEG composite film. Reproduced with permission from ref. 108. Copyright 2025, Elsevier.

to a flame, whereas the PADP coating can effectively form a non-flammable carbon layer on the CPCM surface, therefore the core–shell structured flame-retardant CPCM could not be ignited, indicating a significant improvement in flame retardancy. ARC test results revealed that wrapping a battery with this flame-retardant CPCM could extend the TR trigger time by 675.17 min. Liu *et al.*[122] mixed SiO_2 sol with a paraffin/expanded graphite CPCM. Utilizing the gelation of the SiO_2 sol during aging and drying, they formed a dense ceramic-like protective layer on the CPCM surface, acting as a physical barrier to block oxygen and heat. Cone calorimeter test results showed that compared to pure paraffin, this flame-retardant CPCM reduced the peak heat release rate by 86.4%. In TRP tests, using this flame-retardant CPCM to wrap batteries delayed the TRP time by 375 s.

4.1.3 Using inorganic PCMs. Inorganic PCMs possess the inherent characteristic of non-flammability, granting them an advantage over organic PCMs in the preparation of flame-retardant CPCMs. Hydrated salts are a common type of inorganic PCMs. García *et al.*[123] compared the TRP suppression effectiveness of paraffin, $CaCl_2·6H_2O$, and $Na_2HPO_4·12H_2O$. Their study found that $Na_2HPO_4·12H_2O$ and $CaCl_2·6H_2O$ could limit the maximum temperature of cells adjacent to a TR cell to 44.26 °C and 41.09 °C, respectively, effectively preventing TRP, whereas paraffin failed to do so. Despite their flame-retardant advantage, hydrated salt PCMs also suffer from drawbacks such as supercooling, phase separation, and corrosiveness. Adding nucleating agents to the CPCM is an effective method to reduce the supercooling degree of hydrated salts. Zhi *et al.*[124] prepared a CPCM by adsorbing $Na_2SO_4·10H_2O$ and $KAl(SO_4)_2·12H_2O$ onto polyurethane foam and incorporated expanded graphite as a nucleating agent. Their research showed that the expanded graphite provides nucleation sites for hydrated salts, as the content increased from 2 wt% to 6 wt%, the supercooling degree of the CPCM decreased from 0.63 °C to approximately 0 °C. The CPCM with 4 wt% expanded graphite achieved a UL-94 V-0 flame retardancy rating. In TRP tests, it could maintain the maximum temperature of adjacent cells below 151 °C, completely blocking TRP. Encapsulating hydrated salts within microcapsules can effectively enhance their thermal stability and reduce corrosiveness. Ping *et al.*[125] prepared phase change microcapsules with SiO_2 shells and $Na_2HPO_4·12H_2O$ core material. Their study found that encapsulation reduced the supercooling of the PCM from 13 °C to 8.5 °C, and the enthalpy decreased by only 4.13 kJ kg^{-1} after 15 thermal cycles. These phase change microcapsules did not ignite even after 60 s of flame exposure, and delayed the time for a battery to reach the TR trigger tempera-

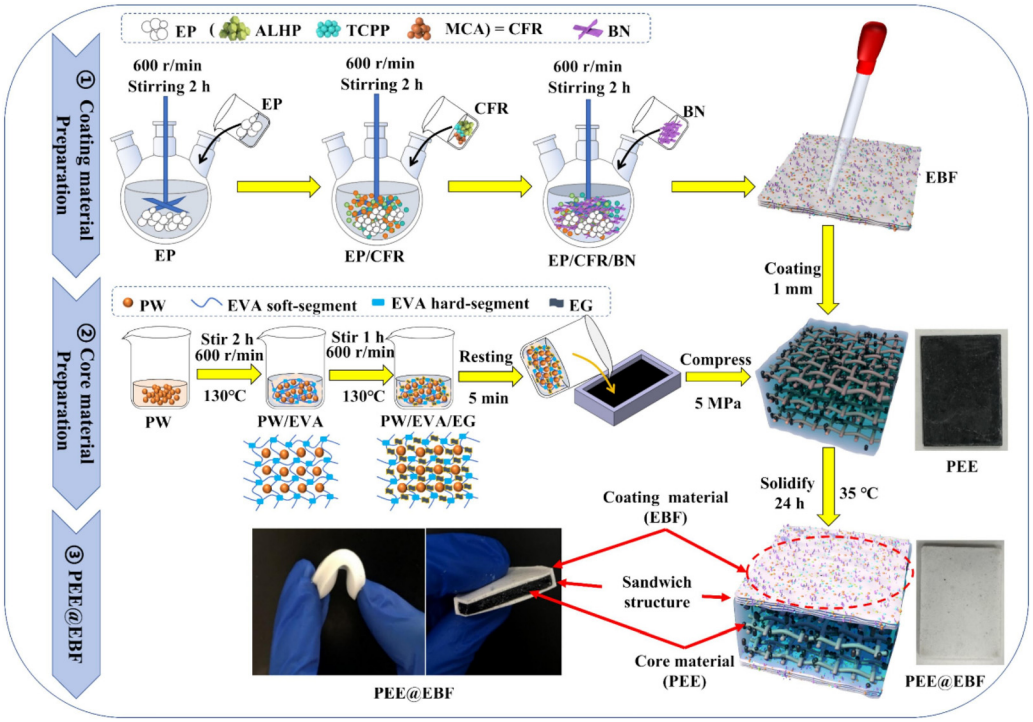

Fig. 10 Preparation process of fire-resistant flexible CPCM with sandwich structure. Reproduced with permission from ref. 120. Copyright 2025, Elsevier.

ture by 495 s. Dai *et al.*[126] prepared phase change microcapsules by encapsulating $Na_2HPO_4{\cdot}12H_2O$ with a carbon nanotube-modified SiO_2 shell and tested their TRP protection performance. The results indicated that wrapping batteries with these microcapsules could extend the TRP time by 345 s compared with the blank module.

Beyond hydrated salts, molten salts and low-melting-point alloys also show potential for TRP suppression. By adjusting their melting points with additives, molten salt PCMs suitable for TRP inhibition can be obtained. Choi *et al.*[109] adjusted the melting point of $LiNO_3$ to 142 °C using KCl, preparing a molten salt PCM with an enthalpy of 308 kJ kg^{-1}. They encapsulated it with stainless steel to form a thermal barrier. Heating tests showed that compared to a commercial aerogel of the same thickness, this barrier delayed the time for a battery to reach the TR trigger temperature by 500 s. Low-melting-point alloys offer high volumetric energy storage density and good thermal stability. Chen *et al.*[127] prepared two types of phase change microcapsules: one with a polymethyl methacrylate shell and a $Bi_{44.7}Pb_{22.6}In_{19.1}Sn_{8.3}Cd_{5.3}$ core, and another with an $Mg(OH)_2$ shell and an $SnBi_{58}$ core (Fig. 11). Their study found that the enthalpies of the two microcapsules reached 231.4 J cm^{-3} and 426.1 J cm^{-3}, respectively, which are higher than those of organic CPCMs. Microcalorimetry showed that a mixture of the two microcapsules had a total heat release of 0 kJ g^{-1}, indicating non-flammability. Heating rod simulation of TR experiments demonstrated that wrapping a simulated battery with a mixture of the two microcapsules could extend the time to reach the TR trigger temperature by 30%.

As evidenced by the studies discussed above, incorporating flame retardants into CPCMs is an effective strategy for enhancing their flame retardancy. Endothermic decomposition-type flame retardants, such as metal hydroxides, demonstrate significant effectiveness in reducing the temperature during TR. The synergistic use of multiple flame retardants yields superior flame-retardant performance in CPCMs, optimizing their composition and ratios is crucial to achieve the best results. Immobilizing flame retardants onto the CPCM carrier matrix offers greater stability, while applying flame-retardant coatings or shells improves flame retardant utilization and minimizes their adverse impact on the thermal storage properties of the CPCM. Inorganic PCMs possess the inherent advantage of non-flammability, future research efforts should prioritize encapsulation technologies to enhance their stability and mitigate their potential corrosive effects on battery components.

4.2 Thermal conductive optimized CPCMs

The thermal conductivity of CPCMs plays a critical role in the TR suppression of LIBs. Current research reveals a non-monotonic relationship between CPCM thermal conductivity and TRP suppression effectiveness: the inhibitory effect initially decreases and then increases as thermal conductivity rises from low to high values. Ma *et al.*[128] investigated the impact of the thermal conductivity of paraffin/expanded graphite CPCMs on TRP prevention through numerical simulation. Their study indicates that low thermal conductivity helps delay heat transfer to adjacent cells, while high thermal conductivity accelerates heat absorption by the CPCM and facilitates rapid heat

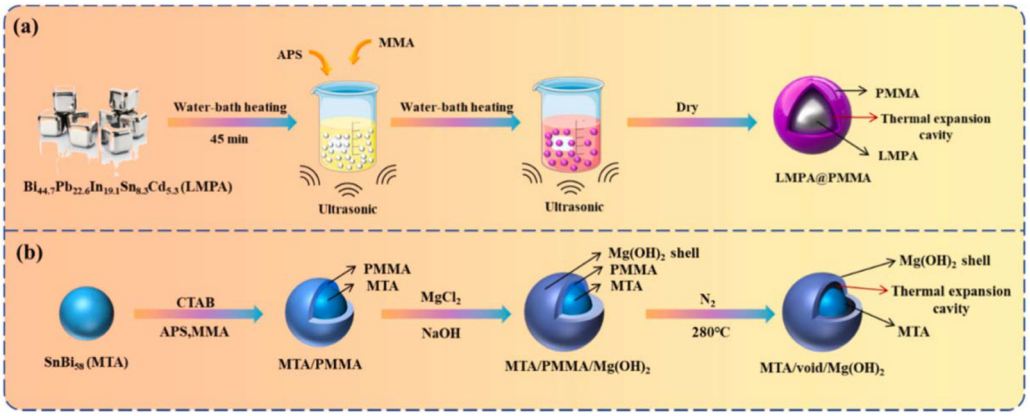

Fig. 11 Synthetic processes of MEPCMs: (a) LMPA@PMMA; (b) MTA@void@$Mg(OH)_2$. Reproduced with permission from ref. 127. Copyright 2025, Elsevier.

dissipation, thereby avoiding the formation of local hot spots. When the thermal conductivity of the CPCM is below 3.49 W m^{-1} K^{-1}, reducing the thermal conductivity contributes to enhancing the TRP suppression performance. Conversely, when it exceeds this value, priority should be given to increasing the thermal conductivity of the CPCM, as illustrated in Fig. 12. Accordingly, both reducing CPCM thermal conductivity to strengthen insulation and increasing it to accelerate heat absorption and temperature homogenization hold promise for improving TRP suppression performance. The following subsections will separately introduce the preparation of low and high thermal conductivity CPCMs and their applications in TRP suppression.

4.2.1 Low thermal conductivity CPCMs. Low thermal conductivity CPCMs suppress TRP by reducing heat transfer from a TR cell to its neighbors. A common method for preparing such CPCMs is compositing PCMs with thermal insulation materials. Aerogel is a common thermal insulation material with an extremely high porosity (over 90%), achieving a thermal conductivity as low as 0.02 W m^{-1} K^{-1}. Liu *et al.*[129] compared the TRP suppression effectiveness of pure paraffin and a paraffin-aerogel composite. Their results showed that using a composite of 3.6 mm paraffin plus 1 mm aerogel delayed the TRP time to 798 s, which is 384 s longer than that of 5.4 mm of pure paraffin. Glass fiber not only possesses high thermal resistance, but also exhibits higher mechanical properties compared to aerogel. Li *et al.*[130] prepared composite sheets by compounding paraffin with glass fiber cloth and vacuum-sealing with aluminum–plastic film. The glass fiber cloth effectively insulates against heat transfer, while vacuum-sealing further reduces the overall thermal conductivity by suppressing gas convection and thermal conduction. Their research showed that the in-plane thermal conductivity of this composite sheet was only 0.178–0.232 W m^{-1} K^{-1}, representing a 42% reduction compared to pure paraffin. TRP test results indicated that compared to aerogel, the composite sheet could reduce the peak temperature of adjacent cells by 77.5 °C and completely prevent TRP. Current research finds that the ratio of the thermal conductivities of the PCM and thermal insulation material influences the TRP suppression performance of the composite. Wu *et al.*[106] designed a three-layer PCM–FR–PCM composite structure using lauric acid as the PCM and aerogel as the flame-retardant (FR) insulation material. They investigated the effect of the PCM-to-FR thermal conductivity ratio (k_{PCM}/k_{FR}) on TRP suppression. Their study found that the optimal TRP inhibition was achieved when k_{PCM}/k_{FR} was in the range of 0.5–1. A ratio that is too high means the FR's insulation is insufficient to prevent heat penetration, while a ratio that is too low prevents the PCM from absorbing heat promptly. Optimizing the structure of the insulation–material–PCM composite can further enhance the thermal insulation performance of CPCMs. Huo *et al.*[131] fabricated CPCM by incorporating glass fibers into paraffin, and systematically investigated the effects of fiber orientation (including random, horizontal, and vertical

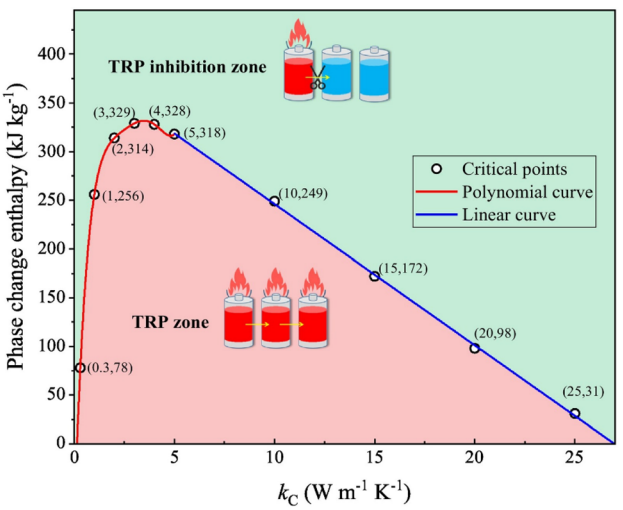

Fig. 12 Critical distribution of k_C and $H_{C,m}$ for preventing TRP. Reproduced with permission from ref. 128. Copyright 2023, Elsevier.

arrangements) on the thermal conductivity. The results indicate that in the horizontal arrangement, heat flow is transmitted along the axial direction of the glass fibers, resulting in the highest thermal conductivity. Random and vertical arrangements are more effective in reducing thermal conductivity, as shown in Fig. 13. When arranged vertically with a glass fiber content of 60%, the thermal conductivity of the CPCM is reduced by 32% compared to that of pure paraffin. TRP simulation results indicated that the CPCM delayed the TRP time by 100 s compared to pure paraffin.

While low thermal conductivity CPCMs aid in suppressing TRP, they are disadvantageous for battery heat dissipation, thereby increasing the risk of TR occurrence. To overcome this contradiction, Chakraborty *et al.*[132] prepared a CPCM with anisotropic thermal conductivity by adsorbing paraffin onto expanded graphite and incorporating air gaps and thin copper foil to block out-of-plane heat transfer and enhance in-plane heat transfer, respectively. Their study showed that this CPCM achieved an in-plane thermal conductivity as high as 32.7 W m^{-1} K^{-1}, enabling efficient lateral heat dissipation. Conversely, its out-of-plane thermal conductivity was as low as 0.5 W m^{-1} K^{-1}, effectively blocking longitudinal heat transfer to adjacent cells. TRP simulation results indicated that this CPCM could maintain the maximum temperature of all cells except the TR cell below 200 °C. Li *et al.*[133] compounded paraffin with an MXene-enhanced melamine formaldehyde (MF) porous matrix to prepare a CPCM with thermally triggered tunable thermal conductivity (Fig. 14). Their research demonstrated that at room temperature, the MXene formed a highly thermal conductive network, enabling rapid heat dissipation. At elevated temperatures, MXene pyrolyzed to form low thermal conductivity TiO_2, causing the thermal conductivity of the CPCM to decrease significantly by 66.1%. TRP experimental results showed that wrapping batteries with this CPCM could delay the TRP time by 857 s.

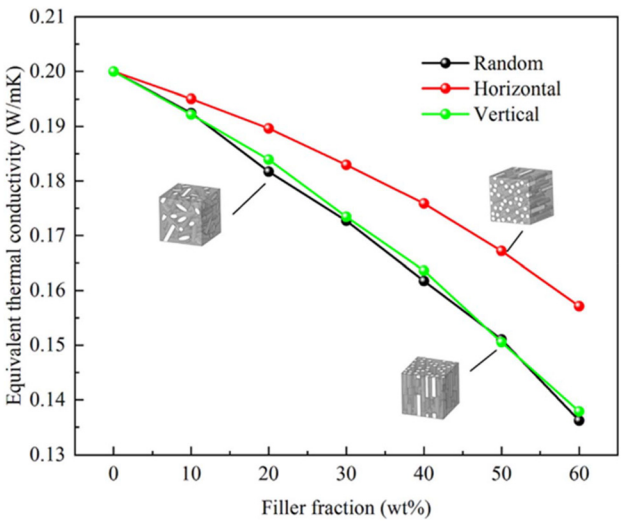

Fig. 13 The influence of glass fiber mass fraction on the thermal conductivity of composites. Reproduced with permission from ref. 131. Copyright 2023, John Wiley and Sons.

4.2.2 High thermal conductivity CPCMs. Improving the thermal conductivity of CPCMs accelerates the transfer of heat generated by a TR cell into the PCM, thereby enhancing the heat absorption and cooling effect. Ni *et al.*[134] investigated the impact of increasing paraffin thermal conductivity on TR protection through numerical simulation. Their study found that as the thermal conductivity increased from 0.28 W m^{-1} K^{-1} to 12 W m^{-1} K^{-1}, the peak TR temperature decreased from 704.26 K to 417.49 K. However, as the heat absorption capacity of the PCM reached saturation, further increasing thermal conductivity yielded only marginal additional cooling benefits. Compositing PCMs with highly thermally conductive materials can effectively enhance their thermal conductivity. Carbon nanotubes (CNTs) possess extremely high thermal conductivity, with axial thermal conductivity exceeding 3000 W m^{-1} K^{-1}.[135] Yang *et al.*[136] constructed a 3D porous aerogel skeleton (MCPC) *via* directional freeze-drying of a mixture of chitosan quaternary ammonium salt (CQS), polyethyleneimine (PEI), CNTs, and MXene, then adsorbed PEG to form a CPCM. CNTs connect the MXene sheets to construct a three-dimensional continuous thermal conductive network, enabling efficient

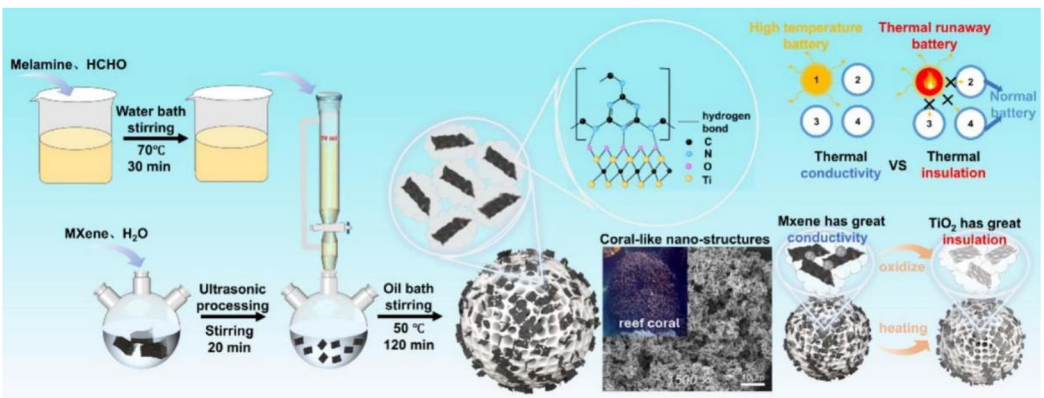

Fig. 14 Conceptual design, preparation process, and fabrication schematic of melamine formaldehyde resin/MXene porous adsorption matrix (MF@MXene). Reproduced with permission from ref. 133. Copyright 2025, Elsevier.

heat transfer. Their research showed that compounding with the MCPC increased the thermal conductivity of PEG by 156%. ARC tests indicated that wrapping batteries with this CPCM delayed the TR trigger time by 40 077 s. Expanded graphite offers not only high thermal conductivity but also the advantage of high porosity.[137] Talele *et al.*[138] studied the effect of compounding paraffin with expanded graphite on its thermal conductivity and TR suppression performance. Their research showed that as the expanded graphite content increased from 3 wt% to 30 wt%, the CPCM's thermal conductivity increased from 0.58 W m^{-1} K^{-1} to 13.85 W m^{-1} K^{-1}. Numerical simulation results demonstrated that increasing the expanded graphite content delayed the time for the battery to reach the TR trigger temperature. At 30 wt% expanded graphite, the CPCM delayed the TR trigger time for LFP and NMC batteries by 1208 s and 1135 s, respectively. Beyond carbon-based materials, metallic materials are also widely used to enhance CPCM thermal conductivity. Weng *et al.*[139] compounded paraffin with aluminum honeycomb (AH) and investigated its TRP suppression effect. Test results showed that wrapping a battery pack with paraffin alone could not prevent TRP, whereas the high thermal conductivity AH promotes heat dissipation, compounding paraffin with AH can maintained the temperature of adjacent cells below 90.9 °C, completely preventing TRP. To accelerate heat transfer throughout the entire battery module, Wu *et al.*[140] compounded paraffin with expanded graphite and attached pyrolytic graphite sheets (PGS) to the module sides to construct a secondary heat transfer network (Fig. 15). TRP simulation results showed that employing PGS could reduce the required volume of CPCM for TRP suppression by 71.4%.

While high-thermal-conductivity CPCMs accelerate heat absorption, if their thermal storage capacity is insufficient to absorb the heat generated during TR, the high conductivity may instead increase the risk of TRP. Wang *et al.*[141] compared the TRP protection effectiveness of pure paraffin and a paraffin/graphene CPCM. Their results showed that although graphene-enhanced thermal conductivity delayed the TR trigger time of the initiating cell by 141 s, it shortened the overall TRP time by 142 s. Combining high thermal conductivity CPCMs with thermal insulation materials can achieve a synergy of rapid heat absorption and thermal blocking, potentially further enhancing TRP suppression. Chen *et al.*[142] prepared a CPCM by compounding paraffin with expanded graphite. They employed an intumescent flame retardant (IFR) and silicon carbide (SiC) to improve its flame retardancy and thermal conductivity, respectively, and combined it with aerogel. Their study demonstrated that SiC particles form a secondary heat transfer network within the CPCM, while the close contact between PA and SiC particles achieved through high-temperature melt blending reduces interfacial thermal resistance. The addition of 10 wt% SiC increases the thermal conductivity of the CPCM by 76.7%. Aerogel, serving as a thermal insulation layer, is inserted between CPCM layers to block heat transfer to adjacent cells. TRP test results indicated that combining the CPCM with aerogel delayed the TRP time by 649 s compared to using the CPCM alone. Boron nitride (BN) not only possesses high thermal conductivity but can also reduce thermal radiation generated during TR through reflection, thereby achieving an insulating effect. Chen *et al.*[143] compared the TRP suppression effectiveness of paraffin/silicone CPCMs separately added with SiC and BN (Fig. 16). Their research showed that although both BN and SiC can construct efficient thermally conductive networks within the CPCM, increasing the thermal conductivity by 266% and 241%, respectively, BN possesses a unique thermal radiation shielding capability—achieving an average reflectance of 88.95% at the wavelength of 2.53 μm (corresponding to the thermal runaway flame temperature of 700–900 °C), which enables significant reflection of thermal radiation from the surface of high-temperature TR batteries. TRP experimental results indicated that the CPCM with added SiC delayed the TRP time by 650 s, while the CPCM with added BN could completely prevent TRP.

In summary, high thermal conductivity CPCMs impose high requirements on heat storage capacity, making them more suitable for small capacity LIBs with relatively low TR heat generation. Low thermal conductivity CPCMs, on the other hand, combine heat absorption and insulation capabilities, providing a solution for suppressing TRP in large capacity LIBs. However, it is essential to ensure that low thermal conductivity materials do not adversely affect battery heat dissipation. The future research focus lies in the synergistic use and structural optimization of high and low thermal conductivity materials within CPCMs, as well as functional designs featuring tunable thermal conductivity, to achieve a balance between heat insulation, rapid heat absorption, and efficient heat dissipation.

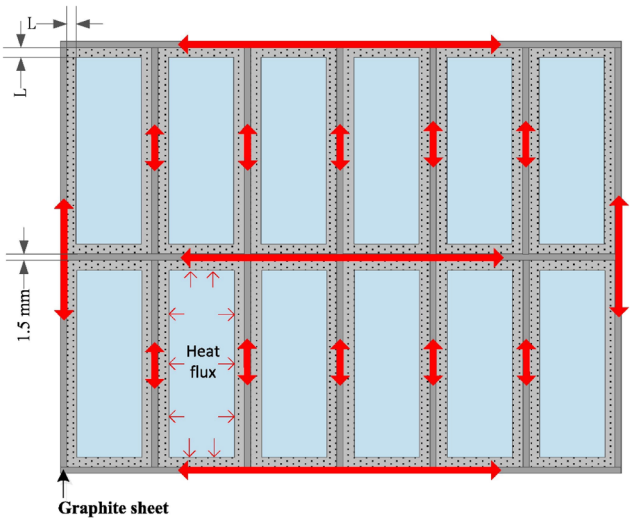

Fig. 15 New design of the battery module (PCM/PGS module). Reproduced with permission from ref. 140. Copyright 2017, Elsevier.

4.3 Flexible CPCMs

The substantial heat and gas generated during TR can cause volumetric expansion of LIBs, exerting compressive stress on protective materials.[144] Employing flexible CPCMs can not

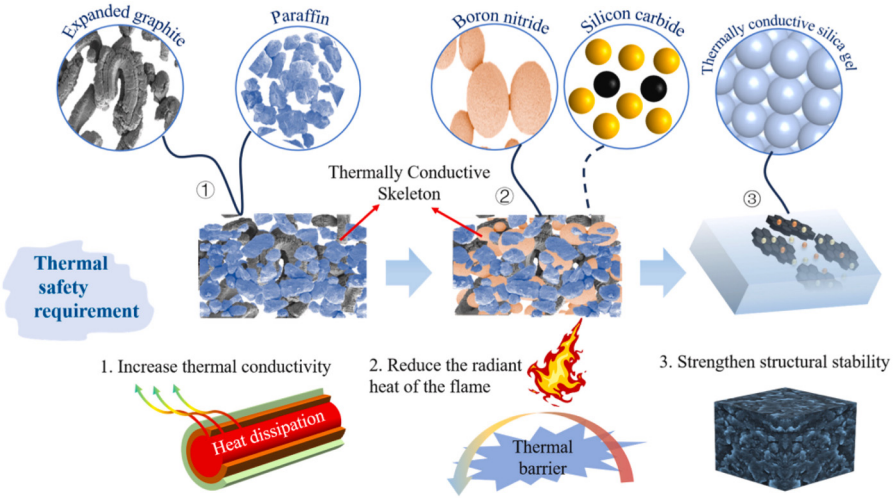

Fig. 16 Material design conception. Reproduced with permission from ref. 143. Copyright 2025, Elsevier.

only prevent fracturing under this expansion-induced pressure but also reduce interfacial thermal resistance by conforming closely to the battery surface.[145] To enhance CPCM flexibility, researchers have incorporated flexible materials into their matrices. Polymer skeleton materials are widely used in the preparation of flexible CPCMs due to their excellent flexibility and structural tunability. Wu *et al.*[146] prepared a CPCM using octadecyl acrylate (OA) as a polymeric skeleton to chemically crosslink and immobilize paraffin, with the addition of expanded graphite and an intumescent flame retardant (IFR). Their study showed that the CPCM transformed into a gel-like state after paraffin phase change, effectively filling interfacial gaps and reducing contact thermal resistance by 23.6%. TRP simulation results indicated that using this flexible CPCM could maintain the temperature of simulated cells adjacent to the TR cell below 150 °C, completely preventing TRP. Zhao *et al.*[147] compounded paraffin with styrene–ethylene/propylene–styrene block copolymer (SEPS) as a flexible material, along with expanded graphite and a flame retardant. SEPS consists of soft and hard segments. When paraffin wax melts, the soft segments are released, rendering the CPCM flexible and enabling it to fold, stretch, and twist (Fig. 17). Simulated TR experiments showed that this flexible CPCM delayed the TR trigger time of a simulated battery by 84 s. Huang *et al.*[148] prepared a flexible CPCM by compounding paraffin with styrene–butadiene–styrene block copolymer (SBS) and adding a flame retardant and expanded graphite. Simulated TRP experiment results demonstrated that this CPCM could control the temperature of simulated cells adjacent to the TR cell below 100 °C, effectively suppressing TRP.

Although the introduction of flexible polymers enhances the flexibility of CPCM, it also increases its flammability, often necessitating the addition of flame retardants. However, the incorporation of flame retardants may adversely affect the flexibility of CPCM. To balance both flexibility and flame retardancy, Liu *et al.*[149] developed a flexible flame-retardant coating

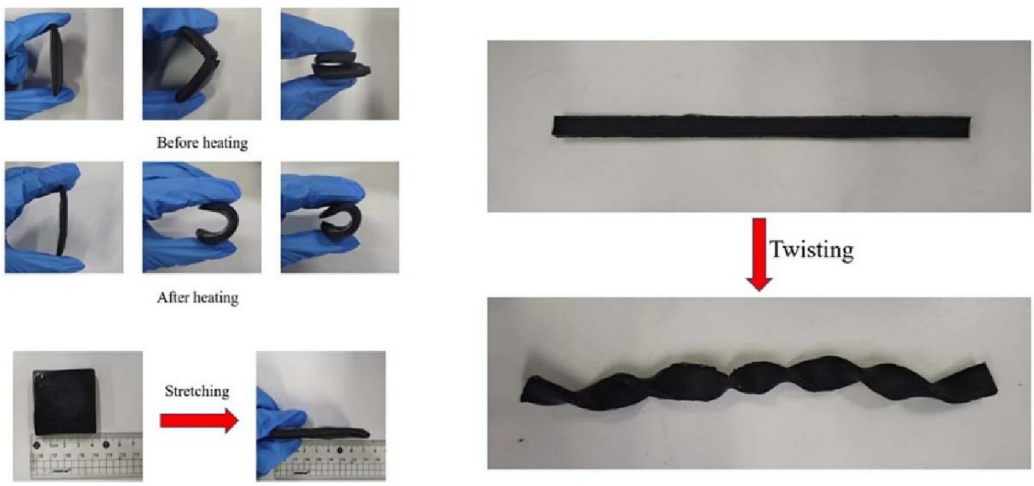

Fig. 17 Thermal-induced flexibility experimental results. Reproduced with permission from ref. 147. Copyright 2024, Elsevier.

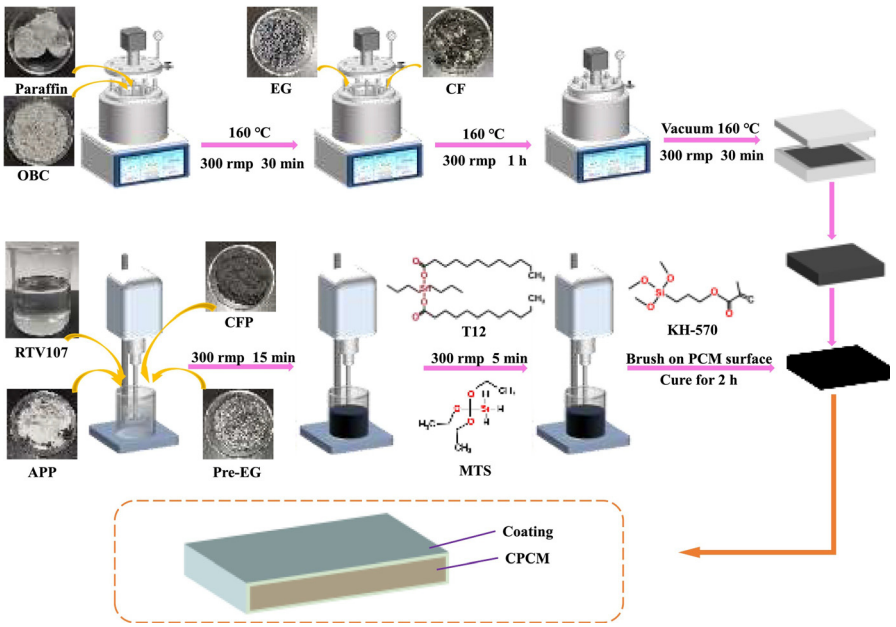

Fig. 18 Preparation of flame-retardant form-stable CPCM. Reproduced with permission from ref. 149. Copyright 2023, Elsevier.

by compounding a flame retardant with room-temperature vulcanized silicone rubber RTV 107. They applied this coating to the surface of a flexible CPCM prepared by compounding paraffin, olefin block copolymer (OBC), expanded graphite, and carbon fiber (Fig. 18). Their study found that the CPCM with flame retardant added *via* direct mixing suffered reduced flexibility and fractured upon bending. In contrast, applying the flexible flame-retardant coating had minimal impact on the CPCM's flexibility. Heating rod simulation of TR experiments indicated that this flexible CPCM maintained shape stability at high temperatures and could adequately envelop the heat source to suppress outward heat transfer. In summary, preparing flexible CPCMs by incorporating flexible polymeric materials helps them withstand the expansion pressure from TR cells and reduces interfacial thermal resistance. Using flexible flame-retardant coatings allows for the integration of flame-retardant functionality without compromising flexibility.

Overall, for CPCMs aimed at suppressing TRP, flame retardancy is a fundamental requirement, thermal conductivity regulation is key to enhancing TRP protection performance, and flexibility addresses engineering compatibility needs. However, the optimization of various performance aspects is not mutually independent; rather, inherent trade-offs exist among them. The incorporation of flexible polymers significantly enhances the flexibility of CPCMs; however, their inherent flammability necessitates the addition of flame retardants. For instance, the flexible CPCM developed by Wu *et al.*[146] required at least 20 wt% flame retardants to achieve a UL-94 V-0 rating, illustrating the trade-off between flame retardancy and flexibility. Flame retardants significantly improve the flame retardancy of CPCMs, but excessive addition can hinder polymer chain movement, thereby reducing flexibility. High-thermal-conductivity fillers, such as carbon materials, often exhibit rigid characteristics, while thermally insulating materials like aerogels tend to be brittle; both can adversely affect CPCM flexibility. Current research has developed various strategies to mitigate these contradictions. One approach is to reduce the content of components that compromise flexibility, for instance, by grafting flame retardants onto the CPCM carrier skeleton to achieve uniform dispersion and enhance flame retardant efficiency. Han *et al.*[107] chemically grafted flame-retardant groups onto the supporting skeleton, achieving comparable flame retardancy with only 5 wt% grafting loading—significantly lower than the 15–30 wt% required for directly added flame retardants. Additionally, structural design approaches have been employed to separate conflicting functions into different regions of the CPCM. For example, Qiu *et al.*[26] applied a flexible flame-retardant coating, which increased the tensile strength of the CPCM by 19.86%, demonstrating the effectiveness of surface coating in balancing mechanical and flame-retardant properties. Future research may further explore the integration of multifunctional features, such as developing flexible flame-retardant coatings with thermal conductivity or thermal insulation capabilities, to achieve a more optimal balance of properties.

5. Application of novel thermal storage materials in suppressing TRP

5.1 Hydrogels for TRP suppression

The enthalpy of traditional solid–liquid PCMs is relatively low (<300 kJ kg^{-1}), which remains insufficient for addressing TRP in high-capacity LIBs. Hydrogels utilize their hydrophilic polymer networks to absorb a large amount of water, which evaporates at 100 °C to absorb heat with an enthalpy of up to

2500 kJ kg^{-1}.[94] Additionally, the generated water vapor can dilute flammable gases, providing flame retardancy. Therefore, researchers have attempted to apply hydrogels for suppressing battery TRP. Zhao *et al.*[150] prepared a sodium polyacrylate hydrogel film and compared the TR protection effectiveness of the hydrogel and paraffin. Their study showed that after nail penetration, the battery wrapped with paraffin underwent TR with a surface temperature exceeding 450 °C, while the hydrogel-wrapped battery did not. The team further tested the hydrogel's effectiveness in suppressing TRP in a battery pack.[151] The results demonstrated that the hydrogel could maintain the temperature of all cells outside the TR cell below 100 °C, successfully preventing TRP. Sun *et al.*[25] proposed a novel thermal structure design composed of a copper structure and hydrogel and investigated its TRP suppression effect *via* numerical simulation. The results indicated that the high thermal conductivity of copper promoted heat absorption by the hydrogel, enabling complete prevention of TRP.

Although hydrogels possess excellent heat absorption and cooling capabilities, their low mechanical strength makes them ill-suited to withstand the expansion and pressure from LIBs during TR. To address this, researchers have attempted to reinforce hydrogels with skeletal materials to enhance their mechanical properties. Zhou *et al.*[152] compounded hydrogel with neopentyl glycol (NPG) and montmorillonite (MMT) to improve mechanical performance (Fig. 19). Their study found that adding NPG and MMT increased the hydrogel's maximum compressive strength from 15.58 MPa to 42.87 MPa. TRP experimental results showed that a 4 mm thick composite hydrogel could extend the TRP time by 820 s. Using thermal insulation materials as a supporting skeleton for hydrogels not only enhances mechanical properties but also allows the skeleton to continue providing heat insulation after the hydrogel thermally decomposes. SiO_2 is characterized by robustness and high-temperature resistance. Furthermore, the surface silanol groups on SiO_2 can form hydrogen bonds with hydrogel polymer chains, enhancing structural stability. Hong *et al.*[28] added 500 wt% nano-SiO_2 to a polyacrylamide hydrogel. Their research found that adding nano-SiO_2 dramatically increased the hydrogel's compressive strength by 645 times. At high temperatures, the composite hydrogel decomposes to form a hierarchical micro/nano porous structure, achieving a thermal conductivity as low as 0.104 W m^{-1} K^{-1}. TRP experiments demonstrated that this composite hydrogel could completely prevent TRP. Li *et al.*[153] prepared a ZrO_2–SiO_2 nanobelt sponge and compounded it with hydrogel. This composite hydrogel exhibited good self-healing properties, rapidly recovering within seconds after damage. At 200 °C, the thermal conductivity of this composite hydrogel was only 0.042 W m^{-1} K^{-1}, indicating good insulation performance. Moreover, this composite hydrogel successfully prevented TRP in nail penetration-triggered TRP experiments, and delayed the TRP time by 316.7 s compared with control modules in thermally triggered TRP experiments. Mineral fibers represent a class of environmentally friendly and low-cost thermal insulation materials. Bausch *et al.*[154] used alkali silicate wool (Superwool 607™) to enhance the mechanical properties of hydrogel. Their results showed that the composite hydrogel achieved a maximum compressive strength of 2.00 MPa and, after thermal decomposition, a thermal conductivity of only 0.031 W m^{-1} K^{-1}. In TRP tests, placing a 2 mm thick layer of this composite hydrogel between cells completely prevented TRP.

To further enhance the TRP suppression performance of hydrogels, researchers have incorporated flame retardants into structurally reinforced hydrogels. Zhou *et al.*[155] compounded glass fiber (GF) with hydrogel and added nano-hydroxyapatite (HAP) as a flame retardant. Their study found that the addition of HAP improved the flame retardancy of the composite hydrogel, reducing the peak heat release rate by 51.17% in cone calorimeter tests. TRP experiments demonstrated that when the heat source was located at the corner, side, and center of the battery pack, a 4 mm thick hydrogel layer could delay TRP

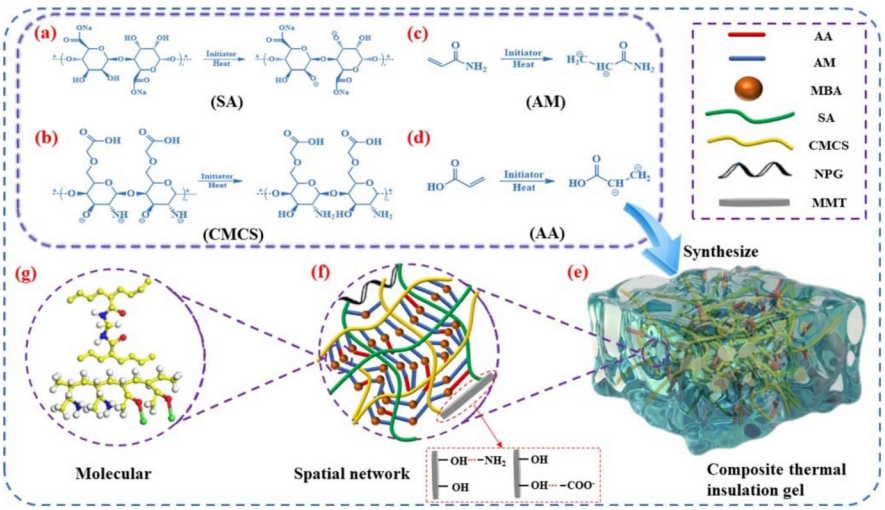

Fig. 19 Synthesis mechanism of thermal insulation hydrogel. Reproduced with permission from ref. 152. Copyright 2024, Elsevier.

by 1442 s, 1319 s, and 1405 s, respectively. Chen *et al.*[156] used ceramic fiber paper (CFP) as a supporting skeleton for the hydrogel and added $Al(OH)_3$ and NH_4HCO_3 as flame retardants, the principle and preparation process are illustrated in Fig. 20. Their research showed that at high temperatures, $Al(OH)_3$ decomposed to form an Al_2O_3 insulation layer and promoted char formation in the hydrogel matrix, in synergy with CFP, the thermal conductivity could be reduced to 0.04 W m^{-1} K^{-1}. NH_4HCO_3 undergoes thermal decomposition at 90 °C, producing non-flammable gases such as NH_3 and CO_2, which dilute the flammable gases generated during TR. Sealed chamber TRP test results indicated that this composite hydrogel could completely prevent TRP, and the lower explosive limit of the gases released during TR was increased by 44%.

Despite the advantages of high enthalpy and flexibility, hydrogels suffer from water evaporation during long-term operation. To address this issue, researchers have developed strategies such as incorporating humectants to enhance their stability. For example, Kang *et al.*[157] introduced glycerol into the hydrogel, which formed hydrogen bonds with water molecules and the hydrophilic groups of the hydrogel, effectively immobilizing the water. The resulting hydrogel exhibited a mass loss of only 0.3% after one week of storage. However, systematic cycling tests under realistic battery operating conditions (*e.g.*, temperature fluctuations and mechanical vibration) remain limited.

In summary, hydrogels leverage the high enthalpy of water evaporation to achieve powerful battery cooling. Their inherent weakness of low mechanical strength is effectively overcome by compounding them with high-strength skeletal materials. Combining hydrogels with thermal insulation materials and flame retardants to achieve synergistic protection mechanisms integrating thermal insulation and flame retardancy represents an important research direction. However, the practical application of hydrogels in battery systems still faces certain obstacles, including the risk of short circuits due to the presence of water, loss of water content over prolonged use due to evaporation, and loss of flexibility caused by freezing under low-temperature conditions. Future research should focus on enhancing the compatibility of hydrogels with battery systems, such as developing insulating encapsulation materials to improve their insulation properties and long-term stability, as well as incorporating antifreeze agents to extend their operational temperature range.

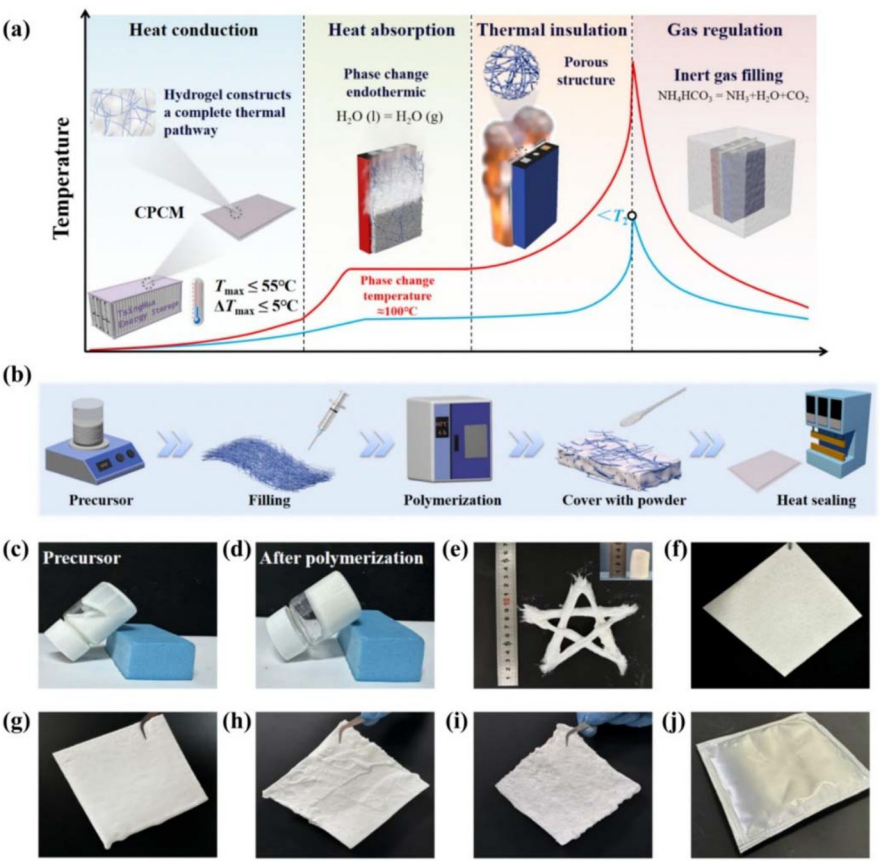

Fig. 20 (a) The function of MFS. (b) MFS preparation process diagram. (c) Physical image of precursors and (d) PSA10. (e) PSA10 exhibits excellent extensibility. (f) Physical image of CFP. (g) CFP infiltrated with precursor. (h) Polymerization of precursor occurs inside CFP. (i) NH_4HCO_3 are uniformly adhered to the surface of PSA10. (j) Appearance of MFS*x* (*x* = 0, 5, 10, 15). Reproduced with permission from ref. 156. Copyright 2025, Elsevier.

5.2 TCMs for TRP suppression

TCMs utilize reversible chemical reactions for thermal energy storage and release, offering ultra-high enthalpy (exceeding 1000 kJ kg^{-1}), an order of magnitude greater than traditional solid–liquid PCMs. In recent years, researchers have begun to explore the use of TCMs that undergo endothermic decomposition near the TR trigger temperature (100–150 °C) to absorb the substantial heat generated during TR. Liu *et al.*[24] prepared a composite TCM material by compounding TCM115 with UV-curable resin (UVCR). Their research showed that this composite undergoes thermal decomposition at 123.2 °C, possessing an ultra-high enthalpy of 1381 kJ kg^{-1}. TRP tests indicated that the composite could maintain the temperature of cells adjacent to a TR cell below 153 °C, successfully preventing TRP, and its protective effectiveness surpassed that of aerogel as illustrated by the results in Fig. 21.

Hydrated salt PCMs are capable of absorbing heat not only through solid–liquid phase transition but also *via* thermochemical energy storage. The crystalline water in hydrated salts is coordinated with metal ions through coordination bonds and interacts with anions and adjacent water molecules *via* hydrogen bonding. At elevated temperatures (typically 100–140 °C), these bonds break, and water molecules are released as vapor, absorbing a substantial amount of reaction heat.[158] Cao *et al.*[110] prepared a CPCM by compounding $CH_3COONa{\cdot}3H_2O$ with expanded graphite and investigated its TRP suppression performance *via* numerical simulation. Their study found that $CH_3COONa{\cdot}3H_2O$ undergoes phase change at 58 °C and thermal decomposition between 106–140 °C. The heat storage process is illustrated in Fig. 22. This CPCM achieved a total enthalpy as high as 793.4 J g^{-1}, enabling effective TRP prevention. To further optimize performance, Lin *et al.*[103] added urea to $CH_3COONa{\cdot}3H_2O$ to lower its thermal

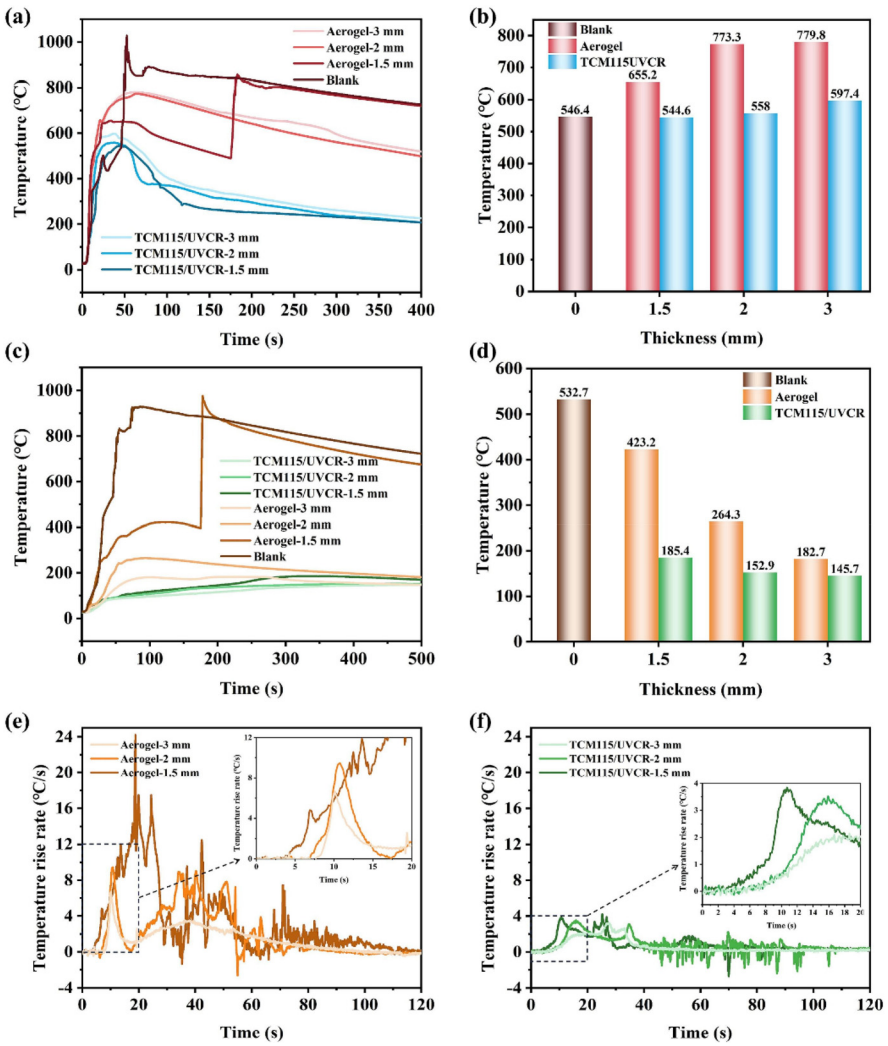

Fig. 21 (a) Temperature variation and (b) comparison of the maximum temperature of TR batteries with different protection materials; (c) temperature variation and (d) comparison of the maximum temperature of adjacent batteries with different protection materials; temperature rise rate of adjacent batteries with different thickness of (e) aerogel and (f) TCM115/UVCR protected. Reproduced with permission from ref. 24. Copyright 2026, Elsevier.

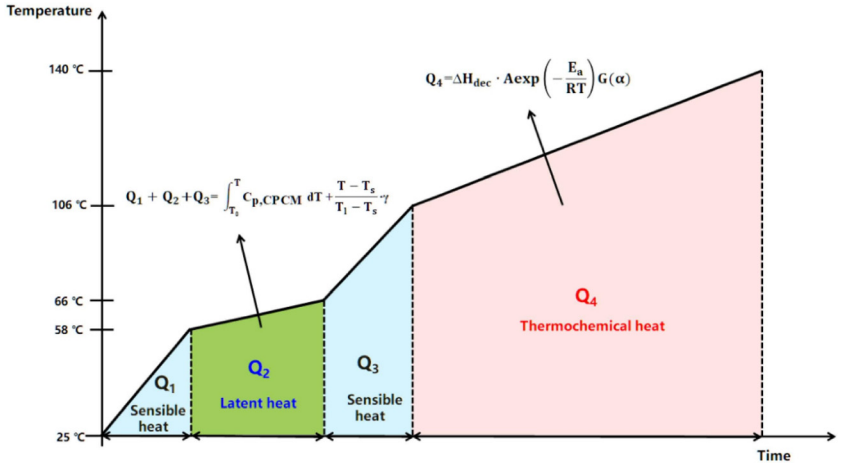

Fig. 22 Schematic of the heat storage process of sodium acetate trihydrate/expanded graphite (SAT/EG). Reproduced with permission from ref. 110. Copyright 2022, Elsevier.

decomposition temperature and compounded it with expanded graphite to prepare a CPCM. This CPCM exhibits phase change at 50.3 °C and thermal decomposition at 114.0 °C, with a total enthalpy of approximately 1000 kJ kg^{-1}. Numerical simulation of TRP demonstrated that using this CPCM successfully prevented TRP, whereas a paraffin/expanded graphite CPCM failed to do so. Zhou *et al.*[29] prepared a CPCM with an enthalpy of 1276 J g^{-1} by compounding a hydrated salt with higher decomposition enthalpy (TCM40) with expanded graphite. Experiments showed that this CPCM could maintain the temperature of all cells except the TR-initiating cell below 95 °C, effectively preventing TRP (Fig. 23), while both aerogel and paraffin/expanded graphite CPCMs failed. The team further investigated the influence of different thermal conductivities (0.50–24.57 W m^{-1} K^{-1}) on the TRP suppression effectiveness of the TCM40/expanded graphite CPCM through numerical simulation.[159] Their study revealed that due to the high-enthalpy CPCM's capacity to sufficiently absorb the heat generated during TR, thermal conductivity had a relatively minor impact on TRP suppression efficacy. With a cell spacing greater than 2 mm, the CPCM effectively prevented TRP regardless of its thermal conductivity level.

Although expanded graphite offers good thermal conductivity and high porosity, its surface is hydrophobic, resulting in poor compatibility with hydrophilic hydrated salts. To enhance the adsorption of hydrated salts onto expanded graphite, Wang *et al.*[160] coated the surface of expanded graphite with $Mg(OH)_2$ and then adsorbed $Na_2HPO_4{\cdot}12H_2O$ to prepare a

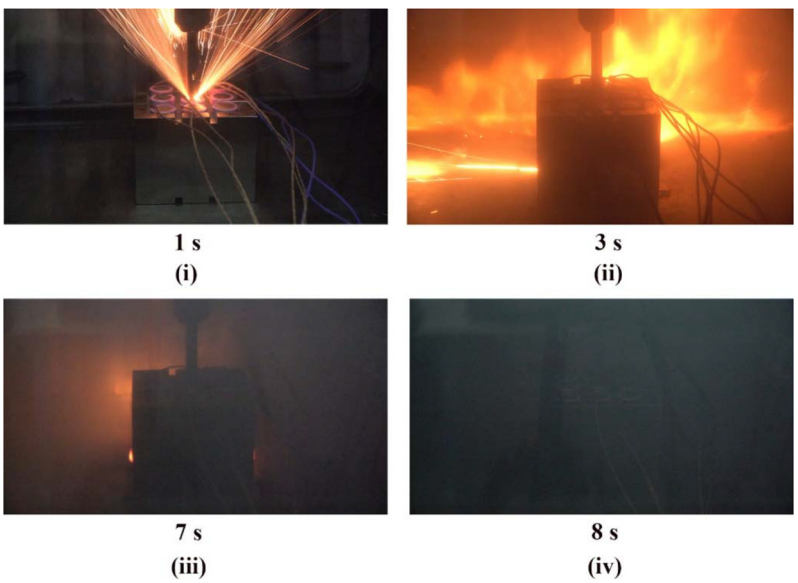

Fig. 23 (i–iv) TR phenomena of battery modules with TCM40/EG at different time. Reproduced with permission from ref. 29. Copyright 2024, Elsevier.

CPCM. Their research showed that after surface modification, the contact angle between the expanded graphite and the hydrated salt decreased from 91.7° to 34.8°, and the adsorption rate for the hydrated salt increased by 75.33%. This CPCM undergoes phase change and thermal decomposition in the ranges of 30–50 °C and 90–120 °C, respectively, achieving a total enthalpy of 1168.5 kJ kg^{-1}. TRP experimental results indicated that compared to the control group, this CPCM delayed the TRP time by a factor of 3.4 and reduced the average peak temperature by 124.1 °C. Given the excellent hydrophilicity of hydrogels, researchers have attempted to compound hydrated salts with hydrogels. Lu *et al.*[27] prepared a hydrated salt gel by compounding $Na_2HPO_4{\cdot}12H_2O$ with sodium polyacrylate hydrogel. Their study showed that the viscosity of this hydrated salt gel before curing was only 150 cP, allowing it to rapidly fill gaps between cells. Its total enthalpy reached 1250.6 kJ kg^{-1}. TRP experiments demonstrated that compared to an unprotected battery pack, the pack filled with the hydrated salt gel exhibited a 239 °C reduction in peak TR temperature, and the temperatures of cells surrounding the TR cell remained within the safe limit of 150 °C.

Compounding TCMs with thermal insulation materials enables synergistic protection combining heat absorption and thermal blocking. Li *et al.*[161] separately prepared a gelatin/sodium alginate biomass aerogel and a $CH_3COONa{\cdot}3H_2O$/thermoplastic polyester elastomer/expanded graphite CPCM, then combined them using an adhesive. Test results showed that this composite material achieved an enthalpy of 811.9 kJ kg^{-1}. After being placed on a 200 °C hot plate for 60 min, the backside temperature was only 88 °C, demonstrating good insulation performance. TR test results indicated that the maximum surface temperature of the TR battery was 228.1 °C, while the maximum backside temperature of the composite material was only 59.8 °C. Miao *et al.*[162] used ceramic fiber (CF) as the thermal insulation material compounded with $CaCl_2{\cdot}6H_2O$, and added $SrCl_2{\cdot}6H_2O$ and hydroxyethyl cellulose nanofibers as nucleating and structural reinforcement agents. Experiments showed that the melting and thermal decomposition enthalpies of this composite were 137 kJ kg^{-1} and 699.5 kJ kg^{-1}, respectively. Furthermore, after heating the surface at 800 °C for 3 min, the backside temperature was only 164.4 °C. Numerical simulation results indicated that wrapping a battery pack with this composite material could effectively prevent TRP (Fig. 24).

Hydrated salts suffer from inherent drawbacks such as phase separation and efflorescence-induced loss of crystal water during long-term use, leading to a gradual degradation of their thermal energy storage performance. Current research indicates that encapsulation is an effective strategy to enhance the long-term stability of hydrated salts. For example, Zhang *et al.*[163] coated the surface of a $Mg(NO_3)_2{\cdot}6H_2O$-based composite phase change material with an epoxy resin layer. After 100 thermal cycles, the mass loss of the coated CPCM was only 0.84%, significantly lower than the 22.92% loss observed for the uncoated CPCM. In summary, TCMs particularly hydrated salts, which combine phase change and thermal decomposition heat absorption capabilities, hold significant promise for TRP suppression. Hydrogels, with their high hydrophilicity and flexibility, serve as excellent carriers for hydrated salts. Combining thermochemical storage materials with insulation materials to achieve synergy between heat absorption and thermal blocking is an important method for enhancing TRP protection performance. However, the practical application of hydrated salts for suppressing TRP still faces several challenges. After repeated melting-solidification cycles, phase separation can lead to a decline in heat storage capacity. Meanwhile, hydrated salts exhibit corrosiveness, which may cause damage to battery casings and electrodes. Future research should focus on enhancing the compatibility and long-term stability of hydrated salts with battery systems, such as employing microencapsulation and multiscale encapsulation techniques to mitigate corrosiveness, as well as incorporating nucleating agents and thickeners to suppress phase separation, thereby improving cycling stability.

Overall, hydrogels and hydrated salts, with their ultra-high enthalpy values, represent a breakthrough compared to the energy storage density of traditional solid–liquid PCMs. Hydrogels exhibit a certain advantage in gravimetric heat storage density over TCMs due to the extremely high evaporation enthalpy of water, making them suitable for applications with stringent weight limitations on the battery system. In contrast, TCMs, with their typically higher density than water, offer superior volumetric heat storage density, rendering them more applicable to compact battery systems. Both material systems face challenges related to stability and compatibility with batteries. Future efforts should focus on researching their long-term stability and encapsulation processes to improve their practical applicability.

6. Coupling thermal storage materials with active cooling systems

6.1 Coupling with liquid cooling systems

Thermal storage materials can effectively absorb the heat generated during battery TR, but their heat absorption capacity is limited, lacking sustained protective capability.[164] For small-capacity batteries, such as 18 650 cylindrical cells, the total heat generated during TR is relatively low, and passive protection relying solely on thermal storage materials is often sufficient to completely prevent TRP. For large-capacity batteries, such as prismatic cells with a capacity exceeding 100 Ah, the prolonged heat release during TR can exhaust the latent heat of the thermal storage materials, necessitating the introduction of an active cooling system for continuous heat dissipation. Although coupling with an active cooling system increases energy consumption and system complexity, this approach is more suitable for applications that demand high safety, such as electric vehicles and large-scale energy storage stations. Among various active cooling methods, liquid cooling is the mainstream choice due to its high heat transfer coefficient and strong cooling capacity.[165,166] In such coupled

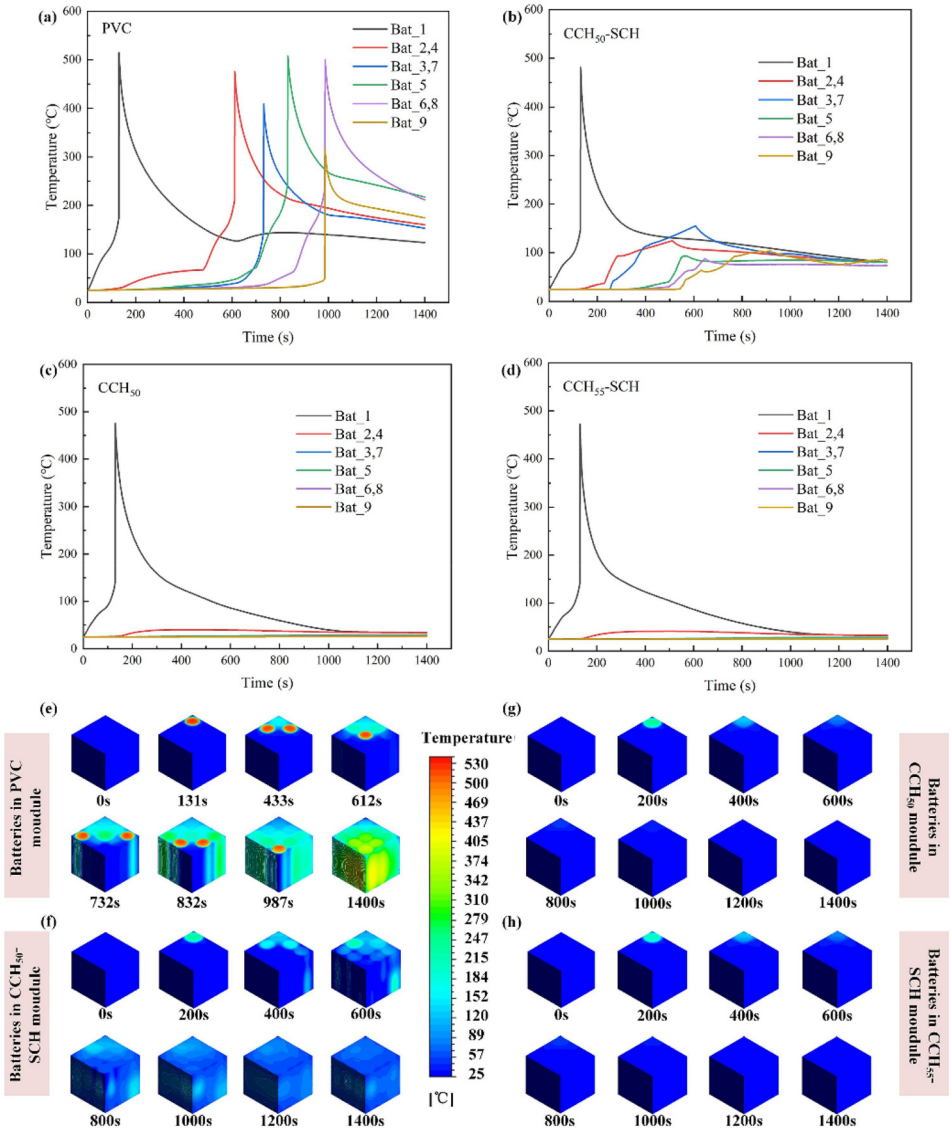

Fig. 24 TR elimination investigation with temperature increase and temperature contours of a battery module in (a, e) PVC-module, (b, f) CCH50-SCH-module, (c, g) CCH50-module and (d, h) CCH55-SCH-module. Reproduced with permission from ref. 162. Copyright 2025, Elsevier.

systems, TRP suppression performance is influenced by multiple parameters. For instance, the structure of the liquid cooling system and the flow rate of the coolant directly determine its cooling efficiency, while the thermal conductivity of the thermal storage material affects its heat absorption rate and the speed of heat transfer to the cooling system. Furthermore, incorporating thermal insulation materials into the coupled system can achieve multi-level protection involving heat absorption, dissipation, and insulation. The following sections will discuss the impact of key parameters, such as system structure, coolant properties, and thermal conductivity of storage materials on the TRP suppression performance of coupled systems, as well as strategies for performance enhancement through multi-level protection.

6.1.1 Structural optimization of coupled systems. To optimize the TRP suppression performance of coupled thermal storage material and liquid cooling systems, researchers have investigated the influence of structural characteristics, such as the layout and shape of cold plates, on TRP suppression. Yang *et al.*[167] combined $CH_3COONa{\cdot}3H_2O$/expanded graphite CPCM with liquid cooling plates and compared the TRP suppression effectiveness under different cooling configurations, including no liquid cooling, bottom cooling, side cooling, and combined bottom-side cooling (Fig. 25), through numerical simulation. Their study found that coupling CPCM with cold plates yielded significantly better TRP suppression than using CPCM alone. Among the configurations, combined cooling achieved the most uniform heat dissipation within the battery module and offered the best protection, completely preventing TRP. Heat transfer occurs fastest along the direction of the large-area contact surface between batteries during TR, which needs to be blocked as a priority. Lu *et al.*[168] designed a coupled system

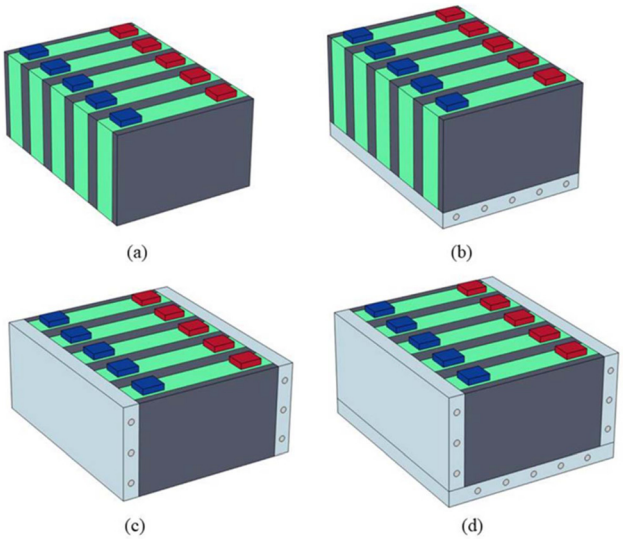

Fig. 25 Schematic diagram of the four schemes: no liquid cooling (a); bottom liquid cooling (b); side liquid cooling (c); and combined liquid cooling (d). Reproduced from ref. 167. CC BY 4.0, MDPI.

where LIBs are wrapped with PCM and liquid-cooled microchannels are vertically arranged between them. The coolant flows from top to bottom, removing heat and suppressing lateral heat transfer. Their study showed that this coupled system could prevent TRP even if four cells undergo TR simultaneously. Wang *et al.*[169] separately combined straight-channel and wavy microchannel cold plates with paraffin/expanded graphite CPCM and compared the protective effectiveness of the two coupled systems using numerical simulation. Their research indicated that compared to the straight-channel microchannel cold plate, using the wavy microchannel cold plate delayed the time for the battery to reach the TR trigger temperature by 440 s. This is because the wavy channels increase the heat exchange area between the cold plate and the CPCM, accelerating heat transfer from the CPCM to the cold plate and enhancing convective heat dissipation by increasing fluid disturbance.

Besides the structure of the liquid cooling system, the integration method between liquid cooling and the PCM also affects TRP suppression. Gong *et al.*[170] placed liquid cold plates between batteries and compared the TRP suppression effectiveness of two layout configurations: embedding strip-shaped CPCMs between the flow channels of the cold plates (Case E), and sandwiching plate-shaped CPCM between the cold plates and the batteries (Case F), shown in Fig. 26. The results showed that under equal CPCM volume conditions, the plate-CPCM layout provided far superior TRP delay compared to the strip-CPCM layout. This is because the plate-CPCM can directly absorb TR heat and has a larger contact area with the cold plate, enabling faster heat dissipation. Liu *et al.*[171] designed four different coupling structures for PCM and microchannel cold plates (Fig. 27) and compared their TRP suppression effectiveness *via* simulation. The results indicated that Design B, where the PCM is placed between batteries and the cold plates are located on both sides of the battery pack, achieved the best TRP suppression, extending the TR trigger time of the adjacent cell by 521 s. The reason is that the PCM between cells effectively blocks heat transfer to neighboring cells through heat absorption and insulation. Furthermore, due to the higher thermal conductivity on the sides of batteries, the cold plates can achieve more efficient heat dissipation in that direction.

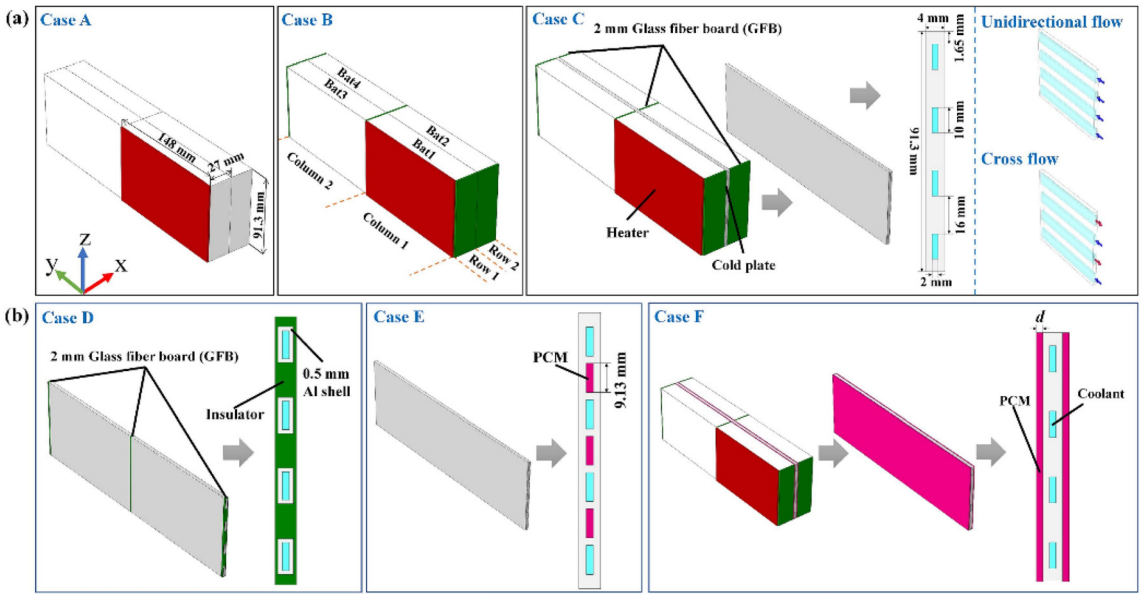

Fig. 26 Configuration of LIB pack assembly and cooling systems: (a) case A, B, C; (b) case D, E, F. Reproduced with permission from ref. 170. Copyright 2025, Elsevier.

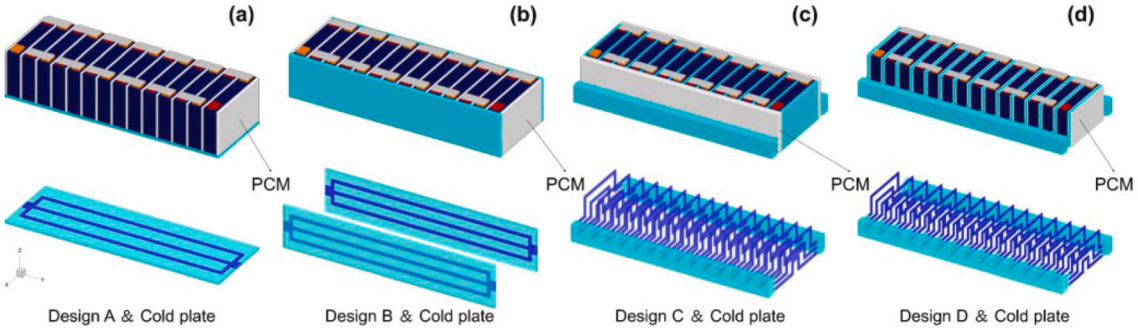

Fig. 27 Schematic structure of the four different hybrid thermal management systems. Reproduced with permission from ref. 171. Copyright 2024, Elsevier.

6.1.2 Optimization of the coolant. Beyond the structural design of the coupled system, optimizing the coolant is equally crucial. Xiao *et al.*[172] investigated the influence of coolant flow velocity on the TRP suppression effectiveness of a CPCM-liquid cooling coupled system through simulation. Their study showed that increasing the flow velocity significantly delays TRP. As the velocity increased from 0.009 m s^{-1} to 0.029 m s^{-1}, the time required for TR to propagate to cells outside the cold plate extended by a factor of 1.84. However, for cells not separated by the cold plate, the influence of flow velocity on TRP was limited due to the insulating effect of the CPCM. While increasing coolant flow velocity facilitates rapid heat dissipation during a TR event within the pack, it also raises energy consumption during normal operation. To address this, Luo *et al.*[173] proposed an intelligent flow rate allocation method based on temperature prediction. This approach first utilizes a Bidirectional Long Short-Term Memory (Bi-LSTM) neural network to predict the future outlet temperature of each microchannel, and then dynamically adjusts the coolant flow rate in each channel according to the predicted cooling demand. The results indicated that compared to a uniform flow distribution, this adaptive strategy could delay the TRP time by 60.6% (85.9 s), as shown in Fig. 28, while reducing the total flow rate by 31.7%.

The temperature of the coolant rises after absorbing TR heat, leading to reduced cooling effectiveness for downstream cells. To mitigate this issue, Kshetrimayum *et al.*[174] positioned microchannel cold plates on both sides of the battery module

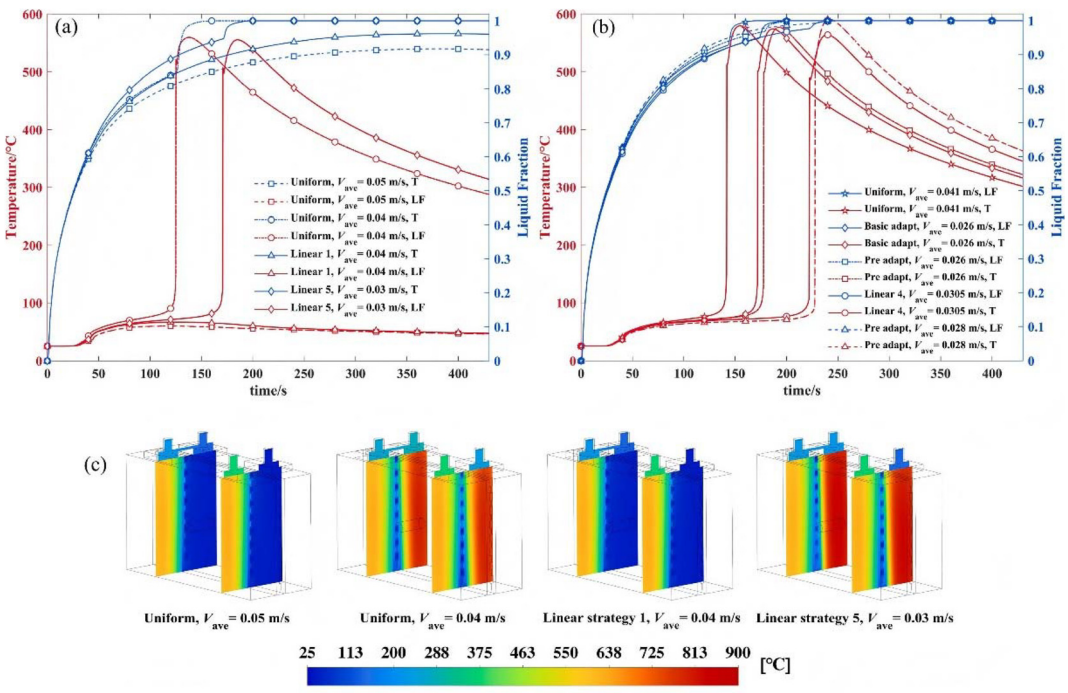

Fig. 28 (a) and (b) Maximum temperature at the interface between battery 2 and PCM, and liquid fraction curves, with different flow rate allocation strategies. (c) Temperature contours of two cross-sections with each strategy at 200 s. Reproduced with permission from ref. 173. Copyright 2024, Elsevier.

and employed a counter-flow configuration where the coolant enters the module from opposite directions. Numerical simulation demonstrated that compared to a parallel-flow configuration where the coolant flows in the same direction, the counter-flow configuration provided better cooling and temperature uniformity for the battery pack. When two cells underwent TR, the maximum temperature and the temperature distribution within the pack using the counter-flow configuration were 4 K and 5 K lower, respectively, than those using the parallel-flow configuration (Fig. 29). Adding nanomaterials to the coolant to enhance its thermal conductivity can improve heat dissipation capability. Ouyang *et al.*[175] prepared a nanofluid by dispersing Al_2O_3 nanoparticles in water and used it as the coolant in the coupled system. Their study showed that as the volume fraction of Al_2O_3 nanoparticles increased from 0% to 3%, the thermal conductivity of the coolant improved by 8.82%. TRP simulation results indicated that compared to using pure water, employing the nanofluid with a 3% Al_2O_3 nanoparticle volume fraction as the coolant reduced the maximum temperature of cells adjacent to the TR cell by 4.54 K.

6.1.3 Optimization of thermal conductivity of thermal storage materials in coupled systems. In coupled systems of thermal storage materials and liquid cooling, the thermal conductivity of the storage material also plays a significant role. Li *et al.*[176] combined paraffin/expanded graphite CPCM with microchannel liquid cold plates. By adjusting the mass fraction of expanded graphite to control the CPCM's thermal conductivity and enthalpy, they investigated its impact on TRP suppression effectiveness. The results indicated that increasing the expanded graphite mass fraction raised the CPCM's thermal conductivity but lowered its enthalpy. Consequently, a greater CPCM thickness was required to compensate for the enthalpy loss to effectively prevent TRP. In coupled systems, spatial constraints sometimes prevent placing sufficient thermal storage material to fully absorb the heat generated during TR. In such cases, increasing the CPCM's thermal conductivity may instead accelerate TRP. Zhang *et al.*[30] designed a thermal management system coupling PCM with liquid cooling and studied the influence of PCM thermal conductivity on TRP through simulation. Their research found that increasing PCM thermal conductivity made the heat generated during TR more easily penetrate to adjacent cells. As the PCM thermal conductivity increased from 0.2 W m^{-1} K^{-1} to 0.6 W m^{-1} K^{-1}, the temperature of cells adjacent to the TR cell rose from 93.3 °C to 171.5 °C. Further increasing thermal conductivity led to TRP. Employing low-thermal-conductivity CPCMs demonstrated superior TRP suppression in coupled systems. Ji

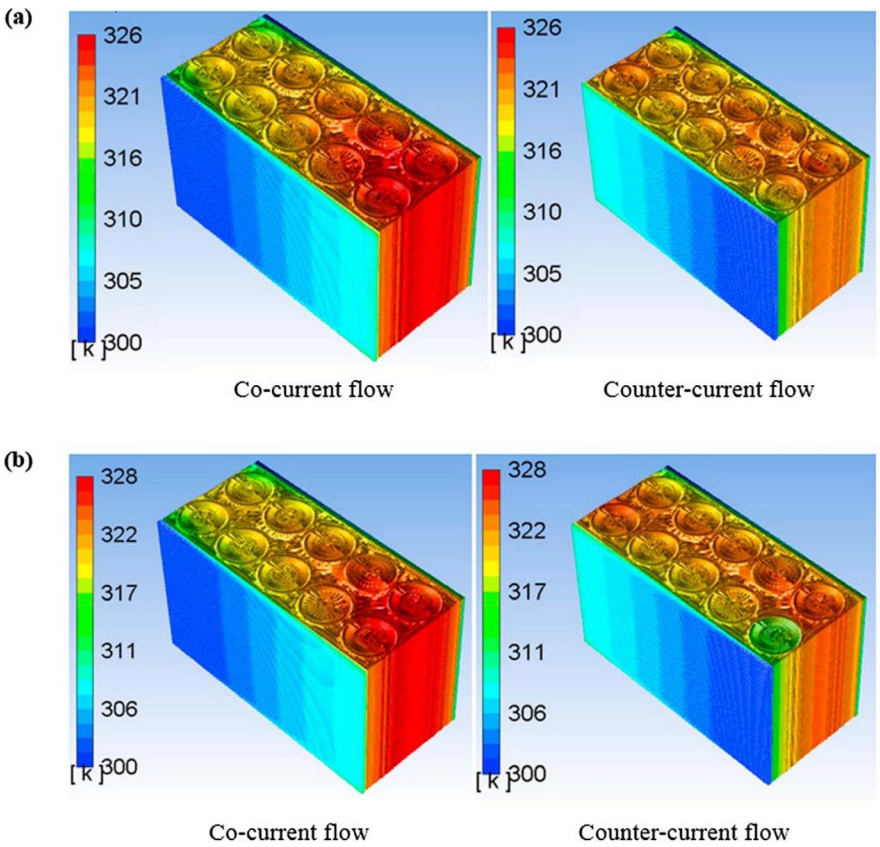

Fig. 29 Temperature contours as a function of flow direction. Temperature contours of (a) 2-cell (cells 7 and 8) and (b) 3-cell (cells 7, 8, and 9) thermal runaway in a battery module with the proposed cooling systems using different flow directions. Reproduced with permission from ref. 174. Copyright 2019, Elsevier.

et al.[177] prepared a low thermal conductivity CPCM by compositing a nano-ceramic fiber substrate with PCM, placed it between cells, and installed a liquid cold plate at the bottom of the battery pack. Their results showed that the through-thickness thermal conductivity of this low-thermal-conductivity CPCM was lower than that of nano-ceramic fiber and glass fiber aerogels. Combining it with liquid cooling could completely prevent TRP.

Using high and low thermal conductivity CPCMs together enables both effective TRP suppression and efficient heat dissipation. Liu *et al.*[178] used pure *n*-nonadecane and *n*-nonadecane/copper foam CPCM as the low-thermal-conductivity PCM (LPCM) and high-thermal-conductivity PCM (HPCM), respectively. The LPCM was sandwiched between HPCM layers, and microchannel liquid cold plates were arranged at the interfaces between HPCM and LPCM (Fig. 30). The HPCM, being close to the heat source, rapidly absorbs heat and transfers it to the cold plates, while the LPCM blocks heat transfer to adjacent cells. Simulation results indicated that using only HPCM could only delay TRP, whereas the HPCM–LPCM sandwich structure could completely prevent it. Wu *et al.*[179] proposed a coupled system designed to mitigate uneven cooling caused by the coolant temperature gradient by rationally arranging PCMs with different thermal conductivities. PCMs with varying thermal conductivities were placed between the cells and the cold plate (with conductivity increasing from the inlet to the outlet), and low-thermal-conductivity PCM was placed between adjacent cells to suppress TRP, as shown in Fig. 31. Simulation results demonstrated that this system could effectively prevent TRP even if any cell within the module underwent TR.

6.1.4 Multi-level protection enhancement strategy for coupled systems. Incorporating thermal insulation materials into the coupled system of thermal storage materials and liquid cooling enables multi-level protection involving heat absorption, dissipation, and insulation, which is beneficial for further enhancing TRP suppression. Ouyang *et al.*[180] designed an integrated thermal management system by filling the gaps between cells with paraffin/expanded graphite CPCM, wrapping an outer layer with aerogel as an insulation barrier, and embedding liquid cooling channels between the aerogel. Their study showed that when using only CPCM and aerogel for protection, heat could not be dissipated promptly. Conversely, when relying solely on a liquid cooling system, the temperature of adjacent cells rose rapidly in the initial stage of TR. The integrated system, however, could both suppress temperature rise and provide continuous heat dissipation, offering optimal protective performance. Simulation results indicated that this integrated system could maintain the maximum temperature of cells adjacent to the TR cell at 358.7 K and could reduce the temperature to a safe range within 400 s. Introducing insulation materials into the coupled thermal storage-liquid cooling system helps block TR heat transfer but can also hinder the system's heat dissipation. Optimizing the system structure can achieve a balance between insulation and cooling. Xie *et al.*[181] grouped three cells into a module encapsulated with CPCM, and four such modules were connected in series to form a battery pack. Aerogel plates were placed between the modules to block inter-module TR propagation. Liquid cold plates were positioned on the sides of the battery pack, allowing the heat within each module to be absorbed by the CPCM and transferred to the cold plates, achieving efficient heat dissipation.

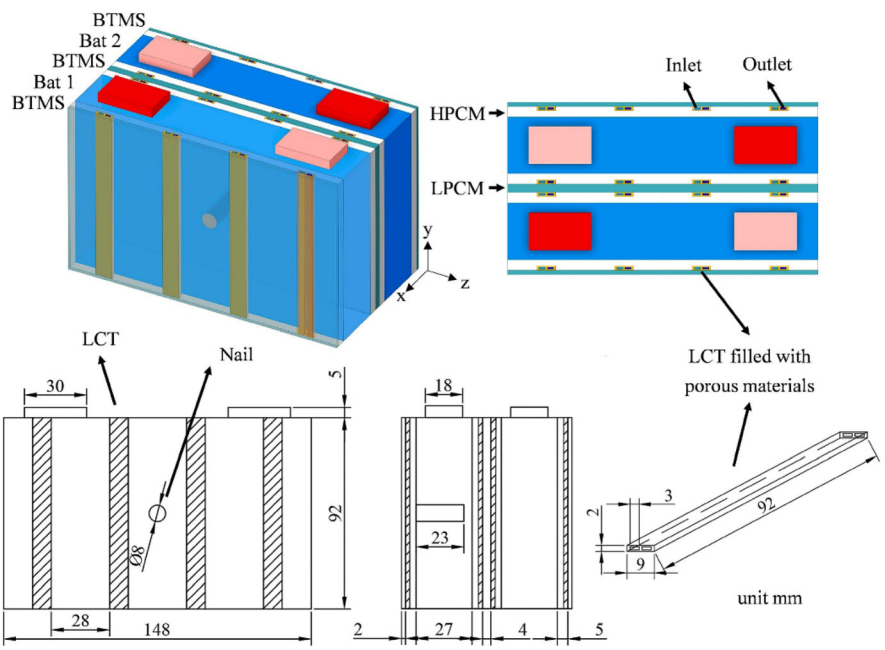

Fig. 30 Proposed phase change-liquid cooling integrated BTMS schematic diagram. Reproduced with permission from ref. 178. Copyright 2025, Elsevier.

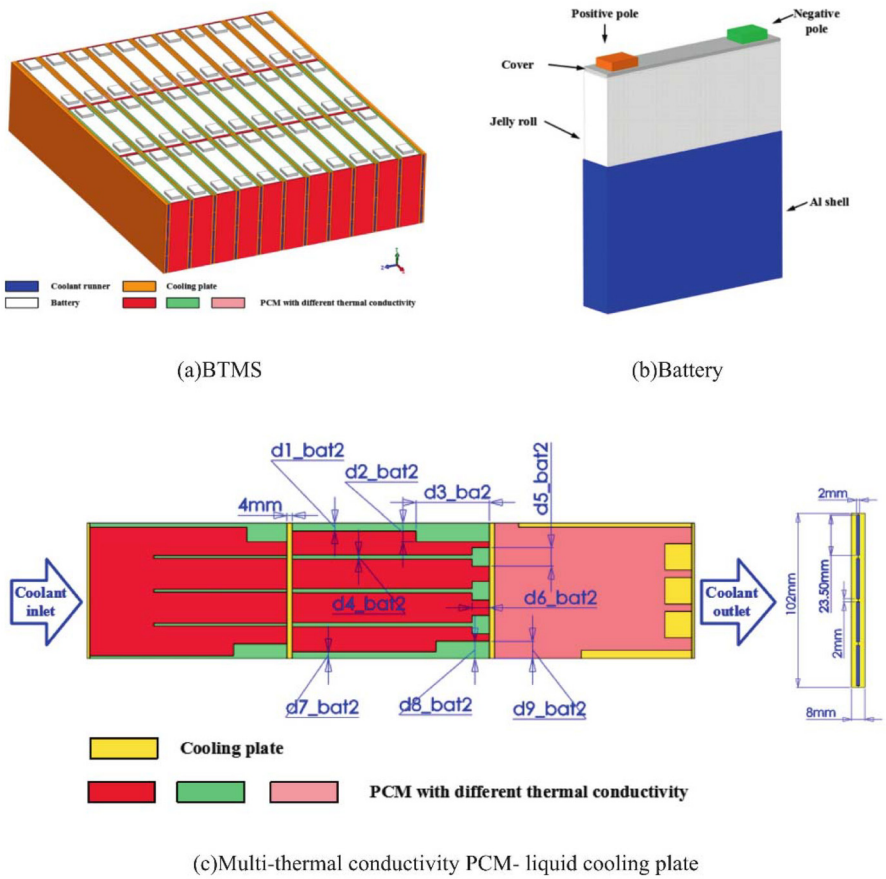

Fig. 31 Battery pack (a), battery (b) and MTCPCM-liquid cooling plate (c). Reproduced with permission from ref. 179. Copyright 2025, Elsevier.

The heat transfer pathways under normal operating conditions (Model I) and TR conditions (Model II) are illustrated in Fig. 32. Simulation results demonstrated that this system could confine TR within a single module. To prevent insulating materials from affecting the PCM's heat absorption, Zuo *et al.*[182] arranged aerogel and liquid cold plates in an aerogel–

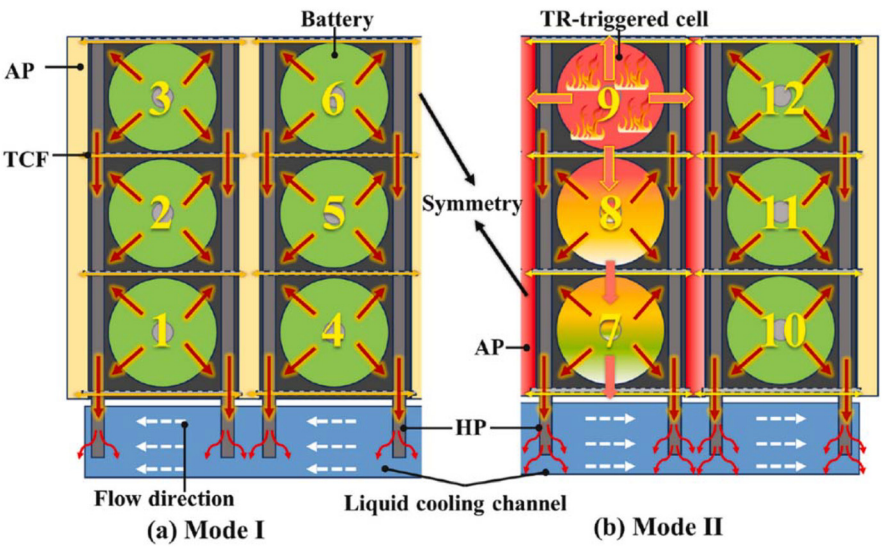

Fig. 32 Heat transfer paths of (a) mode I and (b) mode II. Reproduced with permission from ref. 181. Copyright 2025, Elsevier.

cold plate–aerogel sequence between cells to inhibit inter-cell TRP, while PCM was placed on both sides of the battery pack for heat absorption and dissipation. Simulation results showed that this system could maintain the maximum temperature of cells adjacent to a TR cell below 60 °C, completely preventing TRP.

In summary, coupling the passive cooling of thermal storage materials with the active cooling of liquid systems achieves synergy between absorbing the instantaneous high heat of TR and providing sustained heat dissipation. Increasing the contact area between the cold plate and the thermal storage material, as well as enhancing the flow velocity and thermal conductivity of the coolant, contribute to faster heat dissipation. Adopting a counter-flow configuration enables more uniform cooling. Placing thermal storage materials or cold plates directly between cells is advantageous for blocking the TR heat transfer path. Given the spatial constraints limiting the amount of thermal storage material in coupled systems, employing low-thermal-conductivity CPCMs or incorporating insulation materials to achieve multi-level protection involving heat absorption, dissipation, and insulation proves more effective for enhancing TRP suppression. The future research should focus on the synergistic use of high and low thermal conductivity CPCMs within the system to achieve both TRP suppression and efficient heat dissipation.

6.2 Coupling with other active cooling systems

Beyond liquid cooling, researchers have also explored coupling thermal storage materials with other active cooling methods to enhance TRP suppression. Although air cooling offers weaker heat dissipation capacity, its system structure is simpler, with lower energy consumption and cost. Mehrabi-Kermani *et al.*[183] combined paraffin with copper foam and integrated it with an air-cooling system, investigating its TR suppression effect. Heater-simulated TR tests showed that compared to using only PCM or only air cooling, this coupled system delayed the time for the battery temperature to exceed the limit by 25 minutes and 24 minutes, respectively. Thermoelectric coolers (TECs) are novel cooling devices based on the Peltier effect, offering advantages such as no moving parts, compact size, rapid response, ease of control, and low environmental impact.[184–186] Liu *et al.*[187] wrapped batteries with aluminum–shell-encapsulated paraffin and symmetrically arranged annular thermoelectric coolers (ATECs) on both sides of the batteries. Numerical simulation results indicated that relying solely on PCM heat absorption could not prevent TR caused by overheating. However, activating the ATECs kept the battery temperature below 437 K due to their strong cooling capacity, successfully averting TR. The team further investigated the effect of combining PCM with ATEC on suppressing TRP within a battery pack, as shown in Fig. 33.[31] Their study showed that when only PCM was used, TR propagate throughout the entire battery pack within 150 s, whereas distributing four ATECs within the pack limited TRP to only one adjacent cell. Increasing the ATEC input current (from 3 A to 6 A) only marginally delayed the TRP time (by 7 s). This is because the Joule heating of the ATECs increased significantly at higher currents, leading to a reduction in the Peltier cooling effect. In summary, air cooling systems and TECs feature simple structures and demonstrate certain application potential in compact, coupled TRP protection systems. Optimizing the input current of TECs is necessary to achieve the best energy efficiency ratio.

Overall, coupling thermal storage materials with active cooling systems substantially enhances their sustained protective capability. Future research should focus on developing methods to detect TR occurrence within the system and promptly increase flow rates or cooling power, thereby improving TRP suppression while minimizing the system's energy consumption under normal operating conditions. Furthermore, considering the potential for active cooling system failure under extreme conditions, research should also focus on the protective capability of coupled systems in the event of partial component failure, not solely on their TRP suppression performance under normal operation.

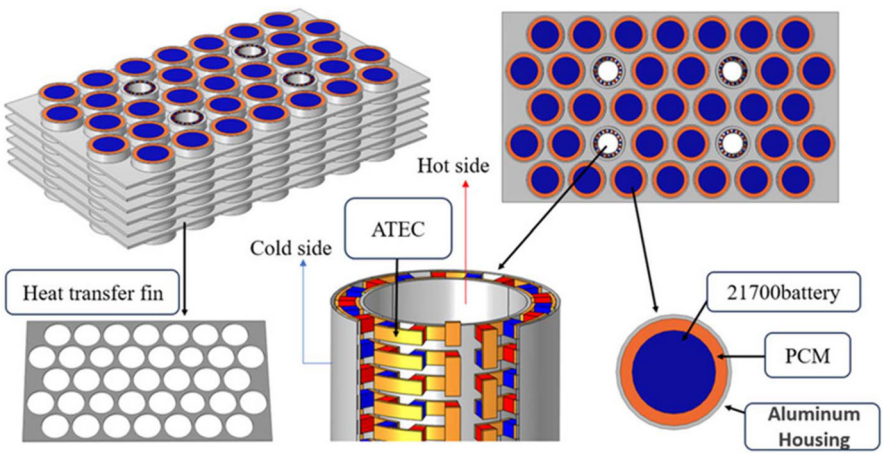

Fig. 33 The 3D model of the system. Reproduced with permission from ref. 31. Copyright 2025, John Wiley and Sons.

Table 2 Comparison of thermal storage materials for TRP suppression: typical heat storage density and thermal conductivity, advantages, disadvantages, and applicable scenarios

Type	Typical heat storage density (kJ kg^{-1})	Typical thermal conductivity (W m^{-1} K^{-1})	Advantages	Disadvantages	Applicable scenarios
Flame-retardant CPCM	60–190	0.4–1.5	Excellent fire resistance	May reduce enthalpy and mechanical strength	Small-capacity battery packs with high safety requirements
Low-thermal-conductivity CPCM	60–160	0.1–0.5	Combines heat absorption and insulation	Hinders normal heat dissipation, prone to heat accumulation	Large-capacity battery packs with low-rate operation
High-thermal-conductivity CPCM	110–230	1–14	Fast thermal response, good temperature uniformity	May accelerate TRP, requires sufficient heat storage capacity	Small-capacity cells or local designs requiring rapid heat dissipation
Flexible CPCM	90–160	1–2	Adapts to battery expansion, low contact resistance	Increased flammability	Battery packs that prone to deformation
Hydrogel	1100–1800	0.2–0.8 (before dehydrated); 0.03–0.1 (after dehydrated)	High gravimetric heat storage density and flexibility	Low mechanical strength, insulation and long-term stability unverified	Weight-sensitive high-energy-density battery packs
Thermochemical material	700–1400	0.05–25 (depending on support materials)	High volumetric heat storage density	Corrosive, long-term stability unverified	Volume-sensitive high-energy-density battery packs
Thermal storage material + active cooling	System-dependent	System-dependent	Combines instantaneous heat absorption and continuous dissipation	Complex system, high cost, risk of failure	Large-scale battery systems

7. Conclusion and outlook

Thermal energy storage materials have demonstrated significant advantages in suppressing TRP in LIBs. This review systematically summarizes recent research progress in this field, highlighting the synergistic optimization of key material properties—flame retardancy, thermal conductivity, and flexibility, the potential of novel high-enthalpy materials (hydrogels and TCMs), and the integration with active cooling systems for enhanced protection. Table 2 provides a comprehensive comparison of these materials, summarizing their advantages, limitations, and applicable scenarios.

Despite the progress achieved in current research, certain limitations still remain. Future research in this field may focus on the following directions:

(1) Development of novel protective materials based on hydrated salts and hydrogels, integrating high energy storage density, flame retardancy, flexibility, and tunable thermal conductivity to meet the comprehensive protection requirements of high-capacity LIBs.

(2) Develop novel smart-responsive thermal storage materials, such as employing thermochromic materials to achieve visual early warning of TR, and utilizing self-healing materials to enable automatic repair after cracking caused by thermal stress, thereby achieving a transition from passive protection to active response.

(3) Integrate the screening and design of novel thermal storage materials with artificial intelligence and machine learning techniques, construct performance prediction models for thermal storage materials, enhance the efficiency of material screening and structural design, and accelerate the development of novel high-performance thermal storage materials.

(4) Investigation into the long-term stability and compatibility of thermal storage materials within battery systems, with emphasis on advanced encapsulation technologies and modification strategies to enhance their reliability and safety in practical applications.

(5) Promoting high-performance thermal storage materials from the laboratory to engineering applications, with a focus on scalable preparation technologies and cost control, while establishing a unified industry-wide testing and evaluation standard system for TRP suppression performance.

(6) Development of intelligent coupled systems integrated with real-time battery state monitoring and early thermal runaway warning technologies, enabling adaptive control of cooling power or flow rate to optimize energy consumption while ensuring safety.

(7) Establishment of more accurate TRP simulation models that comprehensively account for the coupling effects of multiple factors such as venting, combustion, and volume expansion, thereby providing more reliable tools for the precise design and performance prediction of protection solutions.

Author contributions

All authors contributed to the discussion of contents and the editing of the manuscript prior to submission.

Conflicts of interest

The authors declare no competing interests.

Data availability

No primary research results, software or code have been included and no new data were generated or analysed as part of this review.

Acknowledgements

This work is supported by the National Natural Science Foundation of China (No. 22578132, 22278145) and Dongguan Key Research & Development Program (No. 20231200300152).

References

1 V. O. Vega-Muratalla, T. I. Serrano-Arevalo, R. Ochoa-Barragan, L. F. Lira-Barragan, C. Ramirez-Marquez, M. M. El-Halwagi and J. M. Ponce-Ortega, Recent Advances and Engineering Challenges of Lithium Batteries for Grid-Level Energy Storage: A Review, *Ind. Eng. Chem. Res.*, 2025, **65**(3), 1424–1447.

2 X. W. Lin, B. J. Rong, X. Y. Lin, Z. J. Li, X. Y. Ding, D. W. Jing, Y. J. Lu and Z. F. Zhou, Comparative study of thermal management system for wide temperature safety of large-capacity energy storage batteries, *Innovation Energy*, 2026, **3**(1), 100133.

3 D. Luo, L. Jiang, H. Chen, Z. H. Wu and B. Y. Cao, Thermoelectric-based battery thermal management with cooling and energy recovery, *Innovation Energy*, 2026, **3**(1), 100134.

4 X. N. Feng, L. G. Lu, M. G. Ouyang, J. Q. Li and X. M. He, A 3D thermal runaway propagation model for a large format lithium ion battery module, *Energy*, 2016, **115**(1), 194–208.

5 Y. J. Liu, J. X. Liu, Z. W. Zhao, Y. Ma, Q. L. Duan, H. Li, J. H. Sun and Q. S. Wang, The efficiency of dodecafluoro-2-methylpentan-3-one in suppressing NCM 811 lithium-ion battery fire, *Process Saf. Environ. Prot.*, 2024, **186**, 1432–1446.

6 P. J. Liu, C. D. Wang, S. J. Sun, G. J. Zhao, X. Y. Yu, Y. X. Hu, W. X. Mei, K. Q. Jin and Q. S. Wang, Understanding the influence of the confined cabinet on thermal runaway of large format batteries with different chemistries: A comparison and safety assessment study, *J. Energy Storage*, 2023, **74**, 109337.

7 D. X. Ouyang, Y. H. Chung, J. L. Liu, J. L. Bai, Y. X. Zhou, S. C. Chen, Z. R. Wang and C. M. Shu, Characteristics and mechanisms of as well as evaluation methods and countermeasures for thermal runaway propagation in lithium-ion batteries, *Prog. Energy Combust. Sci.*, 2025, **108**, 101209.

8 L. F. Song, Z. H. Huang, W. X. Mei, Z. Z. Jia, Y. Yu, Q. S. Wang and K. Q. Jin, Thermal runaway propagation behavior and energy flow distribution analysis of 280 Ah $LiFePO_4$ battery, *Process Saf. Environ. Prot.*, 2023, **170**, 1066–1078.

9 B. Tong, J. Y. Li, J. H. Sun, Q. S. Wang and P. Qin, Restoring the gas diffusion field before the fire of the $LiNi_{0.7}Co_{0.2}Mn_{0.1}O_2$ lithium-ion battery thermal runaway, *J. Energy Storage*, 2024, **88**, 111548.

10 L. B. Diaz, X. Z. He, Z. W. Hu, F. Restuccia, M. Marinescu, J. V. Barreras, Y. Patel, G. Offer and G. Rein, Meta-Review of Fire Safety of Lithium-Ion Batteries: Industry Challenges and Research Contributions, *J. Electrochem. Soc.*, 2020, **167**(9), 090559.

11 M. Y. Zhang, K. Chen, W. F. Li, S. B. Li, C. Y. Wang, Z. J. Sun, X. M. Cao and H. Ge, Advanced modification strategies for improving the thermal stability of Ni-rich layered cathodes towards next-generation lithium-ion batteries, *J. Power Sources*, 2026, **661**, 238606.

12 Y. D. Zhang, D. H. Wang, C. F. Liang, Y. Han, Z. Li and Y. H. Huang, Design of double layer cathode electrode for improving the safety and stability of lithium-ion batteries, *Chem. Eng. J.*, 2024, **495**, 153344.

13 Y. P. Xiao, T. L. Li, X. Q. Hao, T. J. Zhu, J. Q. Zang, Y. Q. Li and W. J. Wang, Ingenious utilization of Sb-graphite composite and PVDF binder as flame-retardant and performance-improved electrode for safer lithium-ion batteries, *J. Alloys Compd.*, 2024, **1004**, 175871.

14 M. Carter, M. H. Parekh, V. Tomar, J. E. Dietz and V. G. Pol, Flame retardant vermiculite coated on polypropylene separator for lithium-ion batteries, *Appl. Clay Sci.*, 2021, **208**, 106111.

15 Y. Q. Zhang, L. Bo, J. S. Wang, T. D. Zhang, C. H. Zhang, Y. Zhang, C. Yin, X. B. Wang and Q. G. Chi, PVDF-HFP@PW thermal self-regulating separator for long-life and high-safety lithium-ion batteries, *J. Power Sources*, 2025, **660**, 238517.

16 X. M. Wang, J. Zhu, X. H. Niu, H. T. Yang, Q. Z. Liu, W. Lei, J. K. Xie, Y. Z. Wu and W. H. Zhu, Advanced polyethylene separator coated with core-shell structured polydopamine-aluminum nitride composite for enhancing electrochemical performance of high-rate lithium-ion batteries, *J. Energy Storage*, 2026, **152**, 120736.

17 S. F. Song, W. Xue, Y. M. Wang, Z. T. Wang, Y. M. Cui, Z. X. Long, H. Y. Shan, N. Hu, J. F. Wang and F. S. Pan, All-climate all-solid-state batteries enabled by high-entropy amorphous oxyhalide solid electrolytes, *Green Chem.*, 2025, **27**(42), 13281–13292.

18 S. Y. Chen, S. P. Wang, Q. K. Peng, Z. S. Wei, S. Y. Cheng, Z. Fang, P. Y. Duan, Y. Cheng, Y. F. Cheng, K. Q. Jin, L. H. Jiang and Q. S. Wang, *In situ* fabricated succinonitrile-based composite electrolyte for high-performance and safe solid-state lithium batteries, *J. Power Sources*, 2024, **604**, 234473.

19 C. X. Ma, Y. H. Li, P. Z. Zhao, Z. H. Chang, B. Li, M. Yang, W. Zhang and B. Wang, Semi-solid-state high specific energy battery enabled by in situ construction of gel electrolyte, *J. Solid State Electrochem.*, 2026, **30**(2), 953–960.

20 Y. Hong, H. Wu, S. K. Wong, C. Y. Jin, C. S. Xu, H. B. Wang, Y. Peng, Y. J. Zheng, X. N. Feng and M. G. Ouyang, Dynamic thermophysical modeling and

parametric sensitivity analysis of flood cooling suppressing the thermal runaway propagation for electric bicycle battery, *J. Energy Storage*, 2024, **98**, 113084.

21 Y. X. Hu, H. X. Zhu, Y. S. Zhu, R. Tang, X. T. Wu, H. H. Qiu and T. T. Wu, Numerical simulation study on optimizing the temperature characteristics of jet fires in forced air-cooled 18650 battery modules during thermal runaway, *Case Stud. Therm. Eng.*, 2025, **76**, 107369.

22 Y. Yu, Z. H. Huang, W. X. Mei, Z. Z. Jia, L. F. Song and Q. S. Wang, Preventing effect of different interstitial materials on thermal runaway propagation of large-format lithium iron phosphate battery module, *J. Energy Storage*, 2023, **63**, 107082.

23 L. T. Qi, M. Wang, Z. X. Xing, Y. C. Liu, W. Z. Lu, H. Han, T. Y. Zhou, Y. Wu and C. Li, Beyond the thermal barrier: Coupled effects of insulating materials on runaway propagation and toxic gas emissions in lithium-ion batteries, *Case Stud. Therm. Eng.*, 2026, **78**, 107638.

24 Z. Y. Liu, S. L. Zhou, Z. Y. Ling, Z. Zhang, X. M. Fang and S. P. Wang, Achieving no-propagation of battery thermal runaway using ultrathin electrically insulative thermochemical materials with superior heat-absorption capacity, *Appl. Therm. Eng.*, 2026, **283**, 128968.

25 T. Sun, Y. L. Yan, J. Sui, X. H. Wang, G. Rasool and K. Zhang, A novel thermal-cloak-based thermal design for preventing thermal runaway propagation in lithium-ion battery packs, *J. Energy Storage*, 2025, **123**, 116828.

26 H. B. Qiu, Z. G. Zhang, Z. Y. Ling and X. M. Fang, Developing a flame-retardant flexible composite phase change material to realize both temperature control and thermal runaway prevention for lithium-ion battery pack, *Appl. Therm. Eng.*, 2024, **248**, 123301.

27 T. Z. Lu, K. X. Yang, T. H. Wu, Z. Y. Ling, Z. G. Zhang and X. M. Fang, Hydrated salt pouring gel for lithium-ion battery thermal management and thermal runaway prevention, *Chem. Eng. J.*, 2025, **521**, 166984.

28 Y. W. Hong, B. C. Zang, D. H. Yao, X. P. Gao, J. Chen, C. Lu and X. C. Pang, Ultra-high SiO_2-loaded hydrogel with enhanced mechanical strength, thermal regulation, and ablation resistance for lithium-ion battery safety, *Chem. Eng. J.*, 2025, **521**, 166639.

29 S. L. Zhou, W. B. Zhang, S. Lin, Z. Y. Ling, Z. G. Zhang and X. M. Fang, Enhancing lithium-ion battery pack safety: Mitigating thermal runaway with high-energy storage inorganic hydrated salt/expanded graphite composite, *J. Energy Storage*, 2024, **92**, 112089.

30 W. C. Zhang, Z. C. Liang, X. X. Yin and G. Z. Ling, Avoiding thermal runaway propagation of lithium-ion battery modules by using hybrid phase change material and liquid cooling, *Appl. Therm. Eng.*, 2021, **184**, 116380.

31 X. Liu, P. Y. Wu, J. Song and Z. H. Zeng, Performance Analysis of a Hybrid ATEC/PCM Thermal Management System for Battery Packs, *Energy Technol.*, 2025, **14**(1), e202501234.

32 J. Luo, D. Q. Zou, Y. S. Wang, S. Wang and L. Huang, Battery thermal management systems (BTMs) based on phase change material (PCM): A comprehensive review, *Chem. Eng. J.*, 2022, **430**, 132741.

33 J. W. Chen, S. Y. Kang, E. Jiaqiang, Z. H. Huang, K. X. Wei, B. Zhang, H. Zhu, Y. W. Deng, F. Zhang and G. L. Liao, Effects of different phase change material thermal management strategies on the cooling performance of the power lithium ion batteries: A review, *J. Power Sources*, 2019, **442**, 227228.

34 Y. Q. Zhao, B. Y. Zou, T. T. Zhang, Z. Jiang, J. N. Ding and Y. L. Ding, A comprehensive review of composite phase change material based thermal management system for lithium-ion batteries, *Renewable Sustainable Energy Rev.*, 2022, **167**, 112667.

35 K. Z. Li, J. Guo, T. T. Wu, Y. H. Zhang, C. S. Li, H. T. Zhou and Z. J. Zhang, Development of phase change material for thermal management of lithium-ion batteries: a review, *J. Therm. Anal. Calorim.*, 2025, **150**(22), 17947–17972.

36 A. M. F. Faseena and A. Sreekumar, Advances, perspectives and challenges in phase change material based battery thermal management: A comprehensive review, *J. Energy Storage*, 2025, **113**, 115644.

37 D. He, J. L. Wang, Y. J. Peng, B. F. Li, C. Feng, L. Shen and S. X. Ma, Research advances on thermal runaway mechanism of lithium-ion batteries and safety improvement, *Sustainable Mater. Technol.*, 2024, **41**, e01017.

38 G. Assat and J. M. Tarascon, Fundamental understanding and practical challenges of anionic redox activity in Li-ion batteries, *Nat. Energy*, 2018, **3**(5), 373–386.

39 Y. Y. Yu, J. Wang, P. Zhang and J. B. Zhao, A detailed thermal study of usual $LiNi_{0.5}Co_{0.2}Mn_{0.3}O_2$, $LiMn_2O_4$ and $LiFePO_4$ cathode materials for lithium ion batteries, *J. Energy Storage*, 2017, **12**, 37–44.

40 Z. Y. Zhang, R. Ma, J. G. Yang, J. Wang and Y. Peng, A Review on Mechanical, Electrical, Chemical, and Electrochemical Properties of Coating Materials for Silicon Anodes in Lithium-Ion Batteries, *Small*, 2025, **21**(39), e06400.

41 Y. Okamoto, Ab Initio Calculations of Thermal Decomposition Mechanism of $LiPF_6$-Based Electrolytes for Lithium-Ion Batteries, *J. Electrochem. Soc.*, 2013, **160**(2), A404–A409.

42 S. S. Zhang, K. Xu and T. R. Jow, Study of $LiBF_4$ as an electrolyte salt for a Li-ion battery, *J. Electrochem. Soc.*, 2002, **149**(5), A586–A590.

43 N. Lingappan, W. N. Lee, S. Passerini and M. Pecht, A comprehensive review of separator membranes in lithium-ion batteries, *Renewable Sustainable Energy Rev.*, 2023, **187**, 113726.

44 V. G. Choudhari, A. S. Dhoble and T. M. Sathe, A review on effect of heat generation and various thermal management systems for lithium ion battery used for electric vehicle, *J. Energy Storage*, 2020, **32**, 101729.

45 B. Xu, D. N. Qian, Z. Y. Wang and Y. S. L. Meng, Recent progress in cathode materials research for advanced lithium ion batteries, *Mater. Sci. Eng., R*, 2012, **73**(5–6), 51–65.

46 L. H. Saw, Y. H. Ye and A. A. O. Tay, Integration issues of lithium-ion battery into electric vehicles battery pack, *J. Cleaner Prod.*, 2016, **113**, 1032–1045.
47 H. Q. Liu, Z. B. Wei, W. D. He and J. Y. Zhao, Thermal issues about Li-ion batteries and recent progress in battery thermal management systems: A review, *Energy Convers. Manage.*, 2017, **150**, 304–330.
48 S. Landini, J. Leworthy and T. S. O'Donovan, A Review of Phase Change Materials for the Thermal Management and Isothermalisation of Lithium-Ion Cells, *J. Energy Storage*, 2019, **25**, 100887.
49 S. Abada, M. Petit, A. Lecocq, G. Marlair, V. Sauvant-Moynot and F. Huet, Combined experimental and modeling approaches of the thermal runaway of fresh and aged lithium-ion batteries, *J. Power Sources*, 2018, **399**, 264–273.
50 V. Etacheri, R. Marom, R. Elazari, G. Salitra and D. Aurbach, Challenges in the development of advanced Li-ion batteries: a review, *Energy Environ. Sci.*, 2011, **4**(9), 3243–3262.
51 D. Velumani and A. Bansal, Thermal Behavior of Lithium- and Sodium-Ion Batteries: A Review on Heat Generation, Battery Degradation, Thermal Runway – Perspective and Future Directions, *Energy Fuels*, 2022, **36**(23), 14000–14029.
52 Q. S. Wang, J. H. Sun, X. L. Yao and C. H. Chen, Thermal behavior of lithiated graphite with electrolyte in lithium-ion batteries, *J. Electrochem. Soc.*, 2006, **153**(2), A329–A333.
53 G. Gachot, S. Grugeon, G. G. Eshetu, D. Mathiron, P. Ribière, M. Armand and S. Laruelle, Thermal behaviour of the lithiated-graphite/electrolyte interface through GC/MS analysis, *Electrochim. Acta*, 2012, **83**, 402–409.
54 Q. S. Wang, B. B. Mao, S. I. Stoliarov and J. H. Sun, A review of lithium ion battery failure mechanisms and fire prevention strategies, *Prog. Energy Combust. Sci.*, 2019, **73**, 95–131.
55 Y. R. Yang, Y. Gao, Y. Miao, Y. Liang and X. Q. Ren, Research Progress on the Influence of Cathode Materials on Thermal Runaway Behavior of Lithium-Ion Batteries, *Batteries*, 2025, **11**(10), 373.
56 P. Biensan, B. Simon, J. P. Pérès, A. de Guibert, M. Broussely, J. M. Bodet and F. Perton, On safety of lithium-ion cells, *J. Power Sources*, 1999, **81**, 906–912.
57 A. Yamada, S. C. Chung and K. Hinokuma, Optimized $LiFePO_4$ for lithium battery cathodes, *J. Electrochem. Soc.*, 2001, **148**(3), A224–A229.
58 S. K. Martha, O. Haik, E. Zinigrad, I. Exnar, T. Drezen, J. H. Miners and D. Aurbach, On the Thermal Stability of Olivine Cathode Materials for Lithium-Ion Batteries, *J. Electrochem. Soc.*, 2011, **158**(10), A1115–A1122.
59 S. E. Sloop, J. B. Kerr and K. Kinoshita, The role of Li-ion battery electrolyte reactivity in performance decline and self-discharge, *J. Power Sources*, 2003, **119**, 330–337.
60 J. S. Gnanaraj, E. Zinigrad, L. Asraf, H. E. Gottlieb, M. Sprecher, D. Aurbach and M. Schmidt, The use of accelerating rate calorimetry (ARC) for the study of the thermal reactions of Li-ion battery electrolyte solutions, *J. Power Sources*, 2003, **119**, 794–798.
61 E. P. Roth, D. H. Doughty and J. Franklin, DSC investigation of exothermic reactions occurring at elevated temperatures in lithium-ion anodes containing PVDF-based binders, *J. Power Sources*, 2004, **134**(2), 222–234.
62 J. J. Deng, X. L. Yu, D. Q. Pang, B. Fei and J. H. Mo, Cutting-edge gas sensor design for monitoring thermal runaway in lithium-ion batteries: a critical review, *J. Energy Chem.*, 2025, **109**, 769–785.
63 X. N. Feng, D. S. Ren, X. M. He and M. G. Ouyang, Mitigating Thermal Runaway of Lithium-Ion Batteries, *Joule*, 2020, **4**(4), 743–770.
64 P. Ping, X. T. Ren, D. P. Kong, W. Gao, Y. Zhang, C. Yang, G. Q. Wang, Z. K. Feng, J. X. Guo and J. Y. Ren, Multi-scale thermal runaway analysis of sodium-ion batteries and comparative safety assessment with lithium-ion batteries, *Composites, Part B*, 2025, **302**, 112532.
65 S. Mallick and D. Gayen, Thermal behaviour and thermal runaway propagation in lithium-ion battery systems-A critical review, *J. Energy Storage*, 2023, **62**, 106894.
66 X. N. Feng, J. Sun, M. G. Ouyang, F. Wang, X. M. He, L. G. Lu and H. E. Peng, Characterization of penetration induced thermal runaway propagation process within a large format lithium ion battery module, *J. Power Sources*, 2015, **275**, 261–273.
67 Z. H. Huang, J. L. Liu, H. J. Zhai and Q. S. Wang, Experimental investigation on the characteristics of thermal runaway and its propagation of large-format lithium ion batteries under overcharging and overheating conditions, *Energy*, 2021, **233**, 121103.
68 H. Li, Q. L. Duan, C. P. Zhao, Z. H. Huang and Q. S. Wang, Experimental investigation on the thermal runaway and its propagation in the large format battery module with $Li(Ni_{1/3}Co_{1/3}Mn_{1/3})O_2$ as cathode, *J. Hazard. Mater.*, 2019, **375**, 241–254.
69 Z. H. Huang, X. Li, Q. S. Wang, Q. L. Duan, Y. Li, L. N. Li and Q. S. Wang, Experimental investigation on thermal runaway propagation of large format lithium ion battery modules with two cathodes, *Int. J. Heat Mass Transfer*, 2021, **172**, 121077.
70 Z. H. Huang, C. P. Zhao, H. Li, W. Peng, Z. Zhang and Q. S. Wang, Experimental study on thermal runaway and its propagation in the large format lithium ion battery module with two electrical connection modes, *Energy*, 2020, **205**, 117906.
71 C. F. Lopez, J. A. Jeevarajan and P. P. Mukherjee, Experimental Analysis of Thermal Runaway and Propagation in Lithium-Ion Battery Modules, *J. Electrochem. Soc.*, 2015, **162**(9), A1905–A1915.
72 J. H. Zhang, Z. P. Wang, T. F. Jiang, P. Liu, Z. W. Sun, T. X. Shan, B. Chen, Q. Wang and J. C. Hong, Investigation of battery safety states based on thermal propagation and expansion analysis: Experimental studies on different packaging forms, *Appl. Therm. Eng.*, 2025, **258**, 124800.

73 J. Xu, C. J. Lan, Y. Qiao and Y. B. Ma, Prevent thermal runaway of lithium-ion batteries with minichannel cooling, *Appl. Therm. Eng.*, 2017, **110**, 883–890.
74 P. Han, J. Y. Wang, X. M. Zhao, J. W. Liu, C. Wang and X. H. She, Performance study of fin structure in air-cooled thermal management system for column power battery, *J. Energy Storage*, 2024, **104**, 114697.
75 P. Qin, Z. Z. Jia, K. Q. Jin, Q. L. Duan, J. H. Sun and Q. S. Wang, The experimental study on a novel integrated system with thermal management and rapid cooling for battery pack based on $C_6F_{12}O$ spray cooling in a closed-loop, *J. Power Sources*, 2021, **516**, 230659.
76 H. Y. Zhang, J. B. Hu, S. Q. Jing, H. Z. Huang, W. K. Wang, G. Xu, W. J. Ye, Y. Zhang, Z. Z. Tang, W. Zhang and T. Shui, An emerging armor in passive thermal defense for power lithium-ion batteries: Recent advances in aerogels, *Chem. Eng. J.*, 2025, **524**, 169362.
77 H. B. Wei, X. M. Hu, Y. R. Deng, X. X. Wei, Z. Y. Yang and G. Y. Han, Distributed activation energy treatment of polyimide aerogel and its blocking effect on thermal runaway propagation of ternary battery, *J. Energy Storage*, 2024, **90**, 111744.
78 Y. K. Zhao, J. F. Wang, F. Liu, T. Dong and N. Yang, Flexible Al_2SiO_5 Nanofiber Membranes for Thermal Insulation in Lithium-Ion Batteries, *ACS Appl. Nano Mater.*, 2024, **7**(2), 1691–1700.
79 X. M. Sun, Y. J. Dong, P. Sun and B. Zheng, Effects of thermal insulation layer material on thermal runaway of energy storage lithium battery pack, *J. Energy Storage*, 2024, **76**, 109812.
80 Z. Z. Zhou, X. D. Zhou, M. Y. Li, B. Cao, K. M. Liew and L. Z. Yang, Experimentally exploring prevention of thermal runaway propagation of large-format prismatic lithium-ion battery module, *Appl. Energy*, 2022, **327**, 120119.
81 Y. Galazutdinova, S. Ushak, M. Farid, S. Al-Hallaj and M. Grágeda, Development of the inorganic composite phase change materials for passive thermal management of Li-ion batteries: Application, *J. Power Sources*, 2021, **491**, 229624.
82 K. E. N'Tsoukpoe, H. Liu, N. Le Pierrès and L. G. Luo, A review on long-term sorption solar energy storage, *Renewable Sustainable Energy Rev.*, 2009, **13**(9), 2385–2396.
83 P. Tatsidjodoung, N. Le Pierrès and L. G. Luo, A review of potential materials for thermal energy storage in building applications, *Renewable Sustainable Energy Rev.*, 2013, **18**, 327–349.
84 N. V. K. Prasad, K. C. B. Naidu and D. B. Basha, Phase Change Materials for Thermal Energy Storage: A Concise Review, *Nano*, 2024, **19**(14), 2430010.
85 A. Sharma, V. V. Tyagi, C. R. Chen and D. Buddhi, Review on thermal energy storage with phase change materials and applications, *Renewable Sustainable Energy Rev.*, 2009, **13**(2), 318–345.
86 K. Pielichowska and K. Pielichowski, Phase change materials for thermal energy storage, *Prog. Mater. Sci.*, 2014, **65**, 67–123.
87 B. Zalba, J. M. Marín, L. F. Cabeza and H. Mehling, Review on thermal energy storage with phase change: materials, heat transfer analysis and applications, *Appl. Therm. Eng.*, 2003, **23**(3), 251–283.
88 M. M. Umair, Y. Zhang, K. Iqbal, S. F. Zhang and B. T. Tang, Novel strategies and supporting materials applied to shape-stabilize organic phase change materials for thermal energy storage-A review, *Appl. Energy*, 2019, **235**, 846–873.
89 S. Ushak, W. J. Song, P. E. Marín, Y. Milian, D. Zhao, M. Grageda, W. Y. Lin, M. B. Chen and Y. Han, A review on phase change materials employed in Li-ion batteries for thermal management systems, *Appl. Mater. Today*, 2024, **37**, 102021.
90 Z. W. Huang, X. N. Gao, T. Xu, Y. T. Fang and Z. G. Zhang, Thermal property measurement and heat storage analysis of $LiNO_3$/KCl-expanded graphite composite phase change material, *Appl. Energy*, 2014, **115**, 265–271.
91 A. Jamekhorshid, S. M. Sadrameli and M. Farid, A review of microencapsulation methods of phase change materials (PCMs) as a thermal energy storage (TES) medium, *Renewable Sustainable Energy Rev.*, 2014, **31**, 531–542.
92 G. Y. Fang, Z. Chen and H. Li, Synthesis and properties of microencapsulated paraffin composites with SiO_2 shell as thermal energy storage materials, *Chem. Eng. J.*, 2010, **163**(1–2), 154–159.
93 C. Z. Chen, W. M. Liu, Z. Q. Wang, K. L. Peng, W. L. Pan and Q. Xie, Novel form stable phase change materials based on the composites of polyethylene glycol/polymeric solid-solid phase change material, *Sol. Energy Mater. Sol. Cells*, 2015, **134**, 80–88.
94 N. Wu, X. L. Ye, J. J. Li, B. S. Lin, X. L. Zhou and B. Yu, Passive thermal management systems employing hydrogel for the large-format lithium-ion cell: A systematic study, *Energy*, 2021, **231**, 120946.
95 R. R. Li, Z. H. Liu, S. Q. Zheng, C. S. Xu, J. Y. Sun, S. Q. Chen, H. B. Wang, L. G. Lu, T. Deng and X. N. Feng, Trifunctional composite thermal barrier mitigates the thermal runaway propagation of large-format prismatic lithium-ion batteries, *J. Energy Storage*, 2023, **73**, 109178.
96 Y. H. Guo, J. Bae, Z. W. Fang, P. P. Li, F. Zhao and G. H. Yu, Hydrogels and Hydrogel-Derived Materials for Energy and Water Sustainability, *Chem. Rev.*, 2020, **120**(5), 7642–7707.
97 Y. Q. Cui, X. X. Liang, X. Y. Xu, J. Y. Wang, X. L. Zhang, X. Huang, Y. Wang, B. Y. Lu and C. Y. Wang, MoS_2-PVA hydrogel interfacial evaporator for desalination: The role of surface hydroxyl groups-modification towards low evaporation enthalpy and high evaporation efficiency, *J. Environ. Chem. Eng.*, 2025, **13**(5), 118835.
98 D. Aydin, S. P. Casey and S. Riffat, The latest advancements on thermochemical heat storage systems, *Renewable Sustainable Energy Rev.*, 2015, **41**, 356–367.
99 A. Cammarata, V. Verda, A. Sciacovelli and Y. Ding, Hybrid strontium bromide-natural graphite composites for low to

medium temperature thermochemical energy storage: Formulation, fabrication and performance investigation, *Energy Convers. Manage.*, 2018, **166**, 233–240.

100 R. Weber and V. Dorer, Long-term heat storage with NaOH, *Vacuum*, 2008, **82**(7), 708–716.

101 Y. Yuan, Y. J. Li, L. B. Duan, H. T. Liu, J. L. Zhao and Z. Y. Wang, $CaO/Ca(OH)_2$ thermochemical heat storage of carbide slag from calcium looping cycles for CO_2 capture, *Energy Convers. Manage.*, 2018, **174**, 8–19.

102 M. R. Morrell, S. B. Kaudur, J. Shin, S. Flagg, I. Goyal, J. Pyo, E. Barbosa, S. Bharti, C. V. Di Leo, M. T. McDowell and A. K. Menon, Pathways to High-Performance Salt Hydrate Thermochemical Energy Storage Materials and Systems, *ACS Energy Lett.*, 2026, **11**(2), 1021–1034.

103 S. Lin, Z. Y. Ling, S. M. Li, C. Y. Cai, Z. G. Zhang and X. M. Fang, Mitigation of lithium-ion battery thermal runaway and inhibition of thermal runaway propagation using inorganic salt hydrate with integrated latent heat and thermochemical storage, *Energy*, 2023, **266**, 126481.

104 Q. Y. Ma and W. Gao, Preparation and characterization of high-enthalpy inorganic hydrated salt phase change materials based on sodium silicate precursor, *J. Therm. Anal. Calorim.*, 2024, **149**(23), 14449–14461.

105 X. Y. Dai, D. P. Kong, J. Du, Y. Zhang and P. Ping, Investigation on effect of phase change material on the thermal runaway of lithium-ion battery and exploration of flame retardancy improvement, *Process Saf. Environ. Prot.*, 2022, **159**, 232–242.

106 Y. Wu, A. C. Y. Yuen, C. Mo and X. Huang, Modelling and optimization of a thermal management and barrier integration structure by coupling CFD and reduced-order thermal resistance network, *Energy Convers. Manage.*, 2025, **343**, 120188.

107 H. W. Han, F. Xiong, M. L. Qin, Y. K. Jin, H. K. Chu, S. H. Han, K. H. Jia, A. Usman, S. Gao, R. Zhong, Z. Shen and R. Zou, Intrinsic flame-retardant phase change materials for battery thermal management during rapid cycling and thermal runaway, *Energy Storage Mater.*, 2025, **77**, 104175.

108 Q. Huang, S. L. Wang, S. S. Wang, D. J. Xu, W. Y. Zhang, C. C. Liu and L. Q. Huang, Experimental design of thermal conductive and safe phase change composites with carbon foam based on biological polysaccharides, *J. Energy Storage*, 2025, **139**, 118784.

109 J. Y. Choi, M. H. Park and J. J. Yoh, Next-generation battery heat shield based on lithium nitrate molten-salt phase-change material for thermal-runaway prevention, *Cell Rep. Phys. Sci.*, 2025, **6**(11), 102920.

110 J. H. Cao, Z. Y. Ling, S. Lin, Y. J. He, X. M. Fang and Z. G. Zhang, Thermochemical heat storage system for preventing battery thermal runaway propagation using sodium acetate trihydrate/expanded graphite, *Chem. Eng. J.*, 2022, **433**, 133536.

111 Q. Q. Huang, X. X. Li, J. Deng, W. S. Yang, Y. Y. Zeng, Z. H. Rao, F. L. Kong and Y. L. Li, The flame retardant mechanism of composite phase change materials for battery thermal safety: A review, *Energy Storage Mater.*, 2025, **80**, 104344.

112 J. W. Weng, C. R. Xiao, D. X. Ouyang, X. Q. Yang, M. Y. Chen, G. Q. Zhang, R. K. K. Yuen and J. Wang, Mitigation effects on thermal runaway propagation of structure-enhanced phase change material modules with flame retardant additives, *Energy*, 2022, **239**, 122087.

113 J. Mei, G. Q. Shi, H. Liu and Z. Wang, Organic and Inorganic Hybrid Composite Phase Change Material for Inhibiting the Thermal Runaway of Lithium-Ion Batteries, *Batteries*, 2023, **9**(10), 513.

114 J. Mei, G. Q. Shi, H. Liu, Z. Wang and M. Y. Chen, Experimental study on the effect of passive retardation method for thermal runaway mitigation of lithium-ion battery, *Appl. Therm. Eng.*, 2023, **230**, 120861.

115 P. H. Chen, J. Deng, Z. K. Guo, X. X. Li, W. S. Yang, Y. H. Wu, Y. Mao, W. Jia, J. Z. Liu and C. B. Li, Advancing Thermal Safety System for Battery Pack: Introducing Intrinsic Flame–Retardant Solid–Solid Phase Change Materials with Melamine Crosslink, *Adv. Funct. Mater.*, 2025, **35**(29), 2423361.

116 L. Shen, Y. Q. Hu, X. Zhang, D. F. Chen, C. F. Xu, R. Zhou, M. Hao and J. C. Jiang, Research on flame-retardant phase change materials in thermal management of lithium iron phosphate batteries, *J. Energy Storage*, 2025, **137**, 118515.

117 W. S. Yang, C. B. Li, X. X. Li, H. W. Wang, J. Deng, T. Q. Fu, Y. J. Luo, Y. Wang, K. L. Xue, G. Q. Zhang, D. Q. Zhou, Y. X. Du and X. X. Li, High flame retardant composite phase change materials with triphenyl phosphate for thermal safety system of power battery module, *eTransportation*, 2024, **20**, 100325.

118 G. F. Zhao, B. W. Liang, Y. Li, R. F. He, T. Y. Wang, Z. K. Guo, J. Z. Liu and X. X. Li, Investigation on flame retardant microcapsules based composite phase change material for battery thermal safety, *J. Energy Storage*, 2025, **132**, 118010.

119 J. Y. Zhang, X. X. Li, G. Q. Zhang, H. W. Wu, Z. H. Rao, J. W. Guo and D. Q. Zhou, Experimental investigation of the flame retardant and form-stable composite phase change materials for a power battery thermal management system, *J. Power Sources*, 2020, **480**, 229116.

120 J. J. Shen, Y. H. Su, X. B. Xu, X. Chen, X. L. Wang, J. L. Wang and F. Zhou, Performance of sandwich type fire-resistant flexible composite phase change material PEE@EBF for battery thermal management and runaway protection, *Appl. Therm. Eng.*, 2025, **258**, 124813.

121 J. J. Jiang, G. R. Mao, J. J. Xu, Y. T. Chen and J. C. Jiang, Preparation and Application of Aluminum-Phenylphosphinate-Encapsulated Phase Change Materials for Thermal Management of Lithium-Ion Batteries, *Energy Fuels*, 2024, **38**(13), 12111–12120.

122 F. Liu, J. F. Wang, F. Q. Wang, H. Liu, Q. Du, Y. H. Li, B. W. Chen, H. D. Gu and N. Yang, Battery thermal safety management with form-stable and flame-retardant phase change materials, *Int. J. Heat Mass Transfer*, 2024, **218**, 124764.

123 A. García, J. Monsalve-Serrano, A. Dreif and C. Guaraco-Figueira, Multiphysics integrated model of NMC111 battery module for micro-mobility applications using PCM as intercell material, *Appl. Therm. Eng.*, 2024, **249**, 123421.
124 M. Y. Zhi, R. Fan, L. L. Zheng, S. Yue, Z. H. Pan, Q. Sun and Q. Y. Liu, Experimental investigation on hydrated salt phase change material for lithium-ion battery thermal management and thermal runaway mitigation, *Energy*, 2024, **307**, 132685.
125 P. Ping, X. Y. Dai, D. P. Kong, Y. Zhang, H. L. Zhao, X. Z. Gao and W. Gao, Experimental study on nano-encapsulated inorganic phase change material for lithium-ion battery thermal management and thermal runaway suppression, *Chem. Eng. J.*, 2023, **463**, 142401.
126 X. Y. Dai, P. Ping, D. P. Kong, X. Z. Gao, Y. Zhang, G. Q. Wang and R. Q. Peng, Heat transfer enhanced inorganic phase change material compositing carbon nanotubes for battery thermal management and thermal runaway propagation mitigation, *J. Energy Chem.*, 2024, **89**, 226–238.
127 Y. Y. Chen, X. J. Guo, C. W. Shi, X. Zhou and D. Q. Zou, Preparation of metal-based microencapsulated phase change material and its application in a battery for thermal management and thermal runaway protection, *Composites, Part B*, 2025, **298**, 112376.
128 R. X. Ma, X. N. Feng, T. Y. Zhao, W. C. Zhang, M. Liu and W. X. Wu, Composite phase change material for preventing battery thermal runaway propagation: Critical condition and inhibition strategy, *J. Energy Storage*, 2023, **72**, 108237.
129 X. Y. Liu, Z. F. Zhou, W. T. Wu, L. Wei, W. X. Wu, Y. Li, L. S. Gao, Y. B. Li and Y. C. Song, Modelling for the mitigation of lithium ion battery thermal runaway propagation by using phase change material or liquid immersion cooling, *Case Stud. Therm. Eng.*, 2023, **52**, 103749.
130 H. Y. Li, X. B. Hong, J. W. Meng and D. B. Ruan, Novel composite spacer layer for battery modules: Structural design with superior mechanics and thermal runaway resistance, *Therm. Sci. Eng. Prog.*, 2025, **67**, 104208.
131 Z. R. Huo, X. B. Hong, Y. Y. Li, Z. H. Chen and D. B. Ruan, Numerical study of paraffin and glass fiber composites for thermal management of lithium–ion battery packs, *Asia–Pac. J. Chem. Eng.*, 2023, **19**(1), e2989.
132 A. Chakraborty, J. Lee and C. H. Yu, Harnessing anisotropy of phase change composites for taming thermal runaway and fast charging of lithium-ion batteries, *Appl. Energy*, 2025, **389**, 125802.
133 T. Y. Li, J. X. Piao, D. L. Xu, Y. H. Meng, L. F. Zhang, X. Han, X. R. Yang, L. Z. Jin and S. Bi, Thermally triggered tunable-thermal-conductivity phase-change composites for lithium-ion battery thermal management and runaway mitigation, *Chem. Eng. J.*, 2025, **524**, 169799.
134 R. K. Ni, D. J. Zhang, R. Q. Wang, Z. F. Xie and Y. A. Wang, Prevention and suppression effects of phase change material on thermal runaway in batteries, *Case Stud. Therm. Eng.*, 2023, **48**, 103160.
135 P. Kim, L. Shi, A. Majumdar and P. L. McEuen, Thermal transport measurements of individual multiwalled nanotubes, *Phys. Rev. Lett.*, 2001, **87**(21), 215502.
136 J. L. Yang, S. Wang, J. C. Zhao, S. L. Wang, S. S. Wang, Y. L. Peng, Q. Huang and C. C. Liu, Preparation of MXene-based aerogel-derived phase change materials for mitigating thermal runaway risk in batteries, *Chem. Eng. J.*, 2025, **511**, 162039.
137 T. Xu, Q. L. Chen, G. S. Huang, Z. G. Zhang, X. N. Gao and S. S. Lu, Preparation and thermal energy storage properties of D-Mannitol/expanded graphite composite phase change material, *Sol. Energy Mater. Sol. Cells*, 2016, **155**, 141–146.
138 V. Talele, U. Morali, H. N. Khaboshan, M. S. Patil, S. Panchal, R. Fraser and M. Fowler, Improving battery safety by utilizing composite phase change material to delay the occurrence of thermal runaway event, *Int. Commun. Heat Mass Transfer*, 2024, **155**, 107527.
139 J. W. Weng, Y. P. He, D. X. Ouyang, X. Q. Yang, M. Y. Chen, S. T. Cui, G. Q. Zhang, R. K. K. Yuen and J. Wang, Honeycomb-inspired design of a thermal management module and its mitigation effect on thermal runaway propagation, *Appl. Therm. Eng.*, 2021, **195**, 117147.
140 W. X. Wu, W. Wu and S. F. Wang, Thermal optimization of composite PCM based large-format lithium-ion battery modules under extreme operating conditions, *Energy Convers. Manage.*, 2017, **153**, 22–33.
141 Z. Wang and J. Wang, Investigation of external heating-induced failure propagation behaviors in large-size cell modules with different phase change materials, *Energy*, 2020, **204**, 117946.
142 M. Y. Chen, M. H. Zhu, S. Y. Zhang, D. X. Ouyang, J. W. Weng, R. C. Wei, Y. Chen, L. Y. Zhao and J. Wang, Experimental investigation on mitigation of thermal runaway propagation of lithium-ion battery module with flame retardant phase change materials, *Appl. Therm. Eng.*, 2023, **235**, 121401.
143 M. Y. Chen, Y. L. Ye, Y. Yu, L. Y. Zhao, Y. Chen and J. W. Weng, Towards safer lithium-ion battery modules enabled by dual-functionality of silica gel-based phase change materials, *Mater. Today Energy*, 2025, **54**, 102100.
144 W. Y. Dong, C. S. Xu, W. S. Huang, Y. Peng, M. Q. Zhang, H. B. Wang, C. Y. Jin, Y. Z. Fan and X. N. Feng, Dynamic simulation on the deformation of the battery module under thermal runaway propagation based on internal pressure, *Process Saf. Environ. Prot.*, 2025, **195**, 106733.
145 M. Y. Luo, X. M. Lin, Z. Y. Ling, Z. G. Zhang and X. M. Fang, An electric conductive wide-temperature flexible phase change material for all-climate battery thermal management, *Appl. Therm. Eng.*, 2024, **256**, 124051.
146 T. T. Wu, P. C. Chen, Z. H. Zhang, Z. H. Wu, Y. X. Hu, S. T. Cai and C. H. Wang, Synergistically flame-retardant solid-solid phase change composites for battery thermal safety systems, *Appl. Therm. Eng.*, 2025, **279**, 127637.
147 Y. Z. Zhao, X. L. Zhang, S. W. Cai, C. Zhang, M. X. Wu, B. Yang, J. Ji and W. S. Hua, Experimental study on flex-

ible flame retardant phase change materials for reducing thermal runaway propagation of batteries, *J. Energy Storage*, 2024, **89**, 111721.

148 Q. Q. Huang, X. X. Li, G. Q. Zhang, J. W. Weng, Y. Z. Wang and J. Deng, Innovative thermal management and thermal runaway suppression for battery module with flame retardant flexible composite phase change material, *J. Cleaner Prod.*, 2022, **330**, 129718.

149 Q. Liu, Q. Deng, R. Zhao, W. L. Cheng and Y. D. Wang, A novel flexible flame-retardant phase change materials with battery thermal management test, *J. Energy Storage*, 2023, **70**, 108077.

150 R. Zhao, S. L. Zhang, J. J. Gu, J. Liu, S. Carkner and E. Lanoue, An experimental study of lithium ion battery thermal management using flexible hydrogel films, *J. Power Sources*, 2014, **255**, 29–36.

151 R. Zhao, J. Liu and J. J. Gu, Simulation and experimental study on lithium ion battery short circuit, *Appl. Energy*, 2016, **173**, 29–39.

152 G. Zhou, Q. Huang, Q. Zhang, C. X. Niu, H. H. Lu, S. Q. Yang, Y. Liu, Z. K. Wei, S. L. Li and Y. Kong, Thermal insulation phase-change hydrogel with enhanced mechanical properties for inhibiting thermal runaway propagation in lithium-ion battery module, *J. Energy Storage*, 2024, **102**, 114102.

153 L. Li, B. Fang, D. S. Ren, L. Fu, Y. Q. Zhou, C. Yang, F. S. Zhang, X. N. Feng, L. Wang, X. M. He, P. P. Qi, Y. Liu, C. Jia, S. Y. Zhao, F. Xu, X. D. Wei and H. Wu, Thermal-Switchable, Trifunctional Ceramic–Hydrogel Nanocomposites Enable Full-Lifecycle Security in Practical Battery Systems, *ACS Nano*, 2022, **16**, 10729–10741.

154 B. Bausch, S. Frankl, D. Becher, F. Menz, T. Baier, M. Bauer, O. Böse and M. Hölzle, Naturally-derived thermal barrier based on fiber-reinforced hydrogel for the prevention of thermal runaway propagation in high-energetic lithium-ion battery packs, *J. Energy Storage*, 2023, **61**, 106841.

155 G. Zhou, Q. Huang, Z. K. Wei, B. Y. Guo, Q. H. Hu, P. Zhang, H. H. Lu and Q. Zhang, Multifunctional ceramic-reinforced nanocomposite hydrogel for thermal runaway propagation blocking and heat dissipation of lithium-ion battery modules, *Fuel*, 2026, **404**, 136257.

156 J. Y. Chen, C. S. Xu, J. Y. Liu, Y. Sun, S. K. Wong, W. Y. Dong, H. N. Huang, Z. K. Yang, Y. Peng, J. Y. Zhang, L. G. Lu, G. Q. Zhang, X. N. Feng and M. G. Ouyang, Enhanced barrier materials with integrated gas regulation capabilities to mitigate explosion risks in battery systems, *Chem. Eng. J.*, 2025, **503**, 158235.

157 B. S. Kang, S. E. Moon, J. H. Kim and S. M. Kang, Broad-Range Supersensitive and Transparent Patterned Hydrogel-Based Pressure Sensor with Long-Term Stability, *ACS Appl. Polym. Mater.*, 2025, **7**(2), 1012–1019.

158 T. Spietz, R. Fryza, J. Lasek and J. Zuwala, Thermochemical Energy Storage Based on Salt Hydrates: A Comprehensive Review, *Energies*, 2025, **18**(10), 2643.

159 S. L. Zhou, S. Lin, W. B. Zhang, Z. Y. Ling, Z. G. Zhang and X. M. Fang, Kinetics study on inhibiting battery thermal runaway using an inorganic phase change material with a super high thermochemical storage capacity, *Process Saf. Environ. Prot.*, 2024, **191**, 643–657.

160 J. J. Wang, S. P. Wang, Y. Yu, Y. F. Cheng, Z. Y. Li, W. Zeng, C. D. Wang, Y. B. Yue, W. X. Mei and Q. S. Wang, Dual heat-absorbing inorganic flame-retardant composite phase change material for enhanced battery thermal safety, *Chem. Eng. J.*, 2025, **519**, 165205.

161 Z. C. Li, F. Cao, Y. Zhang, S. F. Zhang and B. T. Tang, Enhancing Thermal Protection in Lithium Batteries with Power Bank-Inspired Multi-Network Aerogel and Thermally Induced Flexible Composite Phase Change Material, *Nano-Micro Lett.*, 2025, **17**(1), 166.

162 W. J. Miao, R. X. Quan, J. X. Ju, M. Hu, H. Cao, Q. Xu, Y. X. Xiong, Y. Q. Zhao, Y. L. Ding and X. Ling, Calcium chloride hexahydrate based composite phase change/thermochemical material for wide-temperature range passive battery thermal management, *Chem. Eng. J.*, 2025, **508**, 160800.

163 W. B. Zhang, Y. X. Zhang, Z. Y. Ling, X. M. Fang and Z. G. Zhang, Microinfiltration of $Mg(NO_3)_2{\cdot}6H_2O$ into g-C_3N_4 and macroencapsulation with commercial sealants: A two-step method to enhance the thermal stability of inorganic composite phase change materials, *Appl. Energy*, 2019, **253**, 113540.

164 Y. Yu, J. M. Tian, J. J. Wang, Z. Y. Li, K. Q. Jin, W. X. Mei and Q. S. Wang, In-depth analysis of synergistic suppression of thermal runaway propagation in lithium-ion battery modules via combined active cooling and passive insulation, *Process Saf. Environ. Prot.*, 2025, **197**, 107026.

165 M. Al-Zareer, I. Dincer and M. A. Rosen, A thermal performance management system for lithium-ion battery packs, *Appl. Therm. Eng.*, 2020, **165**, 114378.

166 X. H. Xu, W. Z. Li, B. Xu and J. Qin, Numerical study on a water cooling system for prismatic $LiFePO_4$ batteries at abused operating conditions, *Appl. Energy*, 2019, **250**, 404–412.

167 T. Q. Yang, H. W. Xu, C. F. Xie, L. Z. Xu, M. Liu, L. Y. Chen, Q. Q. Xin, J. Zeng, H. Y. Zhang and J. S. Xiao, A Thermal Runaway Protection Strategy for Prismatic Lithium-Ion Battery Modules Based on Phase Change and Thermal Decomposition of Sodium Acetate Trihydrate, *Batteries*, 2025, **11**(5), 198.

168 D. Lu, N. X. Cui, J. W. Zhou and C. L. Li, Hybrid cooling system with phase change material and liquid microchannels to prevent thermal runaway propagation within lithium-ion battery packs, *Appl. Therm. Eng.*, 2024, **247**, 123118.

169 Y. Wang, Y. T. Wang, T. B. He and N. Mao, A numerical study on a hybrid battery thermal management system based on PCM and wavy microchannel liquid cooling, *Renewable Energy*, 2024, **235**, 121273.

170 J. L. Gong, L. Li and J. H. Gong, Hybrid cooling systems for suppressing thermal runaway propagation in a

lithium-ion battery module, *Therm. Sci. Eng. Prog.*, 2025, **64**, 103845.

171 Y. Liu, Z. F. Zhou, W. T. Wu, L. Wei, J. Lyu, Y. Li, X. Y. Liu, Y. B. Li and Y. C. Song, Simulations on hybrid thermal management of mini-channel cold plate and PCM for lithium-ion batteries under discharging and thermal runaway conditions, *Case Stud. Therm. Eng.*, 2024, **60**, 104837.

172 H. X. Xiao, J. Q. E, S. C. Tian, Y. X. Huang and X. Y. Song, Effect of composite cooling strategy including phase change material and liquid cooling on the thermal safety performance of a lithium-ion battery pack under thermal runaway propagation, *Energy*, 2024, **295**, 131093.

173 P. Luo, K. Gao, L. Hu, B. Chen and Y. J. Zhang, Adaptive hybrid cooling strategy to mitigate battery thermal runaway considering natural convection in phase change material, *Appl. Energy*, 2024, **361**, 122920.

174 K. S. Kshetrimayum, Y. G. Yoon, H. R. Gye and C. J. Lee, Preventing heat propagation and thermal runaway in electric vehicle battery modules using integrated PCM and micro-channel plate cooling system, *Appl. Therm. Eng.*, 2019, **159**, 113797.

175 T. C. Ouyang, B. L. Liu, C. C. Wang, J. L. Ye and S. L. Liu, Novel hybrid thermal management system for preventing Li-ion battery thermal runaway using nanofluids cooling, *Int. J. Heat Mass Transfer*, 2023, **201**, 123652.

176 M. F. Li, Z. Liu, W. W. Yang, Y. W. Lin, K. F. Ji and Z. Y. Jiang, Multi-objective optimization of hybrid battery thermal management design with considering thermal runaway propagation prevention, *Appl. Therm. Eng.*, 2025, **269**, 125990.

177 W. G. Ji, Y. C. Dang, Y. C. Yu, X. L. Zhou and L. Li, Combination of Phase Change Composite Material and Liquid-Cooled Plate Prevents Thermal Runaway Propagation of High-Specific-Energy Battery, *Appl. Sci.*, 2025, **15**(3), 1274.

178 Y. Liu, Y. G. Chen, Z. J. Chang, X. H. Wu, Z. Y. Jiang and S. Z. Tang, Role of porous metal foam on temperature control and thermal runaway propagation of integrated battery thermal management systems, *Appl. Therm. Eng.*, 2025, **267**, 125712.

179 C. K. Wu, J. M. Ni and X. Y. Shi, Research on multiple thermal conductivity phase-change-material-liquid thermal management system considering thermal safety and temperature uniformity of battery pack, *J. Energy Storage*, 2025, **136**, 118456.

180 T. C. Ouyang, B. L. Liu, P. H. Xu, C. C. Wang and J. L. Ye, Electrochemical-thermal coupled modelling and multi-measure prevention strategy for Li-ion battery thermal runaway, *Int. J. Heat Mass Transfer*, 2022, **194**, 123082.

181 J. K. Xie, J. L. Li, C. B. Li, X. Y. Huang, G. Q. Zhang and X. Q. Yang, Multi-level passive-active thermal control for battery thermal runaway prevention and suppression in electric vehicles, *eTransportation*, 2025, **26**, 100467.

182 K. L. Zuo, Z. P. Li, H. M. Liang, Z. R. Wang and T. C. Ouyang, An integrated scheme to prevent the propagation of Li-ion battery thermal runaway, *Int. J. Heat Mass Transfer*, 2025, **241**, 126725.

183 M. Mehrabi-Kermani, E. Houshfar and M. Ashjaee, A novel hybrid thermal management for Li-ion batteries using phase change materials embedded in copper foams combined with forced-air convection, *Int. J. Therm. Sci.*, 2019, **141**, 47–61.

184 H. W. Liu, G. Q. Li, X. D. Zhao, X. L. Ma and C. Shen, Investigation of the impact of the thermoelectric geometry on the cooling performance and thermal-mechanic characteristics in a thermoelectric cooler, *Energy*, 2023, **267**, 126471.

185 X. D. Wang, Q. H. Wang and J. L. Xu, Performance analysis of two-stage TECs (thermoelectric coolers) using a three-dimensional heat-electricity coupled model, *Energy*, 2014, **65**, 419–429.

186 Y. X. Huang, X. D. Wang, C. H. Cheng and D. T. W. Lin, Geometry optimization of thermoelectric coolers using simplified conjugate-gradient method, *Energy*, 2013, **59**, 689–697.

187 X. Liu, P. Y. Wu, C. Q. Su, X. Xiong and Y. P. Wang, Li-ion battery thermal management and thermal runaway suppression method of combining phase change material and annular thermoelectric cooler, *J. Energy Storage*, 2024, **82**, 110564.